# Mapping the recent bio-geomorphological evolution of the man-made Terschelling blowout complex using PlanetScope imagery and airborne LiDAR data

## Personal information


*Name:* Bart Folgerd Maas
*Student Number:* 4237447
*E-mail:* b.f.maas@students.uu.nl
*Master:* Earth Surface and Water

*First supervisor:* Prof. Dr. Gerben Ruessink, Department of Physical Geography
*Second supervisor:* Dr. Wiebe Nijland, Department of Physical Geography

*Number of ECTS:* 37.5

Universiteit Utrecht

*Date: February 2020*

Frontpage image:

*Terschelling blowout complex viewing towards the west near beach pole 19*
*Source: Own collection, 01-02-2020*

# Abstract

For centuries, The Netherlands delivered a constant battle with the sea to protect the country from flooding and to secure its welfare. Its main defence system is the dunes, protecting the vulnerable Dutch lowlands. Throughout the twentieth century, the foredunes were maintained with the philosophy “The higher, the better”, resulting in dune stabilisation that, in turn, contributed to a decline in biodiversity in the landward dunes. To counter the loss of biodiversity a new management strategy aiming to remobilize the foredunes was brought to existence. This strategy included the initiation of blowouts. In 1995 eight foredune notches were excavated, in a pioneering project along the Terschelling coast (km 15-20) in order to create a blowout complex. Now 25 years later, the remobilisation could be marked as a successful project beneficial for both human and nature. In the early years, the area has expanded tremendously. During the last years, indications arose that the blowout complex slowly shifted towards a more ecological development phase. To quantify the bio-geomorphological changes a combination of high resolution 3x3 m PlanetScope multispectral imagery and annual airborne LiDAR data were used. Throughout the six-year study period, the dune area experienced a positive but declining volume growth trend, except for 2013/2014. The volume gain was mainly concentrated around the fore- and back dunes as erosion was found within the dune valley. Furthermore, notches showed signs of closure by filling-in. The landcover change maps showed that regrowth of vegetated area exceeded the area that gets buried by the sand deposition. In autumn most vegetation started to return, net 116.000 $m^2$ landcover turned from sand in to vegetation within two years (2016-2018). By combining the two resulting products, the changing relationship between the abiotic and biotic mechanisms come to light. Abiotic effects decreased at areas where vegetation was returning, decreasing the overall dune dynamics. With the absence of increasing frequency of storm events, it is expected that the blowout complex continues to shift into the ecological development phase and slowly stabilises.



**Keywords:** Terschelling; PlanetScope; LiDAR; dune remobilisation; aeolian sand transport; bio-geomorphology; abiotic-biotic feedback; dune stabilisation

# Acknowledgements

First of all, I would like to thank my supervisors Gerben and Wiebe. They were always available and able to help if I got stuck and helped to enlighten new insights and ideas to improve my thesis even more. Special thanks goes to Loek Schemmekes, during the thesis period we worked in close collaboration on the model that was used in this research, building it up from scratch. Furthermore, we helped each other by motivating and having a critical view on each other's works, which all resulted in a very pleasant time. While digging deeper into the topic I started to enjoy the way of doing research more and more, resulting in that there are no hard feelings or whatsoever while looking back on this period. And last but not least I would like to thank my other fellow MSc students on the fourth floor of VMA for keeping the weeks and hard work enjoyable with good laughter during the daily break routines and other side activities we did together.

# Table of contents

# List of Figures and Tables

# 1. Introduction

With rising sea level and changing weather conditions, extreme water events are a serious threat to reckon, especially in The Netherlands. Here, more than 9 million people live below sea level together with valuable industries that secure the country's welfare (Mulder et al., 2011). In order to defend the vulnerable areas, multiple coastal safety policies have been implemented including hard and soft measures. Most soft measures were applied in order to strengthen the foredunes, which make up 75% of the Dutch primary coastal defence line (Mulder et al., 2011). To increase the dune's resilience against wave and aeolian erosion, marram grass (*Ammophila Arenaria*) was planted on a large scale. At multiple locations this resulted in stabilisation of the foredunes and gain in height and volume, increasing the water safety. The increase of water safety with this method seems perfectly fine, but it also initiated multiple drawbacks. As the dunes increased in height, the amount of aeolian transport over the foredunes declined, creating a deficit of fresh sands and nutrients in the back dunes. This resulted in a drop in biodiversity and morphologic dynamics (e.g. Lithgow et al., 2013; Nordstrom & Arens, 1998; Provoost, Jones, & Edmondson, 2011). Towards the end of the twentieth century, it came to mind that attention should be focussed on a more sustainable measure of which both human and nature would benefit.

One of the locations that suffered from the drawbacks is the northern coast of the Wadden Island of Terschelling. Even though the Wadden coast is the most dynamic coast of The Netherlands, the dunes are often among the least dynamic and are kept the most in shape by vegetation (Van der Valk, Reinders, van der Spek, & Gelder-Maas, 2013). As the dunes were marked as "safe", the new sustainable coastal management strategy was implemented in 1995. This strategy was based on the concept to link the beach, foredunes and back dunes by excavating notches through the foredune. With the presence of the notches, it was expected that aeolian transport could again supply the back dunes with beach sands in order to restore the natural dune dynamics (e.g. Hesp, 2002; Hesp & Hyde, 1995; Nordstrom & Arens, 1998).

As this management strategy was characterized as learning-by-doing it raised concerns by the local inhabitants (*"Eilanders"*) on coastal safety and uncontrolled change to their island. This concern was reinforced when the foredune height started to decrease and undesired aeolian sands deposited on farmlands (Löffler, Landwijzer, Goessen, & Hollands, 2016). In order to limit the nuisance of the sand deposition, minor implications as fences and grasses were placed at selected locations. As the initiation of the remobilisation project started 25 years ago a lot has changed since. Due to the blowouts, the area became much more dynamic and extended even several hundreds of meters landward (Figure 1). The sand volume increased and biodiversity slowly recovered, as is in line with the beforehand expectations.

Over the course of time, the area has been monitored intensively and showed that the initiation of blowouts are a good measure to remobilise the dune area. As much research already has been done, the last published documentations only reach till 2013 (e.g. Arens, Loffler, & Nuijen, 2007; Arens, Slings, Geelen, & Van der Hagen, 2013; Van der Valk et al., 2013). Recent visual observation by local stakeholders indicated that the blowout complex may no longer be as active as in the decades before and that vegetation is recolonising certain parts of the area. To investigate the relationship between the abiotic dune dynamics and biotic dune vegetation this Thesis makes use of remote sensing methods. By combining high-resolution multispectral PlanetScope imagery and airborne LiDAR data, it is aimed to get inside on how the abiotic-biotic feedback mechanisms influence the recent morphological changes of the man-made Terschelling blowout complex.

In the light of this aim first a literature review is presented to provide background on foredunes behaviour and blowout development in mainly natural systems. In addition examples of previous blowout initiation projects are discussed and compared to Terschelling. This is followed by a more extensive study site description including, the climate conditions and bio-morphological developments prior to 2013. Further on, the used data sets and methods are presented and explained. In the results, the observations from the processed LiDAR and PlanetScope data is presented, followed by the interpretations and new insights in the discussion, where it will be compared with the literature study in section 2. Finally, the main findings of this Thesis will be summarised and provided in the conclusion.


*Figure 1 – a) Location of Terschelling and study area indicated in the red box. Source: Planet scope (27-06-2019). b) Zoom-in on the study area. Source: Superview May 2019 50cm; https://www.satellietdataportaal.nl/*

# 2. Background

## 2.1 What are blowouts and how are they formed?

Along the coast of a waterbody with ample sand availability dune rows are formed as the first protection for the hinterland. The most seaward fully developed dune row are called foredunes (Hesp, 2002). As mentioned in the introduction, blowouts are found in the foredunes. To inform the reader thoroughly it is important to include a concise explanation on the foredunes. For a more extensive review on foredune development, the reader is advised to look into Hesp (2002 & 2012).

### 2.1.1 Foredunes

Foredunes are found from modest size, less than a meter vertical elevation, to established sand walls towering ±30 m above ground level which is more often found at areas where humans initiated dune management by planting stabilizing vegetation on the dunes lee side (Arens, Mulder et al., 2013; Hesp, 2002). The foredunes have been classified generally into two types: incipient (also embryo-dunes) and established foredunes, depending on the development state (volume and size). Depending on nine factors mentioned in Hesp (2002), the size, morphology and dynamics of the foredune vary at different locations (Hesp, 2002; Hesp & Thom, 1990). The most important factors concerning foredune development are the presence of vegetation (type and density), ample sand availability and favourable wind conditions (Hesp, 2002).

*Incipient foredune*

The incipient foredune develops seaward of the first dune row and actively depends on the availability of obstacles as vegetation patches or logs to capture aeolian transported sand. Plants tend to increase aerodynamic roughness and therefore affect the mean wind flow and turbulence. This promotes aeolian deposition around the vegetation patches (Hesp, 1983, 1989, 2002; Zarnetske et al., 2015). The growth rate of the embryo-dunes depends on the vegetation species, density and cover, which on their turn depend on the wind regime and beach propagation rates (Hesp, 2002, 2012). Where larger vegetation density and sediment supply will result in increased development of the embryo-dunes. This combination between sand supply and thriving vegetation determines the shape of the embryo dune and possibility it will develop into an established foredune complex or will be eroded in the meantime (Hesp, 2002; Zarnetske et al., 2015). In section 2.2.2, the role of vegetation on foredunes and blowouts will be discussed more thoroughly.

*Established foredune*

Established foredunes develop from incipient foredunes. The difference between an incipient and established foredune is distinguished by vegetation type (more woody and persistent vegetation) but especially by size, volume and morphological complexity (Hesp, 2002). The three most important factors controlling the development rate of established foredunes are 1) beach width/type, 2) sediment supply and 3) wind velocity (Davidson-Arnott & Law, 1996). Depending on the combination of these factors the morphology of the foredune develops in a certain way.

In Hesp (2002), how the evolution of a foredune may progress was presented in a five-step classification. Herein, 1 represents a stable foredune and 5 a highly eroded foredune complex (Figure 2). Depending on the factors mentioned above at the location of the foredune it will evolve according to an erosion or accretion cycle. It is possible for a foredune to undergo an evolution from highly stable (densely vegetated, straight dune row) towards highly erosional, resulting in remnant knobs and blowouts. This process could be reversed when the conditions changes in favour of a densely vegetated foredune (e.g. mild climatic conditions and ample sand supply), the accretion cycle. The time it takes for the foredune complex to progress through the stages depends on the local climatic regime and potential storm event feedbacks (Hesp, 2002).

This Thesis will focus on blowout evolution within the foredunes. Therefore, stages 3-5 of the Hesp (2002) classification are the most interesting, considering both the erosional as the accretional cycle, see Figure 2.

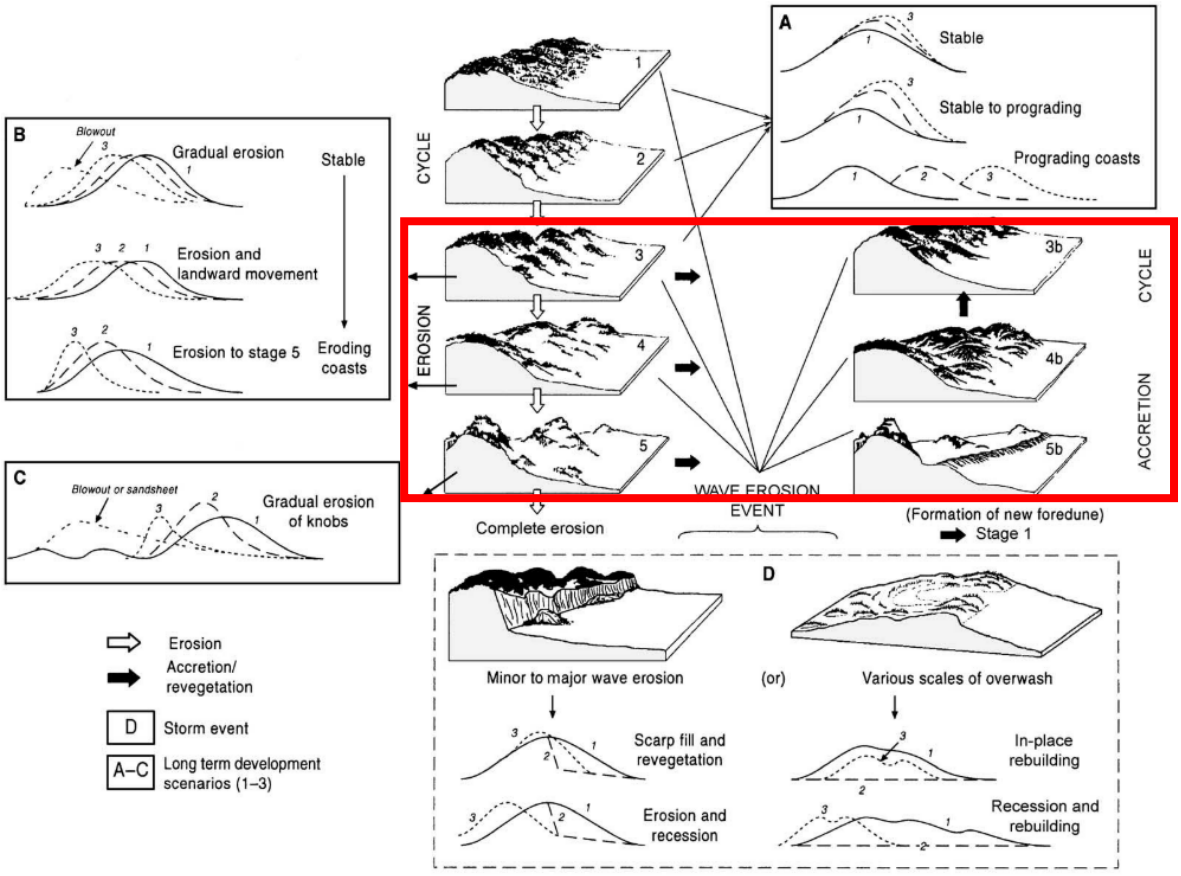


*Figure 2 - Evolutional trends of established foredune morphology. It includes 5 stages for stable (1,2), erosional (3-5) and accreting (3b-5b) dunes. In the red box, the erosion and accretion cycles are marked, which are most interesting for blowout development. Adopted from Hesp (2002).*

### 2.1.2 Blowouts

Blowouts are defined as sandy erosional landforms shaped by wind activity. Besides the already mentioned foredunes, blowouts are found in almost every dune type in coastal as well as desert environments (Hesp, 2012). Within blowouts three different erosional forms are distinguished: saucer-, cup- and trough-shaped blowouts, where saucer- and trough-shaped are most common (Figure 3) (Hesp, 2002). The type of blowout that will form depends on dune morphology, extent and type of vegetation and local climate conditions (Duran & Moore, 2013; Gonzalez-Villanueva, Costas, Duarte, Perez-Arlucea, & Alejo, 2011; Hesp, 2012; Schwarz, Brinkkemper, & Ruessink, 2018). The saucer blowout is a shallow disc-like shaped feature with a large width-to-depth ratio, the cup-shaped blowout are deeper and are formed by continuous saucer erosion (Hesp, 2002). Trough blowouts are V- or U-shaped notches in the foredunes. Compared to saucer blowouts the trough blowouts are often more elongated with a lower width-to-depth ratio due to the characteristic high erosional walls (Hesp, 2012). A blowout is subdivided into three morphological features: 1) Depositional lobe, 2) Deflation basin, 3) and Erosional walls (Figure 3) (Hesp, 2002). These features together are considered to be the blowout. The deflation basin is a non-vegetated area where most of the erosion and aeolian transport takes place. The blowout becomes larger when sand is eroded from the deflation basin and

transported in windward direction onto a ramp towards the depositional lobe or back dunes. The sidewalls are bounded by the rim, which is the boundary of the blowout.

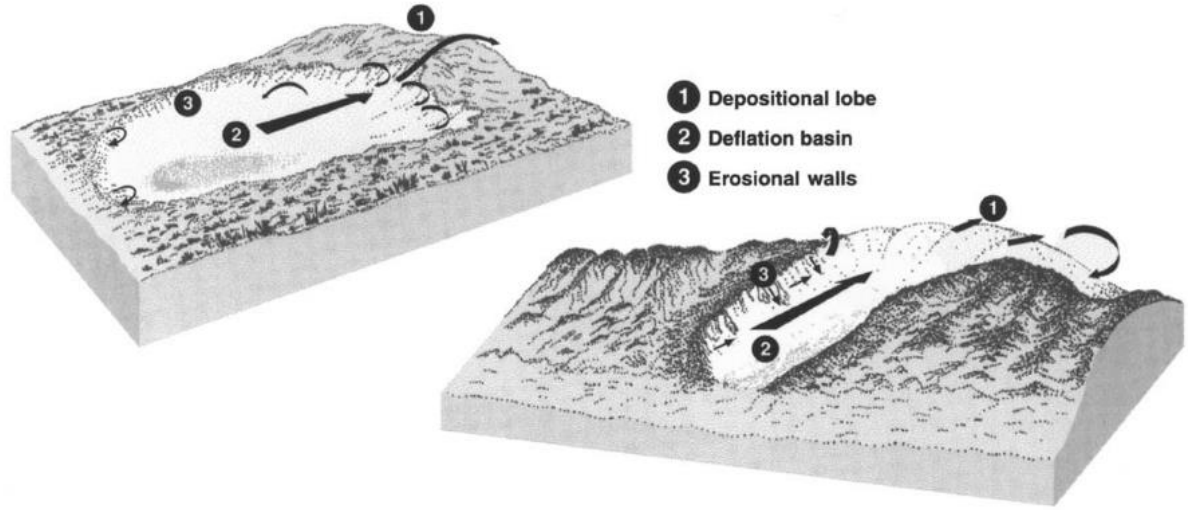


*Figure 3 - Morphology of the two most common blowouts. Left: Saucer blowout, right: Trough blowout with the inclusion of the dominant wind and transport direction. Source: Hesp (2002).*

### *Initiation of blowouts*

Blowouts develop in different sizes and shapes, depending on a wide variety of conditions. They are commonly found along coastal environment where the erosion/accretional cycles (Figure 2) are dynamic. Nonetheless, blowouts are also found along more stable regions with prevailing winds and waves, like in The Netherlands and Denmark (Arens, Mulder, et al., 2013; Clemmensen, Hansen, & Kroon, 2014). Furthermore, the dune shape and wind direction and strength are of importance for the type of blowout that will form (Gonzalez-Villanueva et al., 2011; Jungerius, Witter, & van Boxel, 1991). On foredunes with a broad crest saucer blowouts are the general form to initiate, while on foredunes with a steep, windward facing, slope trough blowouts are more common (Hesp, 2012). Blowouts always form in the direction of the predominant wind direction. Where the morphology of the foredune is one important factor, Hesp (2002) mentioned a total of seven other conditions for blowout initiation:

1) Wave-driven erosion. Continuous wave action erodes the toe of the foredune, in conjunction with wind, the fresh unvegetated part is eroded and the foredune starts slumping. This indicates an onset for a blowout.
2) Wind erosion induced by topography. Small scarps or cliff in the dune could function to funnel and accelerate the wind. Increasing wind velocity results in a higher erosional rate increasing the size of the depression and initiating a blowout (Gares & Nordstrom, 1995).
3) Climate change. This is an important factor in the short and long timescale. When protective vegetation is weakened by a prolonged dry period and the water table has dropped, this allows blowouts to form by wind erosion. On longer time scales changes in wind direction and velocity are drivers for changes in blowout initiation.
4) Vegetation variations. Vegetation density and species are often varying alongshore. Regions with less dense or resilient vegetation cover are more prone to be eroded. For example, this could be initiated by soil nutrient depletion and animals grazing or routing the top layer.
5) Water erosion. After severe storm events, rills and gullies could form. After formation, the perturbations are prone to wind erosion as described under condition 2. The water erosion inside these perturbations is of minor importance according to Hesp (2002).

6) Extreme wind erosion. During extreme storm events or hurricanes, vegetation could be undercut and buried. This creates a bare surface favourable for the blowout to initiate.
7) Human impact. Nowadays this might be the most important factor for initiation of blowouts. Since humans started to live in the coastal area the dunes got cultivated, the landscape got damaged by trampling and track creation and most important of all the vegetation growth got affected and altered (Arens, Slings, Geelen, & Van der Hagen, 2013; Hesp, 2002; Schwarz et al., 2018). Furthermore, since the last decade, an increasing total of foredunes are excavated to artificially create blowouts, for example, a large project in Zuid-Kennemerland, The Netherlands (Ruessink, Arens, Kuipers, & Donker, 2018).

In the light of this thesis initiation conditions, the fourth (vegetation variations) and seventh (Human impact) are most relevant. The blowouts at Terschelling (1995) started as excavated foredune notches to transport beach sand into the back dunes. Without human intervention, the landscape evolution now visible would not have occurred and the foredunes would have remained static (Arens, Loffler, & Nuijen, 2007). The importance of vegetation on the potential blowout site is recognized by multiple studies considering blowout initiation (Arens, Slings, et al., 2013; Duran & Moore, 2013; Gares & Nordstrom, 1995; Hesp, 2002; Martínez, Gallego-Fernández, & Hesp, 2013). Arens, Slings et al. (2013) considered that the problem between mobile or stable foredunes is a matter of dominating force. When vegetation is dominating sand supply, the dune remains stable and the other way around. Where both factors are now more than ever influenced by human activities. Arens, Slings et al. (2013) summarized the two pathways from mobile to stable foredune and vice versa, presented in Figure 4.

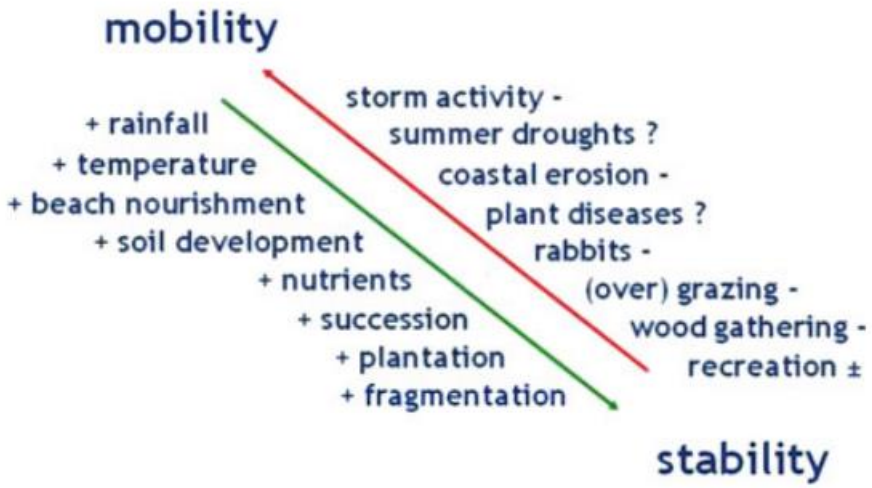


*Figure 4 - Environmental stress factors on dune mobility. Two pathways are presented towards dune mobility and stability. Source: Arens, Slings et al. (2013).*

## 2.2 Dynamic blowout development cycle

When blowouts are initiated they often grow larger and reach their maximum extent depending on local morphologic and ecologic conditions. Eventually, the blowout will become more static until a point the sand transport is negligible, a stable blowout is reached. Then, vegetation is the dominant force and the blowout will often evolve in a parabolic dune (Carter, Hesp, & Nordstrom, 1990). This development cycle is a decadal scale process, though the dimensions of the blowout affect the exact duration (Gares & Nordstrom, 1995; Gonzalez-Villanueva et al., 2011). The development of a blowout is a cycle existing out of an interplay of abiotic (environmental) and biotic (ecological) processes. The abiotic processes include: sand transport, wind speed, rainfall and temperature. Biotic processes

consist out of vegetation growth rate, seasonal variability and competition (Schwarz et al., 2018). The combination of the abiotic and biotic processes give an indication for the presence of blowouts.

The blowout development cycle presented in Schwarz et al. (2018) consist of three phases describing the process from blowout initiation till stabilization and recovery of the foredune, called the bio-geomorphological succession. Figure 5 shows a simple conceptual model of the three phases and the relative influence of abiotic/biotic processes. In the geomorphologic phase, abiotic processes are prevailing and are shaping the new erosional landform. The seven conditions for initiation of a blowout discussed in Hesp (2002) are all part of the geomorphologic phase. Vegetation is subjected to local physical conditions and often dispersed or removed (Corenblit et al., 2015). When the blowout gets its distinct shape (e.g. trough, saucer) the cycle shifts to the bio-morphological phase. When the impact of abiotic processes decreases relatively as the vegetation starts to resettle along the deflation basin and depositional lobe. As a result, the abiotic and biotic processes start to interact and lead to bio-morphodynamic feedbacks in the bio-geomorphological phase. When the intensities of the abiotic and biotic processes are balanced, the bio-morphodynamic feedback mechanisms are most effective and blowout development is most dynamical (Schwarz, Brinkkemper, & Ruessink, 2018). Plants interact with the aeolian sand transport increasing drag, resulting in an increased local sand deposition. Eventually, with the absence of large storm events which could act as a reset, plants will re-colonize the blowout and take over the environmental development during the ecological phase (Corenblit et al., 2015; Schwarz et al., 2018; Van Boxel, Jungerius, Kieffer, & Hampele, 1997). Soil development will result in blowout stabilization and recovery of the foredune. Depending on the abiotic processes governing around the former blowout might be re-activated and the cycle may be started over (Barchyn & Hugenholtz, 2013).

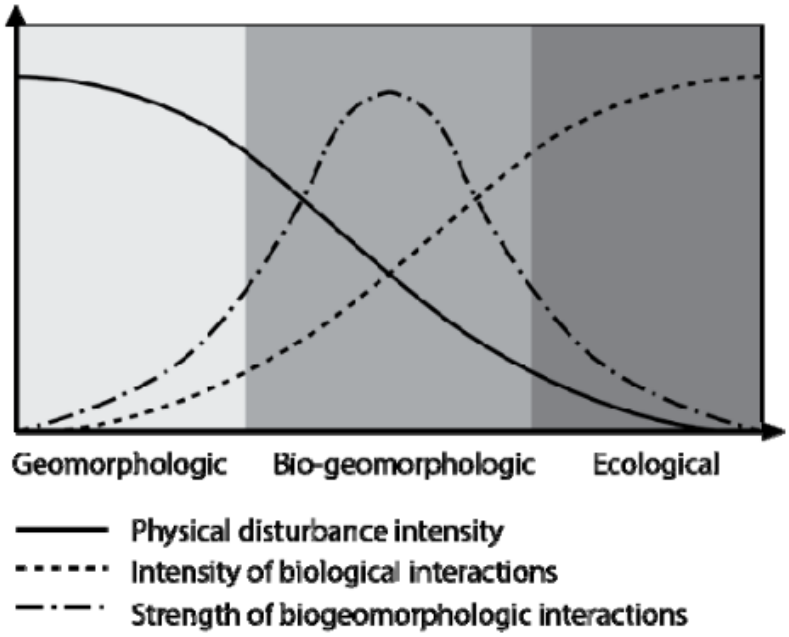


*Figure 5 - The bio-geomorphological succession on blowout development including three phases and intensity of abiotic and biotic feedbacks. Source: Schwarz et al. (2018), adopted from Corenblit et al. (2015).*

### 2.2.1 Aeolian sediment transport

As stated among others Arens, Slings et al. (2013) the development of a blowout is the conjunction between sand supply and vegetation. The sand transported through the blowout originates from the beach and the deflation basin to deposit it on the depositional lobe and back dunes (Carter, Hesp, & Nordstrom, 1990; Hesp, 2002; Hesp & Hyde, 1996). To understand the development of a blowout it is

vital information to understand in what way the sand is transported and how it affects the blowouts morphology.

Most natural formed blowouts are found at locations with persisting onshore winds, depending on morphology which shape of blowout will form (Gonzalez-Villanueva, Costas, Duarte, Perez-Arlucea, & Alejo, 2011; Hesp, 2002; Hesp & Hyde, 1996). When wind velocity increases a certain threshold, sand will be lifted up and transported by saltation towards the stoss side of the foredunes. The threshold is mainly driven by surface conditions as soil moisture and grain size (Bauer et al., 2009). Jungerius et al. (1991) stated that when high wind velocity is prevailing from a fixed direction a blowout tends to develop into a more elongated shape, whereas with a more changing wind direction the shape is less defined. Besides, the effect on blowout development by low frequency extreme aeolian events are small relative to persisting winds with a lower magnitude (Jungerius, Witter, & van Boxel, 1991). Contrasting, for the initiation of blowouts, storm events are helpful to trigger the start of formation. Early studies concerning aeolian processes in coastal areas by Riley (1943) and Olson (1958) (in Hesp & Hyde, 1996) found that wind blowing over the beach will accelerate over the stoss side of the foredunes. Flow separation will occur on the lee side with the effect of a decrease in velocity and sediment deposition. This effect by the topography is a driving force inside a blowout considering the aeolian dynamics and transport. Independent of the blowout shape, sediment is transported at the windward direction (stoss side), explaining the location of the deflation basin. And on the lee side, the wind decelerates, on top of the depositional lobe (Figure 3). This process results in the landward migration of the depositional lobe (Arens, Mulder et al., 2013). Meanwhile, trough and saucer blowouts have a distinct morphological shape and therefore evolve in different ways and will be discussed separately. For example, the width to length ratio of a trough blowout is 1:4 where for saucers blowouts it is measured 1:2/1:3 (Hesp, 2012). An important factor is the jet flow that is induced inside the trough blowout, resulting in a more elongated shape as will be discussed below.

### *Trough blowouts*

Trough blowout form at foredunes with a steep stoss side, resulting in a relatively deep notch flanked by vegetated dunes. The trough blowouts are important for sediment transport and function as a transport corridor between the beach and back dunes. Sediment transport is most effective when the wind speeds are highest and soil moisture is low (Pluis, 1992). This is reached when the wind is aligned with the blowout axis (Hesp & Hyde, 1996). Due to the presence of the erosional walls wind gets accelerated within the trough blowout forming a jet flow. The jet flow reaches its highest velocity above the deflation basin, resulting in the highest amounts of erosion and transportation at this location (Hesp & Hyde, 1996). Erosion of the deflation basin will continue till the base of the deflation basin is reached (e.g. indurated layer or water table). This also applies to saucer blowouts (Hesp, 2002). Furthermore, when the deflation basin gets deeper the erosional walls get undercut and start slumping. When the walls collapse the trough shape can get too wide to create a jet flow and the sediment transport will decrease (Carter et al., 1990). When one of these two factors applies sediment transport will decrease and vegetation will become the dominating force controlling blowout evolution (Carter et al., 1990). The blowout will shift towards the ecological phase (Figure 5).

Summarizing, trough blowouts develop from small erosional disturbances in the foredune to incipient blowouts. Increasing jet flow and erosion of the deflation basin cause it to grow till it becomes too wide or a deficit of sediment occurs. Then it will decay and vegetation will recolonize the blowout (Carter et al., 1990; Gares & Nordstrom, 1995). Even after the closure of the trough, the depositional lobe often will migrate landward to eventually evolve into a parabolic dune (Hesp, 2012).

#### *Saucer blowouts*

Saucer blowouts form on wide dune crests, lacking a steep stoss side of the foredune (Hesp, 2002). The processes discussed at trough blowouts do also occur to some extent at saucer blowouts. When the wind is directed aligned to the blowout axis a jet flow is still created, but the wind is less accelerated because the saucer blowout is relatively wider and less deep. When the wind is multi-directional the jet flow is absent, which is in contrast with trough blowouts (Hesp & Hyde, 1996). Furthermore, the shape of the saucer is more depended on wind direction than the fixed shape of the trough blowout, therefore the depositional lobe is often found to be wider (Carter et al., 1990). The deflation basin is located at the most upwind location. Therefore, saucer blowouts grow in length in the upwind direction, contrary to trough blowouts (Jungerius & van der Meulen, 1989). Dimensions of the saucer blowout increase as evolution continue, resulting in decelerating of the flow, decreasing transport capacity. This could lead to sand accretion on the deflation basin, re-colonizing of vegetation and eventually closure (Schwarz et al., 2018).

### 2.2.2 Role of vegetation on blowout development

Till this point, the literature study mainly focused on the role of sand in the bio-geological blowout succession and discussed the first phase and first part of the second phase. Without the existence of vegetation in the dune system, the coastal region would only exist of wandering dunes and everything would be subject to aeolian transport. Vegetation is the driving force in the latter part of the bio-geological cycle, stabilizing the sediment. Furthermore, our region of interest at Terschelling is experiencing this phase. Even when the abiotic processes are dominating, vegetation is still influencing the system. Assume seasonal effects, in summer and autumn vegetation is thriving and keeps hold on the sand during mild weather conditions. Whereas during winter plants are dead or covered, sediment transport is larger (Byrne, 1997). The rate of how vegetation recovers and will influence the blowout evolution depends on species, density and season (Maun, 1998; Schwarz et al., 2018).

#### *The (bio-)geomorphologic phase*

According to Schwarz et al. (2018), two distinct controls on vegetation survival during the bio-geomorphological phases can be identified: 1) On the deflation basin, where sand erosion dominates vegetation survival and 2) on the depositional lobe, where sand deposition dominates vegetation survival.

#### Erosion in the deflation basin

Initiation of a blowout often takes place at a location were surface vegetation is already scarce (Hesp, 2002). Continues erosion at the forming deflation basin will affect seedlings and developed plants by undercutting the root system resulting in desiccation and eventually removal (Maun, 1994). This negative feedback will increase the stress above the surface, causing more sand transport. When erosion is more episodically it could initiate seeds, that were buried during the accretion phase of the foredune, to germinate which could settle in the deflation basin. Depending on species, the ideal depth for seeds to germinate is 2-7 cm (Zhang & Maun, 1990). Another condition for seeds to germinate is that the blowout is of recent origin, as seeds are viable between 5-20 years, depending on the species (Maun, 1998).

#### Accretion of the depositional lobe

Considering plant survival at a location where burial is dominating Maun (1998) classified them into three types: 1) burial-intolerant, 2) burial-tolerant and 3) burial dependent (Figure 6). As the classification names insinuate plants are not per definition suffering from sand transport/accretion. Burial-intolerant plants will experience stress and a decrease in health when sand accumulates. At burial-intolerant plants, stress-levels will not change unless vital parts for photosynthesis get buried (Maun, 1998). When vegetation gets buried soil properties will change, increase of soil moisture,

depletion of oxygen, decreasing soil porosity and temperature (Maun, 1994). If plants will survive depends on the accretion rate, if this exceeds a certain threshold the individual plant will eventually die (Figure 6). This accretion rate is also important for the survival of burial dependent. Contrary to burial-intolerant species, burial dependent species will increase plant performance (e.g. bio-mass production, carbon uptake) when buried partly (Figure 6) (Cheplick & Grandstaff, 1997; Zhang & Maun, 1990). Overall, for all plant species applies when all above-ground leaves are buried the plant is not able to apply photosynthesis which results in death (Cheplick & Grandstaff, 1997; Maun, 1998).

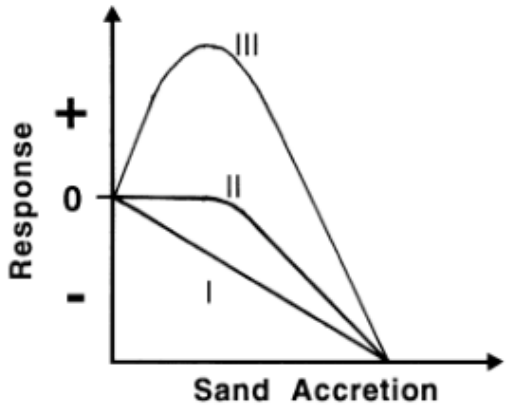


*Figure 6 - Relation between plant species activity and an increasing amount of sand accretion. Here (I) represents burial-intolerant species, (II) burial-tolerant and (III) burial depended. Source: Maun (1998).*

#### *The ecological phase*

Entering the ecological phase biotic processes start to dominate over the abiotic processes, the blowout starts to close. As the lack of vegetation is important for initiation of the blowout, the reduced wind speed and recolonization rate determine the rate of closure. Blowout closure is an interplay between three main factors: 1) Vegetation species, 2) sand availability outside the blowout and 3) climatic variability (Gares & Nordstrom, 1995; Martínez, Gallego-Fernández, & Hesp, 2013). These factors determine the re-colonization rate. Rhizomes are most likely to recolonize the deflation basin as rhizomes grow faster and are less vulnerable to erosion than seedlings (Maun, 1998). The new plants originate from adjacent locations as the rim when the erosional wall is undercut and starts mass sloping (Schwarz et al., 2018). Due to the milder wind conditions on the depositional lobe seedlings are more common to re-colonize the bare areas than rhizomes. Depending on the accretion rate and change in soil properties burial-intolerant or burial-depended plants will flourish (Maun, 1998). Moreover, a reason that erosion of the deflation basin decreases is the increased soil moisture content when the base reaches the water table (Barchyn & Hugenholtz, 2013). At first, the increased soil moisture makes the sediment more cohesive and less prone to aeolian transport. Secondly, capillary forces will drag water towards the surface allowing seeds to reactivate and germinate, also increase cohesiveness.

Furthermore, the temporal aspect is important for blowout closure. When seedlings emerge in spring, climatic conditions are favourable (e.g. no storms, enough precipitation) to develop into mature plant near autumn. When plants emerge during periods of unfavourable conditions for plant survival the rate of blowout closure will decrease and might go back in the development cycle (Maun, 1998; Pye, Blott, & Howe, 2014).

### 2.2.3 Summarizing blowout development

Schwarz et al. (2018) created a conceptual model summarizing the bio-geomorphologic blowout development as described in detail in the previous paragraphs, see Figure 7. In Figure 7a they presented the changes in stage-morphology in a cross- and along-shore orientation. In Figure 7b the

relation between abiotic and biotic feedback mechanisms are illustrated. The integer numbers 1, 2 and 3 represent the phases stated in 6a and thoroughly discussed above. The stages 1.5 and 2.5 are transitions between the main phases. Stage 1.5 illustrates positive biotic feedbacks (e.g. decrease wind speed → reactivation of vegetation → more sand accretion). Where stage 2.5 represents positive abiotic feedback mechanisms (e.g. increase wind speed → vegetation gets buried → surface erosion), which could initiate blowout reopening. This conceptual model indicates the importance of the type of sediment favouring vegetation. If no erosion-tolerant species are available, it may take longer for the blowout to reach the bio-geomorphological phase (Maun, 1994). When burial-depended species have conquered large parts of the deflation basin and depositional lobe soil stability increases resulting in a more stable blowout. This initiates positive feedback throughout the ecological phase. When morphologic stability increases the governing species will shift gradually towards burial-intolerant plants (Schwarz et al., 2018).

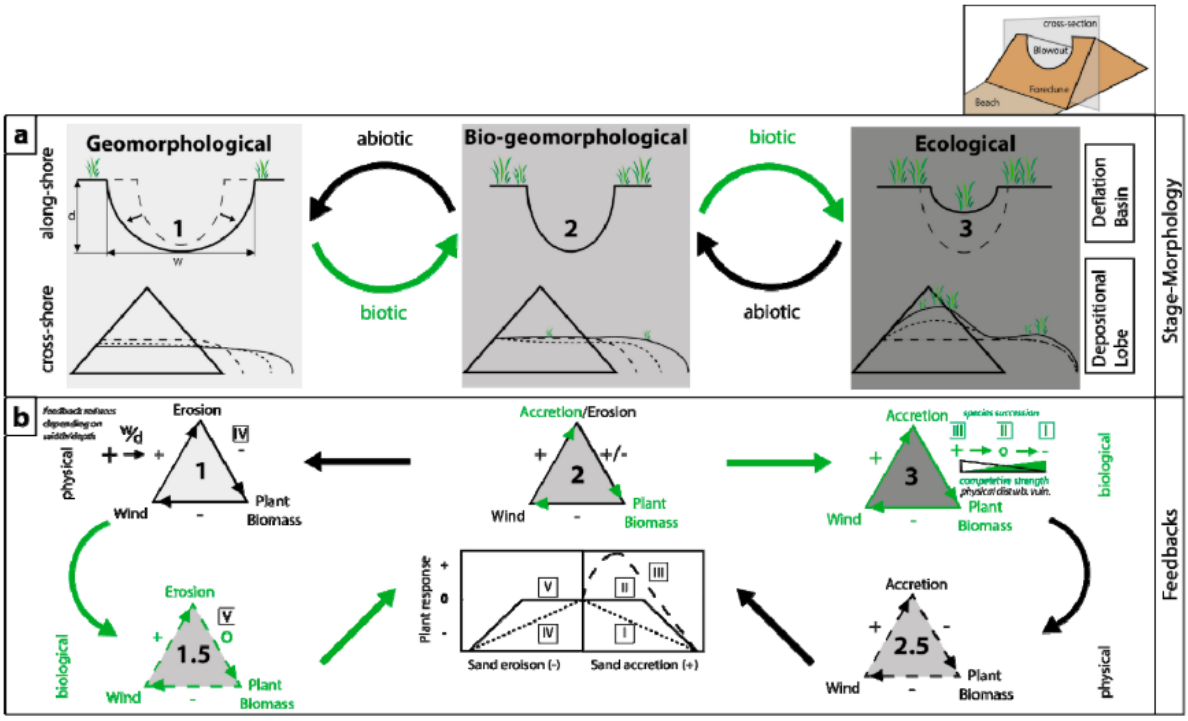


*Figure 7 - Conceptual model summarizing the bio-morphological blowout development cycle. 7a includes the stage-morphology in cross- and along-shore direction. 7b includes biotic and abiotic feedback mechanisms resulting in the evolution of the blowout. Source: Schwarz et al. (2018).*

## 2.3 Recent coastal restoration projects

During the twentieth century, coastal dune regions all around the world were subjected to anthropogenic alterations. Coastal cities grew, increasing pressure on land use of the area. The building of industries increased tourism and commuters started polluting the region resulting in degradation or loss of coastal biodiversity (e.g. Lithgow et al., 2013; Nordstrom & Arens, 1998; Provoost, Jones, & Edmondson, 2011). Furthermore, for coastal safety reasons the most popular strategy was planting of European marram grass (*Ammophila Arenaria*) resulting in a decline in aeolian activity and therefore stabilisation of the foredunes and even more decrease in biodiversity (Arens et al., 2007; Clemmensen et al., 2014; Martínez, Hesp, & Gallego-Fernández, 2013; Provoost et al., 2011; Pye et al., 2014). Particularly for The Netherlands coastal safety is a hot topic. According to the Dutch Water Act of 2009 and former legal documents concerning coastal management, the prevention or reduction of flooding is the core objective. For example, since 1990 the Basal Coast Line (BCL) was introduced to ensure that structural erosion of the Dutch coast would stop by invoking a constant nourishing policy (Mulder, Hommes, & Horstman, 2011). By continuedly supplying sand to the shore, sand availability is abundant to develop extensive foredunes. In combination with the planting of vegetation, foredunes continued to develop till a point that beach sediments could not be transported into the back dunes. This resulted in a depletion of important needs for a healthy dune ecology, resulting in a decline in ecological value (Martínez, Hesp, et al., 2013). Another danger considering coastal safety is that the back dune barrier cannot grow in elevation to keep up with sea-level rise (Arens, Mulder, et al., 2013). Since the 1980's projects have started to remobilize the back dunes and improve coastal dune biodiversity. For example, small individual blowouts were reactivated to cause increased sand transport (Van Boxel et al., 1997) or vegetation removal on parabolic dunes (Arens, Slings, & de Vries, 2004). Overall, most implemented measures were not sustainable for longer time periods without human interference. An important underlying cause for the difficulty to keep the dunes reactivated is attributed to the hysteresis relation between vegetation and wind speed for dune stabilize/de-stabilization (Figure 8) (Tsoar, 2005). To destabilize a vegetated dune, high wind energy is needed to initiate and keep the dune mobile. When vegetation is recolonizing the dune, lower energy levels are required to fixate the dune which are often more frequent in the study areas, resulting in the short time scales measures remained self-maintaining.

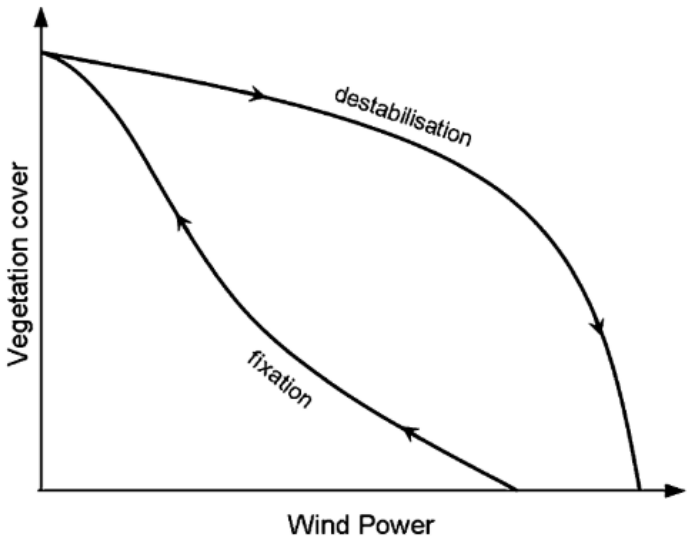


*Figure 8 - Hysteresis curve for the relation between destabilizing and stabilizing of coastal dunes. Source: Provoost et al. (2011) adapted from Tsoar (2005).*

The present international and Dutch management approach is shifted towards the foredunes by excavating notches, creating new blowouts which could act as a corridor for aeolian transported beach sands into the back dunes (Arens, Mulder, et al., 2013; Pye et al., 2014; Riksen, Goossens, Huiskes, Krol, & Slim, 2016; Ruessink et al., 2018). According to Arens, Mulder, et al., (2013) measures implemented in the foredunes are expected to be much more successful than the ones taken in the inner dune area. The stress factors needed for dynamic blowout development, wind and sand, are much larger at the foredunes than in the back dunes, resulting in a longer self-maintaining period. This durability of the blowout system is depended on dimension, quantity and sand supply.

Within The Netherlands, there are differences in success rate between these foredune notch projects. For example, at the northern coasts of Terschelling a large project started in 1995 and is still active at the time of writing (Arens, Slings, et al., 2013). Here sediment gets transported more than 300 m downwind. As this area will be the main study area of this research, it will be explained more extensively in Chapter 3. The initiated blowout complex on the neighbouring barrier island Ameland was less successful in transporting sand into the back dunes and started to close within a few years (Riksen et al., 2016). The beach sands have only transported a maximum of 60 m into the back dunes, having little effect on the dune ecology. In 2012 five large foredune excavations were realised in a 20 m high foredune complex at the Dutch National Park Zuid-Kennemerland (Ruessink et al., 2018). The notches were V-shaped and had a depth varying between 9 and 12.5 m and a width of 50-100 m. The dimensions of these notches are multiple times larger than the ones excavated on Terschelling and Ameland. The current results are promising for reactivation of the back dunes. Ruessink et al., (2018) found 1) an increase in aeolian activity: erosion, transport and deposition, 2) new aeolian landforms developed, 3) vegetated area decreased, bare sand increased, and 4) a positive sand budget landward of the foredune. 75% of the total sand budget was now found on the landward side of the blowout, where during the pre-notch period (2006-2012) this all was deposited at the stoss side of the foredune (Ruessink et al., 2018). Outside The Netherlands, large blowout initiation projects are conducted as well. For example in Wales, Pye & Blott (2016) described the development of 27 notches at 3 different location with a wide variety in dimensions. The overall result was a positive sand budget transported through the notches into the back dunes. The success rate for an active back dune system was mostly determined by the beach morphology, sand availability, wet climatic conditions favouring vegetational regrowth. Furthermore, the most successful notches were all oriented in the direction of the prevailing wind direction (Pye & Blott, 2016).

## 2.4 Research questions

Over the last couple of years, the initiation of human-induced blowouts has become an increasingly used method in coastal management to restore dune dynamics in previously stabilised foredunes. It is hoped that the projects will support sediment supply into the back dunes for decades. Nowadays there is still much unknown about the period the blowouts remain open and the time scales of the development cycle of an individual blowout. Gares & Nordstrom (1995) did cover the three development phases but these were divided over three separate blowouts, where Ruessink et al., (2018) and Pye & Blott (2016) extensively covered the first phase of the bio-geomorphological cycle. Due to the novelty of this management-strategy, only a little amount of monitored extensive blowout areas have developed past the geomorphologic phase. One of them is the blowout complex at Terschelling (1995-present) which is still dynamic. Over the last six years visual observations indicated that the blowout complex shows considerable abiotic-biotic feedback mechanisms and indications that vegetation is recovering in certain parts of the area. Only for this period it lacks quantified documentation. Therefore, the aim of the MSc Thesis is to investigate the development of a Terschelling blowout since 2013 through its bio-geomorphological cycle. The main research question and associated sub-questions are:

***How has the Terschelling blowout complex evolved since 2013 as a function of climate variability and vegetation regrowth?***

- How is the blowout complex surface area and volume changing on annual time scales using LiDAR data (2013 – 2019)?
- What is the effect of seasonal vegetation cover change on blowout development at Terschelling using NDVI- and landcover maps (2016–present)?
- Are there indications for a shift in the bio-geomorphological development phase?

# 3. Study area

## 3.1 History

Terschelling is the third Dutch barrier island going from west to east. With a surface area of 86,16 km$^2$, it counts as the second largest barrier island behind Texel (Tourist Info Terschelling). On the western and northern part of the island a sandy shoreline is present stretching over 30 km. The particular study area is located along the northern coast between 15 and 20 km (beach pole 15-20), which is nowadays a dynamic blowout complex (Figure 1). From the 1960s till 1990s *Rijkswaterstaat* monitored and maintained this foredune area by planting marram grass and installing natural fences to trap aeolian sediment. The foredunes grew and were maintained as perfectly straight lines functioning as primary flood defence, Figure 9. At the end of the 1980s, they concluded that this way of coastal preservation was not future proof. In the past 50 years, the Terschelling coasts between beach pole 15-20 lost cross-shore 400 m of the beach (Rijkswaterstaat & Staatsbosbeheer, 2015). Together with the implementation of the Basal Coast Line (BCL) management strategy, it was needed to implement a new durable coastal development strategy (Mulder et al., 2011). Therefore, since the 1990s, projects have been implemented to ensure dynamic coastal development along the entire shoreline. In 1995 a large project started to restore the foredune dynamics in the study area. The main project goal was to increase the aeolian transport into the hinterland to allow the dunes to grow with rising sea level. Furthermore, this project promotes the increase of ecological variation and formation of young dunes (Arens et al., 2007; Van der Valk, Reinders, van der Spek, & Gelder-Maas, 2013). Activities have been executed between 1995 and 2003. The measures consisted of excavating eight notches in the foredune, placing fences to direct the transported sand, planting marram grass at strategic locations and removal of vegetation on the seaward side of the foredune to stimulate aeolian transport. The eight foredune notches have been dug in a WNW-ESE orientation according to the direction of the strongest winds. Till 2003 vegetation was actively removed on the seaward side of the foredunes to stimulate the aeolian processes. After 2003 this was assumed unnecessary and the system remained self-maintaining (Arens et al., 2007; Van der Valk et al., 2013).


*Figure 9 - The study area in 1987. The foredune row was maintained as a straight and static dune row (Rijkswaterstaat, 2015).*

## 3.2 Climate

When focusing on the bio-geomorphological and ecological phase of blowout development the local climate is of importance for ecological behaviour. The growth rate of vegetation is mainly determined by the amount of precipitation and temperature. The wind climate determines the amount of aeolian transport the vegetation is subjected to. The Frisian Barrier Islands are experiencing a maritime climate with average winter temperatures of 6°C and in summer around 17°C, Figure 10. The air temperature is strongly dependent on the North Sea surface temperature. The average annual precipitation is 60 mm per month, however, the annual precipitation regime shows seasonal variation. In autumn, September – November the precipitation average exceeds 100 mm a month (KNMI, 2019), Figure 10. The prevailing wind direction is from the south-west with an average wind speed of 7.6 m/s (Figure 11). In autumn and winter storms are more frequent when the wind blows over the North Sea from the north-west. These storms are expected to result in the largest abiotic morphological changes in the area.

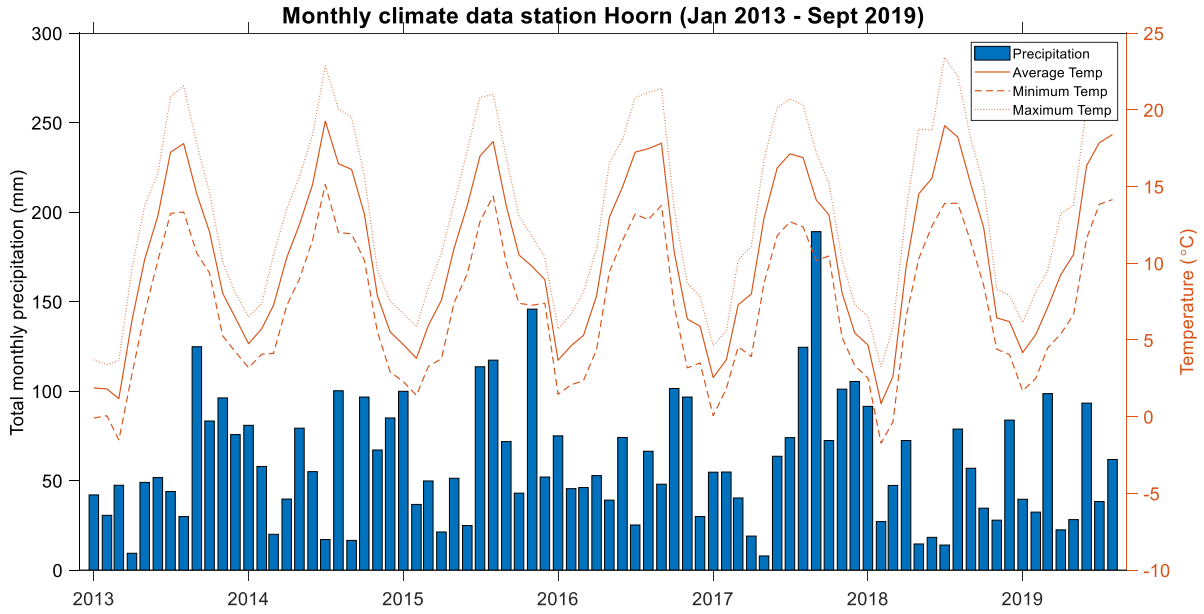


*Figure 11 - Monthly precipitation and temperature data from KNMI weather station Hoorn, Terschelling (01-01-2013 – 01-09-2019).*

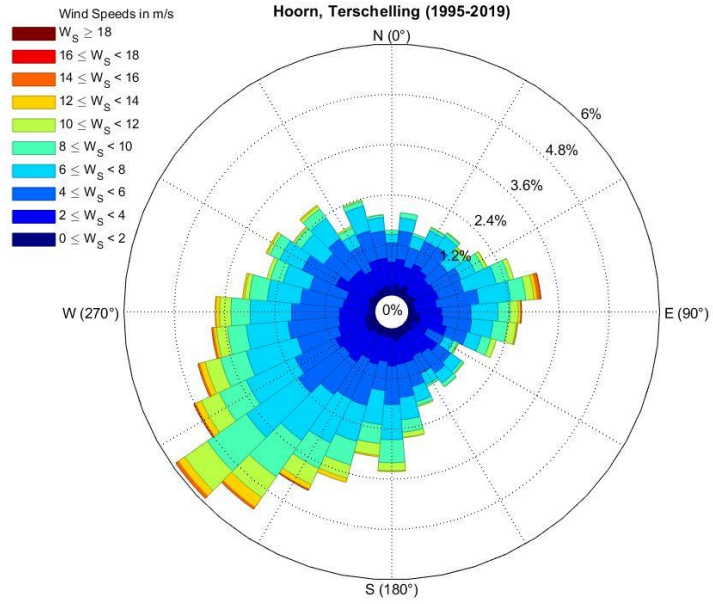


*Figure 10 - Wind rose for the period 1995-2019 from the meteorological station at Hoorn, Terschelling (KNMI, 2019). Inspired by Matlab-code of Daniel Pereira (2015): https://nl.mathworks.com/matlabcentral/fileexchange/47248-wind-rose?s_tid=FX_rc1_behav*

## 3.3 Morphological development

Rapidly after the foredune notches were completed the sand transport into the hinterland started to increase and, for Dutch proportions, a large dynamic dune landscape developed. The intensity of the sand spray was beyond expectations satisfying the involved organizations. The notches were eroded to an extent of half their original depth and the hinterland was raised several centimetres (Arens et al., 2007). Over a period of 14 years (1997-2010), the average deposition over the area amounted to 0.3 m. Furthermore, at several locations, the sand was transported further than 300 m away from the dunefoot, where before the remobilization the maximum extent reached no more than 80 m (Arens, Mulder, et al., 2013). Locally the foredune row migrated over 200 m landward in the period 1995-2004. After this period the foredune row continued to migrate landward but on a slightly lower rate due to the return of vegetation. After 2003, vegetation seaward of the foredunes was not removed anymore resulting in the creation of a new incipient foredune row in front of the original. As the incipient foredunes are catching-in sediment the original foredunes become more eroded due to the decline of incoming sands. The erosion of the foredune row resulted in large sand deposition just landward, locally up to 5m (Figure 12). Nowadays a lower elevated but wider foredune area has developed with an established second dune row. After implementation, the dune volume increased with several cubic tons of sand per year and is expected to continue growing (Rijkswaterstaat, Staatsbosbeheer, & Vitens, 2014).

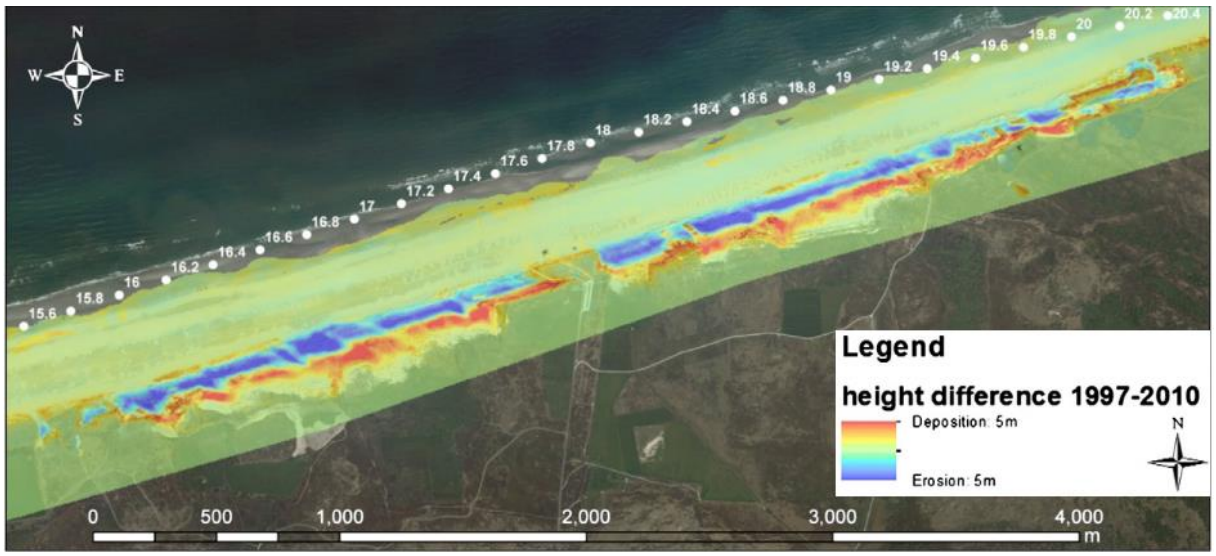


*Figure 12 - Total erosion and deposition for the period 1997-2010 after remobilization. Extracted from Lidar data by Arens, Mulder, et al. (2013).*

## 3.4 Ecological development

This blowout complex is one of the largest in Western Europe. As these natural areas are scarce, it gives exquisite opportunities for new floral and faunal development. The complex consists of wet and dry valleys and alternating vegetated and barren dunes. For years the back dunes were poor in calcite rich sands (RWS & SBB, 2015). Due to the sand spray, new calcite rich sand is deposited further into the dunes. Furthermore, within the dune valley, a freshwater bubble developed of which the seepage promotes the appearance of new and rare fauna (Löffler et al., 2016). Overall, this has a positive effect on a variety of species. Especially mosses benefit from fresh sand deposition and started to expand. On the lee side of the foredune, the large deposition rate resulted in eutrophication and proliferation of thistles which was undesired (Arens et al., 2007).

# 4. Methodology

## 4.1 Data sets

The research will be conducted by analysing the change in abiotic (sand) and biotic (vegetation) surface areas in the Terschelling blowout complex. The available dataset consists of high-resolution (3x3m) of PlanetScope satellite imagery (RGB-NIR) and annual airborne LiDAR data. PlanetScope provides almost daily imagery, but the usability of the imagery obviously depends on atmospheric disturbances (e.g. clouds, haze), solar angle and flight path. The multispectral PlanetScope data makes it possible to separate sand from vegetation due to overall high reflectance values in the NIR-band. The annual LiDAR data is available since 1997 but will be used here for the years 2013-2019. The available 3D point clouds will be averaged into Digital Elevation Models (DEM) with a grid of 3x3 m to calculate the change in sand volume for the set time period.

From autumn 2016 the PlanetScope scenes will be used to look for changes in the visual and the multispectral spectrum within a year. The PlanetScope images will be used to create Normalized Difference Vegetation Index (NDVI) maps to detect the division between sand and vegetation. This is made possible by the difference in reflectance spectrum sand and vegetation have (Figure 13). As vegetation shows higher NDVI values (eq. in Fig. 13). To detect the effect of seasonal vegetation growth NDVI sets of the four seasons will be investigated and compared. For validation purposes, a small field campaign with a portable spectrometer was organized to compare real-life multispectral vegetation data with the PlanetScope data.

Besides the available imagery, meteorological data of the Royal Dutch Meteorological Institute (KNMI) will be used for coupling with perceived bio-geomorphological change. This dataset includes wind direction, speeds (m/s), precipitation (mm/day), temperature (°C) and solar radiation (W/m$^2$) data for the period 1995-2019 from the meteorological station at Hoorn, Terschelling.

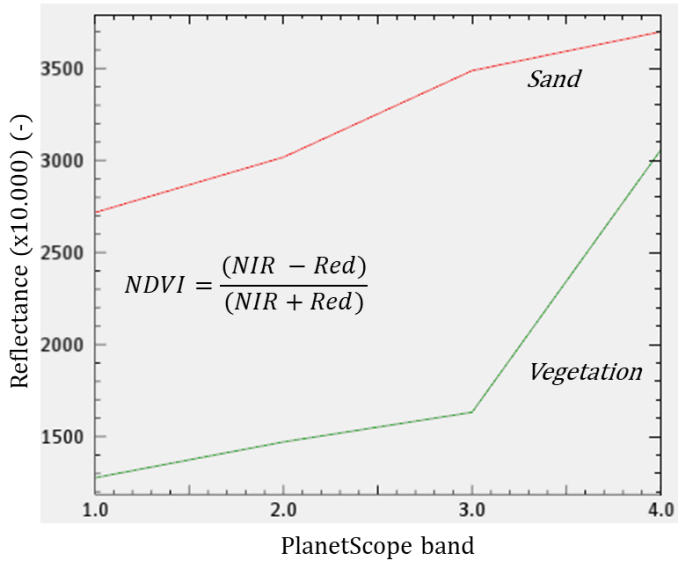


*Figure 13 - Spectral profiles for sand and vegetation derived with ENVI. The PlanetScope band represent 1: Blue, 2: Green, 3: Red and 4: NIR.*

### 4.1.1 Planet: 3- & 4-Band PlanetScope Scene Product

Planet is a commercial company which provides a web-based platform where satellite data is presented for imagery processing and analyzation. The used PlanetScope scenes are acquired by so-called CubeSats 3U ("Doves") satellites with a dimension of 0.1x0.1x0.3 m (Planet Labs Inc., 2019). Currently, more than 130 CubeSats are deployed which result in a nearly daily worldwide coverage

(max latitude = 81.5°). The satellites are launched in groups into a sun-synchronous orbit at an altitude of 475 km. Because of this orbit altitude, the satellites cross a certain location every day at roughly the same time of the day. For our study area, this is around 10:15 UTC. The used scenes are acquired by different CubeSats.

In this study Level 3B PlanetScope Ortho Scene Product (Surface Reflectance) data is used (Planet Labs Inc., 2019). This data is orthorectified with help of ground control points (GCPs) resulting in an RMSE < 10m and scaled to surface reflectance. Furthermore, the data is atmospherically corrected by the 6SV2.1 radiative transfer code with near-daily data retrieved from the MODIS satellite (Planet Labs Inc., 2019). They offer visual (PSScene3Band) and analytic (PSScene4Band) scene products. Every PSScene4Band item has a corresponding PSScene3Band item which does not contain the near-infrared (NIR) band but is optimized for visual inspection purposes. In Table 1 the four spectral bandwidths are presented.

*Table 1- CubeSats 3U band widths*

| **Spectral Band** | **Spectral Width** |
|---|---|
| 1 (Blue) | 455 – 515 nm |
| 2 (Green) | 500 – 590 nm |
| 3 (Red) | 591 – 670 nm |
| 4 (NIR) | 780 – 860 nm |

The scenes have an approximate dimension of 24 by 8 km with a pixel size of 3 meters. The default projection is in UTM WGS84. The reflectance values [0 – 1] are scaled by 10.000 to reduce quantization errors.

The first usable PSScene4Band data for the study area was available from 21 September 2016 where the last scene was taken as 24 August, 2019. As more CubeSat groups were launched with time, the data density increased through the years. Therefore, the time interval between scenes decreases towards the end of the study period.

The PlanetScope image processing chain is included as Appendix 1 go give an overview of how the raw data is converted into the visual and analytic ortho scene products.

### 4.1.2 LiDAR

LiDAR (Light Detection And Ranging) is a remote sensing method using laser illumination to measure the distance from its source (airborne vehicle) to an object (here; dune surface). The results of a survey are presented as LiDAR 3D point clouds, which will be the main source to analyse the abiotic morphological change in the study area. The annual airborne LiDAR elevation data is collected by *Rijkswaterstaat* and stored as *.LAZ-files* accessible via the UU servers. The data is available from 1995 till 2019 of which the data from 2013 and onwards will be used. Before the data gets published it underwent an extensive quality check to detect a possible measuring error. The quality control concerns errors in point density, absolute and relative altimetry and filtering. For the extensive quality control, the reader is referred to the *Kwaliteitsdocument laseralimetrie 201X* by *Rijkswaterstaat.* The default coordinate system is RD_New, which is the same coordinate system as the PlanetScope scenes will be converted to. Before retrieving valuable elevation and volume data it is necessary to process the data in multiple steps using LASTools (Rapidlasso GmbH, 2019) and MATLAB *ver. R2018b*. This will be explained in more detail in the image processing section. The data is retrieved halfway March each year.

### 4.1.3 Field spectrometer data

In addition to the spectral data of the PlanetScope scenes more specific data was gathered during a one-day field campaign to the blowout complex in the *Zuid-Kennemerland National Park*. That the field campaign was conducted here instead of Terschelling has to do with logistic reasons and the fact that it was not expected to find distinctive different results. Furthermore, this location was visited as it is the study area of L.M. Schemmekes.

The spectral data was gathered by a Spectral Evolution DARWin SP spectrometer operated by a handheld device with the DARWin *v*1.2 data acquisition software. The software presents a user-friendly interface which allows measurements to complete within two clicks. Due to constantly changing atmospheric conditions it is necessary to conduct a reference measurement in advance of measuring the target object. For the reference measurement, a white tile is used which reflects the complete solar electromagnetic spectrum. The target measurement indicates the percentage of light that reflects per wavelength relative to the reference results. All measurements were executed with an 8° lens mounted at the end of the optical fibre.

The measurement location was recorded using an RTK-GPS with a horizontal and vertical accuracy of a few centimetres.

### 4.1.4 KNMI meteorological data

The Royal Dutch Meteorological Institute provides free downloadable datasets consisting of daily meteorological data from 50 measuring stations. For this study, the data originates from the station in Hoorn (station 251), just 2 km south of the study area. The meteorological data will be correlated with encountered morphological change quantified from the PlanetScope and LiDAR image analysis. The downloaded dataset consists of the measurements presented in Table 2 and spreads over 6 years, from 1$^{st}$ of January 2013 till the 1$^{st}$ of September 2019, a total of 2423 days. To create the wind rose in Figure 11 vector mean wind direction data from 01-09-1995 till 01-09-2019 was used, as this represents the start of the project. To read the ASCII-files a MATLAB script was created and the default units were converted to conventional units, Table 2. Furthermore, to be able to clearly interpret the meteorological data it is chosen to average the daily temperature data to monthly averaged and the daily precipitation data are summed to create the total monthly precipitation sum. The wind data will remain on a daily basis because daily storm events could have a significant effect on the blowout morphology.

*Table 2 - KNMI meteorological data from the station in Hoorn (Terschelling).*

| KNMI code | Measurement | KNMI Unit | Converted Unit |
|---|---|---|---|
| DDVEC | Vector mean wind direction | Degree | Degree |
| FHVEC | Vector mean wind speed | 0.1 m/s | m/s |
| FHX | Highest hourly mean wind speed | 0.1 m/s | m/s |
| TG | Mean daily temperature | ˚C | ˚C |
| TN | Minimum temperature | ˚C | ˚C |
| TX | Maximum temperature | ˚C | ˚C |
| Q | Solar radiation on surface | J/cm$^2$ | W/m$^2$ |
| RH | Sum of daily precipitation | 0.1 mm | mm |

## 4.2 Image processing

Before the desired PSScene4Band data for the study area and period is ready to be classified and analysed it is necessary to run through a specific workflow. To get access to the PlanetScope database it is required to have a Planet account with sufficient amount of downloadable data. For this study, an

Education and Research Program Basic account was used, with a download space of 10.000 km$^2$/month. To download data from the Planet database an API-key should be acquired. To retrieve the API-key a Python-programmed workflow was developed, ran in Anaconda3 Prompt. The workflow is added as Appendix 2 and will be explained in more detail in the section below.

### 4.2.1 Acquire data using Planet environment

To acquire the necessary Planet API-key a virtual Python environment (Python 3.6) called "planet" was created in which multiple programs were later installed. The two key programs that had to be installed were: *Planet*, to communicate with the Planet database and *Porder* (version 0.4.3) which is the client that makes it possible to interact with the ordersv2 API and allows you to order and download the desired data (Samapriya Roy, 2019). Before getting started multiple other packages outside the default Python 3.6 libraries were installed to allow the program to work: *GDAL* (v. 2.4.1), *numpy* (v. 1.15.4), *pyproj* (v. 2.2.2), *shapely* (v. 1.6.4.post2), *fiona* (v. 1.8.6) and *geopandas* (v. 0.5.1). For further information on the installation process consult: https://pypi.org/project/porder/#porder-version.

A single PSScene4Band image has a dimension of 24 by 8 km where the study area measures 4.5 by 1.8 km (626x1521 pixels). With the constraint of a maximum of 10.000 km$^2$/month of downloadable data, it was chosen to select an area of interest using a *.geojson*-file (created at http://geojson.io) before ordering the data using *Porder*. Besides the selected area of interest more conditions concerning, date range, cloud cover and area overlap percentage (Table 3) were included in the order statement. Its product is a *.csv* file which contains all PSScene(3/4)Band data which meet the stated conditions. Before downloading, the list needs to be sorted out by checking the data manually in the Planet web-interface to delete possible unusable scenes. The download output contains of three files per scene: 4-band *.tiff*-file, DN-file and *.xml*-metadata. The downloaded data has a default projecting in UTM WGS84 where for this study the *Rijksdriekhoekscoördinatenstelsel* (RD) projection is used. To convert the data into RD-coordinates the batch file *reproject.bat* (provided by B.G. Ruessink) was applied. The next step is to restore the image clip created by the *.geojson* file for the re-projected scenes using the batch file *clipNotches.bat* (provided by B.G. Ruessink).

If area coverage is less than 100% and more than one scene per day is available it is possible to combine the two scenes into a merge-image. An already existing script (*3stu_planet_merge.py*) provided by C. S. Schwarz was adjusted and applied. It requires a different Python environment "planetlabs" in version 2.7 to run. This merging tool was applied to 21 scenes which summed up to 31% of the total data set.

*Table 3 - Porder download settings*

| | |
|---|---|
| **Date range** | 01-09-2016 – 31-08-2019 |
| **Cloud cover** | 0 – 40 % |
| **Area overlap** | 50 % |
| **Item** | PSScene3Band or PSScene4Band |
| **Asset** | Visual or Analytic_sr |

### 4.2.2 Image registration

Due to the facts that the multiple CubeSats cross the study area at slightly different orbits and the changing RMSE position, not all scenes are perfectly aligned with each other. This influences pixel-by-pixel analyses and causes false results comparing the scenes through time and space. Therefore, images that visually deviated from the average position were registered using the Control Point Selection Tool (*cpselect*) in MATLAB version 2018b (MathWorks, 2019). The *cpselect tool* displays an interface with a fixed (reference scene) and moving (displaced scene) image (Figure 14). Locations that

do not change through time (e.g. road junctions, buildings) should be selected and will be overlain. Applying the *inwarp* function to the displaced scene, it gets geospatial transformed into the coordinate system of a geospatial reference scene. https://nl.mathworks.com/help/images/ref/cpselect.html

*Cpselect* tool only supports grayscale or 3-band RGB images to warp, where the data set consists out of 4-band RGB-NIR. To apply the tool all single bands were extracted and transformed from original matrix values into a grayscale image to support the *cpselect* interface for selecting control points and calculating the transformation matrix. Assuming that all 4 bands were correctly aligned relative to each other the same transformation matrix was applied and the bands were combined to restore the 4-band scene.

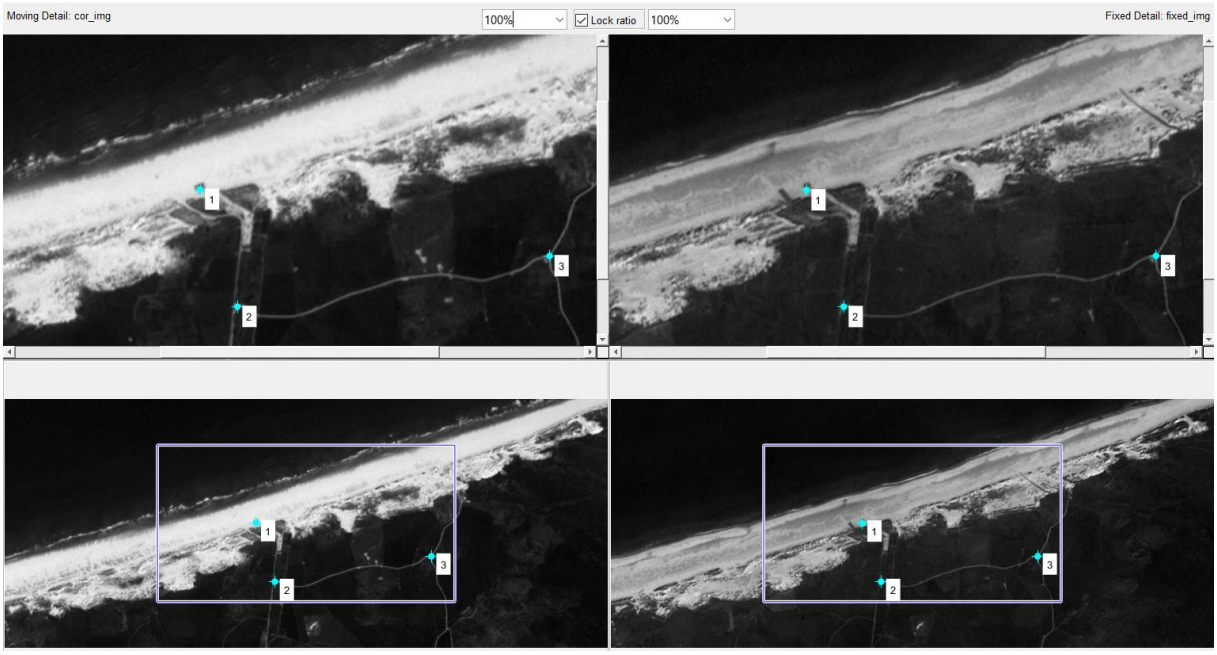


*Figure 14 - CPSelect tool MATLAB interface. The left panels represent the displaced image that needs to be geospatially transformed relative to the reference image in the right panels.*

### 4.2.3 Masking area of interest

The scenes have a rectangular shape containing areas that are of no interest and could make classification more complicated, resp. sea and densely vegetated hinterland. A smaller research area is expected to result in less noise and uncertainties. Therefore, it was chosen to apply a mask over these areas and convert the reflectance values to NaN. The mask covers a surface area of 6.04 $km^2$ reducing the area of interest to 2.53 $km^2$. The mask was created using the *drawpolygon* function in MATLAB *ver.* 2018b. Afterwards, the mask was saved and multiplied by the 4-band scenes resulting in a diagonal area of interest which will be used in further image classification, Figure 15a.

The same method was used to mask out certain areas in order to conduct area-specific volume calculations. The mask function was applied to divide the area into three districts: beach, dunes and hinterland (Figure 15b). Furthermore, to investigate the abiotic morphological change around the blowouts, a mask based on the 2013 DEM was created. This mask covered the eight most distinct notches present at that time (Figure 15c).

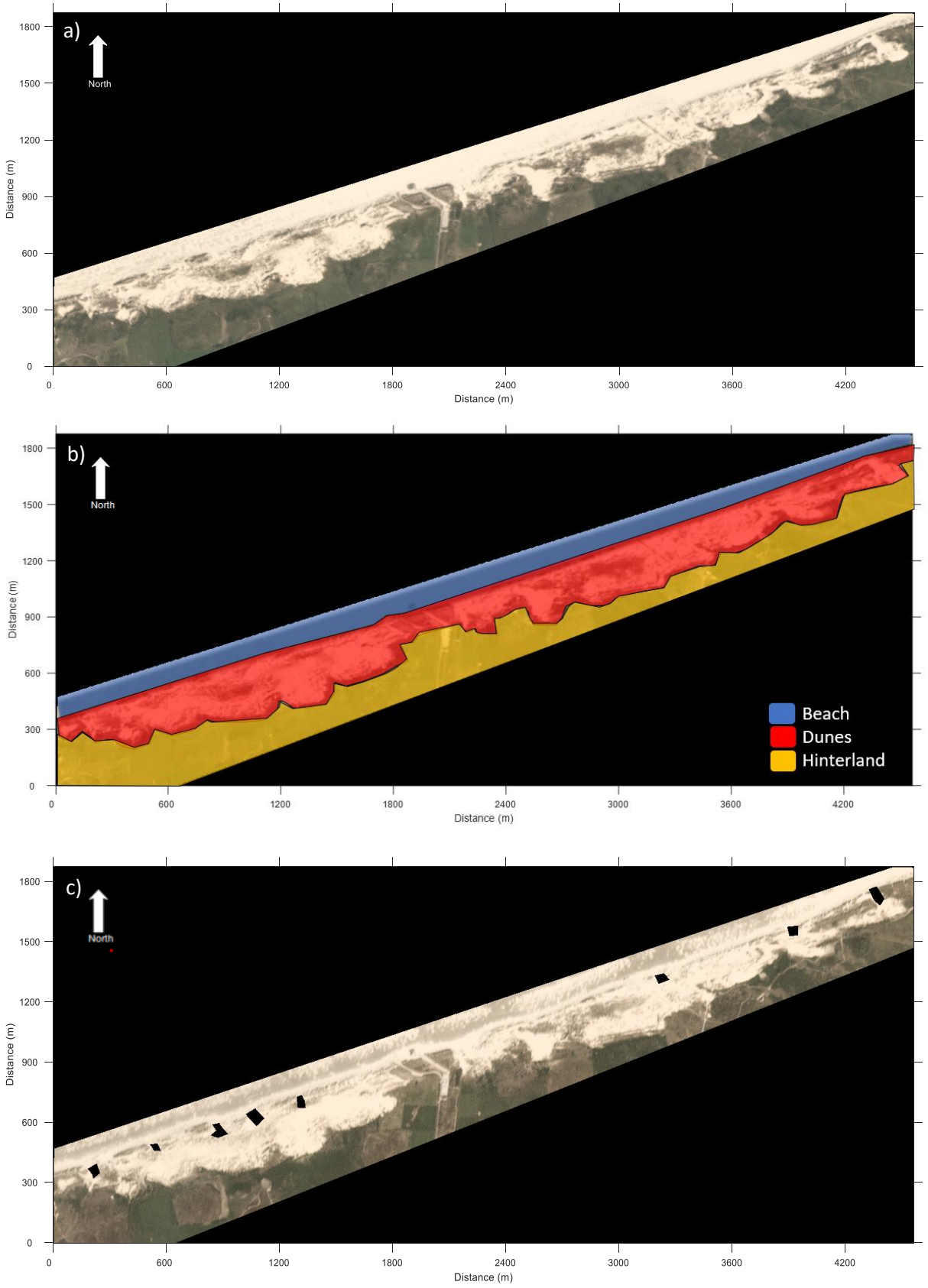


*Figure 15 – a) A PSScene3Band image after applying the mask shows the area of interest that will be used for this study. b) Size and location of the masks subdividing the three districts: beach, dunes and hinterland. c) Size and location of the masks covering the eight foredune notches.*

## 4.3 Data analysis

### 4.3.1 LiDAR

*LASTools*

For processing the LiDAR data the program LASTools created by Martin Isenburg (Rapidlasso GmbH, 2019) was used, a program specially designed to process *.LAZ* files. This is necessary as the LiDAR data is supplied in predetermined area tiles which do not match the exact study area (Kwaliteitsdocument Laseraltimetrie Rijkswaterstaat, 2013). The study area is separated over two tiles: 1DZ1 and 1DZ2. To retrieve the area of interest from the two tiles the application *las2las* was used. *Las2las* provides tools to merge and clip the 3D point cloud accordingly that it overlaps the study area. The 3D point cloud was clipped accordingly to the corner coordinates retrieved from the clipped PlanetScope scenes in ENVI.

The annual datasets had different flight lines and point cloud density increased with consecutive years. For comparison between the LiDAR data, it was important to display the data in one common grid. The grid should have 3x3 m resolution as this matches the resolution of the PlanetScope scenes. The application *lasgrid* was used to grid the merged and clipped *.las* files. The important input values were pixel/step size: 3m and op: average. With these input arguments *lasgrid* rastered the average elevations from all points that fall into cells of size 3x3 m and stored the resulting grid in a *.asc* raster file with the dimension 626 by 1521 pixels.

The last step in pre-processing the LiDAR data was to create a DEM. This was done using the application *las2dem*, reading the raster LiDAR points, triangulated them temporarily into a TIN (Triangulated Irregular Networks), and then rastered the TIN onto a DEM (Rapidlasso GmbH, 2019). Also with this application, it was important to set the step size to the step size of the grid (3 m). Furthermore, as for some years, the LiDAR raster data consists of NaN values. To compare the annual DEM's it is desired to have full coverage over the study area. Therefore, the *kill triangles* option was set at 200 m, these raster triangles with edges below 200 m, where the default was set to 100 m. The DEM was saved as a *.asc* file.

*MATLAB*

To retrieve data for further investigation on absolute and changing volumes and elevation a MATLAB script was created (LIDAR_DEM.m). To read the *.asc* DEM files the function *readASC2XYZ*, created by B.G. Ruessink, was implemented into the code. This function converted the *.asc* file into three separate X, Y and Z matrices with the same 626 by 1521 dimension. The next step was to apply the same mask as used for the PlanetScope scenes to the three matrices. Due to the inconsistency of the annual LiDAR measurement area, there are differences in the covered area. In 2016 the covered measure area contained the least measurement points. To make sure the measured areas are the same for each year all Z matrices were multiplied by a binary contour matrix of Z2016. As all Z matrices had the same surface dimensions change maps could be created to compare change throughout the years.

From the processed LiDAR data multiple data products were created. Besides the annual DEM maps annual and total change maps were generated. The annual elevation change maps were calculated by subtracting the current year by the previous year (e.g. DEM2014 – DEM2013). Furthermore, the total change maps display the elevation change compared to DEM2013. This was executed to give insights in and detect large morphological changes in the area. Moreover, to interpret the abiotic sand transport it is preferable to investigate changing sand volumes. By multiplying the elevation data by the pixel area (9 $m^2$) annual total and relative volume change was calculated. This was calculated for the total area as well for the subdivided districts as presented in Figure 15b. Furthermore, in order to

compare the relative volume change per area, the volume changes were normalized for their surface area. This normalisation was also applied to the volume changes at the selected notches.

Along- and cross-shore transects were drawn to investigate the development of the foredune notches and blowout system. The blowout transects are NW-SE oriented in the direction of the prevailing onshore wind. Besides the blowout area, the transect includes the beach and vegetated hinterland. The location of the along- and cross-shore transects are presented in Figure 17.

### 4.3.2 Image classification

After sorting out, downloading and masking the PlanetScope imagery, continued for some images by merging, and registration, the data set was accessible to start the image classification. Image classification was executed using a MATLAB environment with a pixel-by-pixel based method. The classification script was developed during this study in close corporation with L. M. Schemmekes and is operable at every location covered by PlanetScope satellites. The classification method is based on classifying the pixels to a maximum of 5 classes based on the difference in the reflectance spectrum, Table 4. To create the classification method ENVI software and field multispectrometer data were used to check and compare the scenes' reflectance spectra to find specific features which define landcover classes.

*Table 4 - Classification options*

| **Class** | **Landcover type** |
|---|---|
| NaN | Non classified/mixed pixels |
| 1 | Vegetation |
| 2 | Sand |
| 3 | Shadow -> No-Change |
| 4 | Masked area |

The central question of this study revolves around the changing division between sand and vegetation in the study area. The most important distinction in the spectral profiles are the differences in B3 (red) reflectance value and the sum of B4 – B3. The latter one is important when making a distinction using NDVI values. NDVI values become larger when the sum of (B4-B3)/(B4+B3) increase indicating a healthy vegetated landcover. Furthermore, pixel intensity could change per scene which could affect the separability in pixel values. An advantage using NDVI instead of absolute reflectance values is that NDVI compensates for illumination differences as it is a fraction of two bands within a scene.

To make a division over multiple seasons it is recommended to use a flexible threshold value instead of a fixed NDVI value because the NDVI is seasonally varying. For this case the study made use of the Otsu threshold applied to the individual scenes' NDVI values. This method is based on an unsupervised method, to create a scene-specific threshold between the two main classes (here, sand/vegetation) (Otsu, 1979).

As mentioned above the Otsu NDVI threshold is the most important data source to classify the individual pixels. Nevertheless, this threshold is not trivial all year round, due to changing occurrence of sorts of vegetation throughout the seasons. Therefore, classification conditions were designed and composed out of the 4 spectral bands, to conform to the landcover classes spectral profile. Furthermore, the classification conditions were based on mean band values individual values significantly differ throughout the year due to illumination changes and atmospheric conditions. The classification code will be explained per landcover class. During the classification, an empty matrix ("*clas*") will be filled with values according to the landcover code.

*Classification Vegetation (1):*

```
if NDVI_mask(a,j,k) >= T015(k) && NIR_mask(a,j,k) > n(:,k)
        clas(a,j,k) = 1;
    end
if  Green_mask(a,j,k) < g(:,k) && Red_mask(a,j,k) < r(:,k) &&
NDVI_mask(a,j,k) < T015(k)
        clas(a,j,k) = 1;
    end
```

In this classification, a combination with an absolute NDVI value (0.15) and the flexible Otsu threshold was applied. If the Otsu threshold value appeared lower dan 0.15 that value is used instead of the NDVI value of 0.15. This is the case for scenes taken in the winter season, where it seems that NDVI values sometimes appear below 0.15 and would therefore not be classified as vegetation. Overall, it is assumed that the vegetation patches meet the condition that the pixel NDVI value exceeds an NDVI value of at least 0.15, derived from trial and error and literature (e.g. EOS, 2019; Weier & Herring, 2000). Furthermore, the classification on NDVI has an important advantage, it corrects for illumination differences because it is a ratio between the NIR and Red band. In combination with the second criterion, the NIR reflectance value should exceed the mean NIR reflectance value of the scene. This criterion is used to exclude wet sand, which sometimes appears to have an NDVI value exceeding 0.15 or the Otsu threshold.

*Classification Sand (2):*

```
if NDVI_mask(a,j,k) < 0.05
      clas(a,j,k) = 2;
    end

if Red_mask(a,j,k) >= (r(:,k)) && NDVI_mask(a,j,k) < T015(k)/2
        clas(a,j,k) = 2;
    end
```

For the classification of sand, a classification based on NDVI was used again. Compared to the vegetation classification no flexible threshold was used in the first classification, instead, a fixed value of 0.05 is applied (EOS, 2019; Weier & Herring, 2000). The second criteria is a combination of the third band and again NDVI value, based on an alteration of the Otsu threshold used at the vegetation classification. As displayed in Figure 13, a significant difference between the vegetational and sand class are the values in the third band (Red). Therefore, to classify pixels as sand it should meet the condition that the band 3-pixel value exceeds the mean image band 3 value and the NDVI pixel value should be lower than 0.10 to exclude mixed pixels including vegetation.

*Classification No Change/Shadow (3):*

```
if  Green_mask(a,j,k) < g(:,k) && Red_mask(a,j,k) < r(:,k) &&
NIR_mask(a,j,k) < n(:,k) && NDVI_mask(a,j,k) < T015(k)
        clas(a,j,k) = 3;
    end
```

At winter scenes another problem occurs due to the low sun inclination angle, shadows appear on the scene. At the moment the scene is shot, the sun is located in the SSE relative to the study area. This created a shadow on the NNW side of the foredune row, projected on the beach. As is recognized from visual images the landcover class which is projected as shadow is often sand (2). The spectral profile of the shadow area is characterized by low reflection values in all four bands, especially in the NIR band. So it does not match the sand (2) classification condition due to the low red (band 3) values.

Eventually, the shadow class should be classified as the landcover class it is. To achieve this the following condition was used:

```
for a = 1:Size(:,1)
    for j = 1:Size(:,2)
         if clas(a,j,1) == 3
              clas(a,j,1) = clas(a,j,7);        % image 7 had lowest amount
of pixel value = 3
         end
    end
end
for l = 2:Size(:,3)
    for a = 1:Size(:,1)
        for j = 1:Size(:,2)
            if clas(a,j,l) == 3
                 clas(a,j,l) = clas(a,j,l-1);
            end
        end
    end
end
```

In the first image of September 21st 2016, 1.185 x$10^3$ pixels were classified as no change/shadow. This is 0.42% of the total amount of pixels, 2.810 x$10^5$. It states that if a pixel was classified as shadow it would be changed in the pixels value it was in the previous scene. In scenes of spring 2017, no shadow is present in the study area, so after these dates no pixel was classified as shadow anymore. Only for the first scene, this method did not apply, the pixels of the first image were compared to the ones of the seventh image as this images contained the least pixels classified as no change/shadow. Furthermore, by visual inspection it seemed that the no-change/shadow areas in the first scene agree with the classified pixels in the seventh pixel.

*Non classified/mixed pixels (NaN):*

Not all landcover pixels meet the exact criteria to be classified to one landcover type. These pixels remained therefore NaN values. To still assign the pixels to the vegetation or sand class it was necessary to create a second classification method. This method was based on the mean endmembers of the classified vegetation and sand pixels. For every scene, all pixels classified as a certain landcover class, the mean pixel value for every band was calculated. This resulted in a mean spectral profile for vegetation and sand per scene. Then, an average of the two spectral profiles was calculated (emBound) to function as a boundary layer for the following classification, Figure 16.

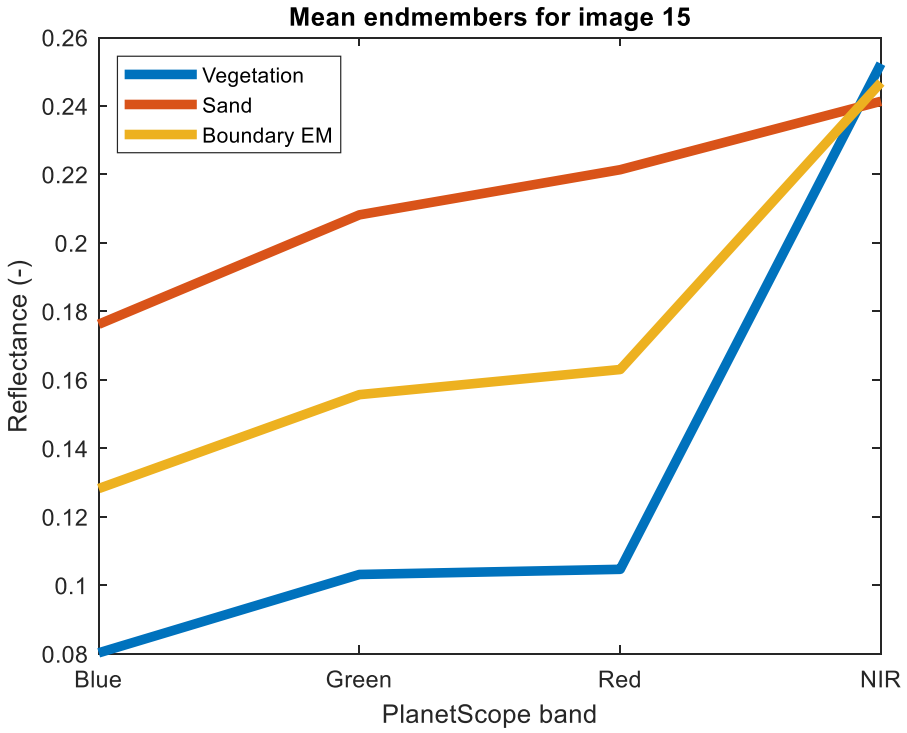


*Figure 16 - Example spectral profile of mean endmembers for vegetation and sand.*

```
if isnan(clas(a,j,k)) && Blue_mask(a,j,k) < emBound(1,k) &&
Green_mask(a,j,k) < emBound(2,k) && Red_mask(a,j,k) < emBound(3,k) &&
NDVI_mask(a,j,k) >= NDVIemB(k)
    clas(a,j,k) = 1;
end
if isnan(clas(a,j,k)) && Blue_mask(a,j,k) > emBound(1,k) &&
Green_mask(a,j,k) > emBound(2,k) && Red_mask(a,j,k) > emBound(3,k)
    clas(a,j,k) = 2;
end
```

The applied classification assumed the average endmember (emBound) as a threshold. If pixel values for the first (Blue), second (Green) and third (Red) band are below the ones stated in emBound they will be classified as vegetation. If the pixel values for the resp. bands were above emBound they were classified as sand. The fourth criterion is the NDVI value. It is assumed that the NDVI value for vegetation is higher than for sand, therefore the emBound NDVI was calculated for each scene. If the NDVI of the pixel is higher than the emBound NDVI it was assigned to vegetation and vice versa. The forth (NIR) band was not included in this classification as the pixel value for that band shows no distinct difference between the vegetation and sand classification.

Even after applying this classification not all pixels were assigned to a certain class. The first classified image of September 21$^{st}$ 2016 consist of 2.534 x10$^{3}$ unclassified pixels, which was 0.9% of the total amount of pixels inside the study area (= 2.810 x10$^{5}$). Even though this percentage is minim, the same method in assigning the correct landcover class as for the no change/shadow class was applied to reduce the NaN values to zero:

```
for a = 1:Size(:,1)
    for j = 1:Size(:,2)
        for l=2:Size(:,3)
           if isnan(clas(a,j,l))
              clas(a,j,l) = clas(a,j,l-1);
           end
           % For the first image
           if isnan(clas(a,j,1))
              clas(a,j,1) = clas(a,j,2);
           end
        end
    end
end
```

When the classifications were completed all individual classified pixels were counted and calculated to present the annual change in landcover class. The number of pixels were multiplied by the pixel size (9 $m^2$) to represent the surface area in $m^2$. The *clas* matrix is filled with numbers between NaN and 4 and plotted in a landcover map.

### 4.3.3 Landcover change map

With all pixels classified it was possible to create fully covered landcover maps. To investigate the change in landcover over the study period it is important to be able to compare the classified images with each other. To show the most reliable change, three landcover classifications around the same time of year were compared. This has been done for scenes in autumn, winter, spring and summer, Table 5. Furthermore, the classification applied a pixel by pixel-based method to compare the first and second scenes and the second and third scenes with each other. Seven classes were assigned depending on the type of (no)-change, Table 6. The code is pasted below the tables.

*Table 5 - Dates of landcover change maps.*

| Season | Date |
|---|---|
| Autumn | 22 Oct 2016<br>15 Oct 2017<br>14 Oct 2018 |
| Winter | 19 Jan 2017<br>21 Jan 2018<br>03 Feb 2019 |
| Spring | 25 Apr 2017<br>22 Apr 2018<br>19 Apr 2019 |
| Summer | 17 Jul 2017<br>15 Jul 2018<br>24 Jul 2019 |

*Table 6 - Landcover change map classification.*

| Type of change | Classification |
|---|---|
| No Change Vegetation | 1 |
| No Change Sand | 2 |
| Change sand -> plant 17/18 | 3 |
| Change plant -> sand 17/18 | 4 |
| Change sand -> plant 18/19 | 5 |
| Change plant -> sand 18/19 | 6 |
| Masked part | 7 |

```
for a = 1:Size(:,1)
      for j = 1:Size(:,2)
           if clas(a,j,cnr1) == 1 && clas(a,j,cnr2) == 1 && clas(a,j,cnr3)
== 1
              change(a,j) = 1;                        % No Change Vegetation
           elseif clas(a,j,cnr1) == 2 && clas(a,j,cnr2) == 2 &&
clas(a,j,cnr3) == 2
              change(a,j) = 2;                        % No Change Sand
           elseif clas(a,j,cnr1) == 2 && clas(a,j,cnr2) == 1
              change(a,j) = 3;                  % Change sand -> plant 17/18
           elseif clas(a,j,cnr1) == 1 && clas(a,j,cnr2) == 2
              change(a,j) = 5;                  % Change plant -> sand 17/18
           elseif clas(a,j,cnr2) == 2 && clas(a,j,cnr3) == 1
              change(a,j) = 4;                  % Change sand -> plant 18/19
           elseif clas(a,j,cnr2) == 1 && clas(a,j,cnr3) == 2
              change(a,j) = 6;                  % Change plant -> sand 18/19
           elseif clas(a,j,cnr1) == 4
              change(a,j) = 7;
        end
    end
end
```

### 4.3.4 KNMI meteorological data

The available meteorological data as presented in section 4.1.4 was used to couple the abiotic changes quantified from the annual LiDAR data and biotic changes in the 2D landcover change maps. To find optimal climate conditions for sediment transportation the wind data was filtered on both a certain wind speed threshold and wind direction region. Based on literature the wind speed threshold for semi-fixed dunes was chosen to be 6 m/s (Liu, Skidmore, Hasi, Wagner, & Tatarko, 2005; Sloss et al., 2012). This should be convenient to transport sand on a modest scale. The wind direction depends on how the direction of the notches are facing. Based on Hesp and Hyde (1996) winds blowing under an angle of 50° relative to the blowout axis, are found to support the optimal wind circumstances. As the blowouts are orientated under different angles the wind direction area includes the degrees between 270° (West) and 20° (North/Northeast).

For abiotic morphological change (sediment transport), the following climate characteristics were favoured: High averaged wind speeds, wind direction aligned with the blowout notches and low precipitation rates (Bauer et al., 2009; Hesp, 2002; Jungerius et al., 1991). An important factor that was unavailable, is the soil moisture content of the sand. Considering the biotic morphological change a combination of precipitation, temperature and solar radiation will be limited for the change (Schwarz et al., 2018).

Bounded by the limited data availability of the LiDAR (1 per year) and change maps (seasonal) it was chosen to provide the climate data on monthly and seasonal time scales. Therefore, extreme one-off events were excluded to be presented solely as this is beyond the scope of the research goals.

# 5. Results

## 5.1 LiDAR

In this section the processed LiDAR data for the period 2013 till 2019 will be presented to show the morphological change. At first the total area, including the three area districts: beach, dunes and vegetated hinterland. As the dune area is the most interestingly in the study area this will be investigated into more depth than the beach and hinterland. The in-depth investigation will highlight the regions that changed the most, before zooming in to the shape and volume change of the eight foredune notches as they were present in 2013. Furthermore, a distinction will be made between total and annual elevation and volume changes throughout the study period.

### 5.1.1 LiDAR Digital Elevation Model

In Figure 17a and b the DEM's of the first year (2013) and last year (2019) are displayed to provide an overview of the dune locations. The annual DEM's over the total study period are included as Appendix 3. Based on the elevation map the dune area could be subdivided in a foredune row, valley (dune slack) and a parabolic shaped dune row. Between X = 1800-2300 m the valley and parabolic dune row are not present as this area was unaltered during the blowouts initiation. Comparing the DEM 2013 to 2019 shows two distinct changes 1) widening of the dune valley at the western part and 2) a more pronounced continuous landward dune row. The total study area increased with an average elevation of 0.18 m per $m^2$. This indicates an overall increase of 4.65 $x10^5$ $m^3$ or 18.5 $m^3$/m/year (when dividing by the beach length excluding the fixed dune row) of sand within the system. Obviously, the elevation increase is not equal over the area. In Figure 17c the elevation change between 2013 and 2019 is presented, showing the change in elevation within the area. The largest elevation changes are visible inside the dunes area varying from -7 m to +7 m. The largest changes are found aligned 315° (NW) direction. Compared to the dunes the net elevation change in the beach and hinterland districts are small.

Comparing Figure 17a and b, little to no change is visible for the beach and vegetated hinterland. For the beach, Figure 17c shows an elevation increase of <1 m at the shoreward face where closer to the dunefoot the elevation change is approx. zero. In the vegetated hinterland, the elevation change is less gradual, even though the average elevation change is around zero. At the western part, left of X = 2250 m, the boundaries between cultivated land patches are visible. Within these areas the elevation change is rather constant, varying around zero. In the eastern part, right of X = 2250 m, the elevation change is less bound to constricted areas. In most of the area hardly any elevation change is present, except for multiple patches exceeding a 1 m increase in elevation.

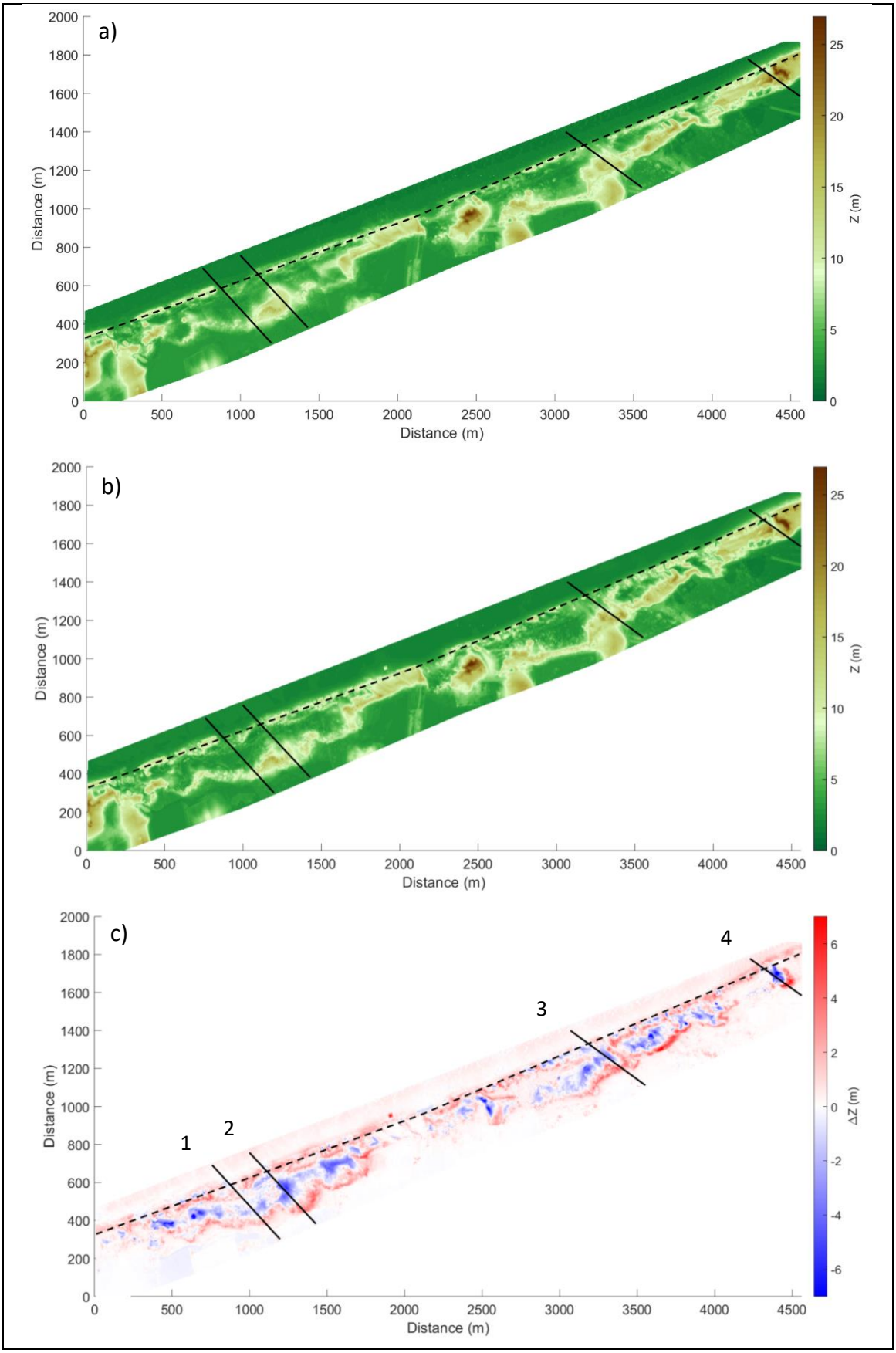


*Figure 17 - Elevation maps of the total study area. a) DEM 2013, b) DEM 2019 c) Difference DEM 2019 – 2013, in blue negative elevation change, in red positive elevation change (m). The black dotted line represents the alongshore foredune transect, presented in Figure 18. The black solid lines represent the four cross-sections through the blowout complex, presented in Figure 19.*

Considering the dunes, in addition to Figure 17 an alongshore profile (Figure 18) over the foredune row and four blowout cross-shore profiles (Figure 19) will be used to evaluate abiotic morphological change.

### *Foredune profile*

In Figure 17a could be seen that the static and straight foredune row before 1995 (Figure 9) has changed drastically into a foredune row with multiple notches. The initiated notches were still recognizable in the alongshore transect for 2013 and 2019. In the western part (X = 0 – 2100 m), the notches were more distinct than in the eastern part where there is a higher alternation between notch and crest and smaller differences in elevation. Over the total length of the transect, an elevation increase of the dune crests was visible. The 2019 crest relief tends to follow the 2013 relief, with often only a vertical change. The height increase varied between 0.1 and 3 m, where the largest peaks were found mainly in the eastern part (X = 2500 – 2800 m and 3700 – 4300 m). In contrast to the crests, the notches did not show a uniform tendency of erosion/accretion. In the western part only three out of seven notches showed (partial) erosion patterns at X = 550, 650 and 850 m, over widths of respectively 40, 75 and 30 m. A large erosion area of the foredune was found in the eastern part between X = 2850 – 3650 m. Here, the difference between notch and crest were less distinct than in the western part as the elevation differences were less and showed a faster alternation. Throughout the six years the notches became more distinct by deepening and eroding the lateral wall. This resulted in a narrower but higher peak. West and east of this area the foredune increased in height in both crest and notch, with five significant exceptions at X = 2550, 2790, 4000, 4300 and 4375 m. Overall, the erosion/accretion at the notches and crests showed roughly the same range between 0 and ±3 m. Derived from Figure 17b the elevation change along the transect amounts 895,5 m which is an average height increase of 0.19 m per meter.

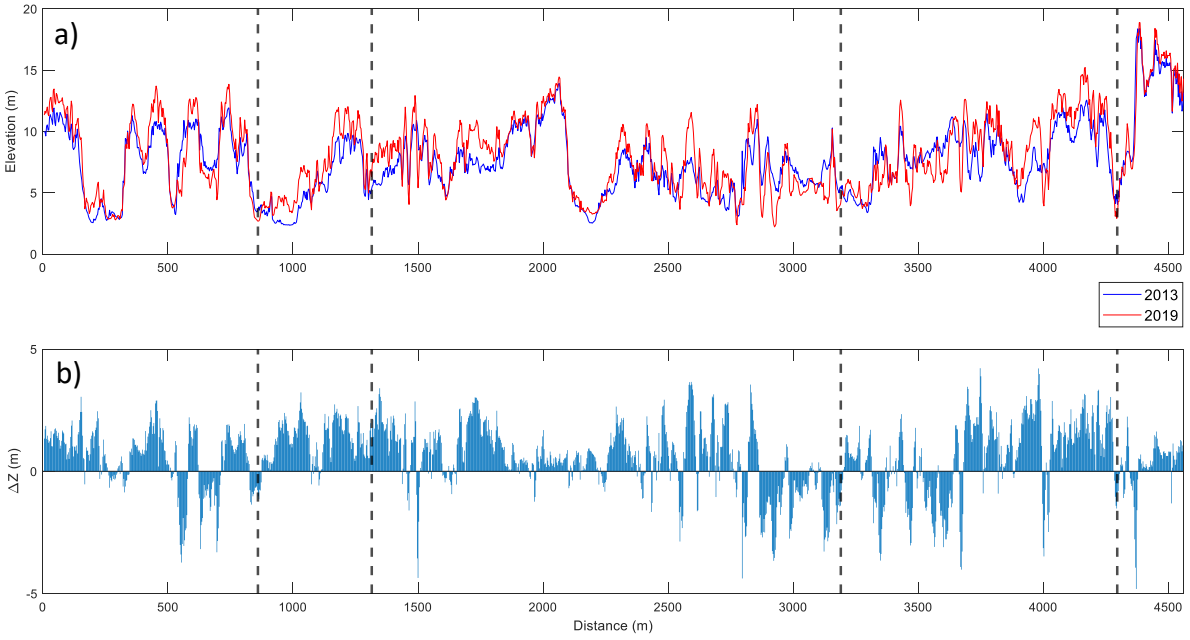


*Figure 18 – a) Alongshore profile over foredune row, comparing 2013 to 2019. Orientation is west (left) to east (right). b) shows the change in elevation between 2013 and 2019. The dashed lines represent the cross-sections displayed in Figure 17.*

### *Blowout cross-sections*

Considering the elevation change map in Figure 17c the largest increase in elevation was perceived most landward along the sand-vegetation border as a parabolic shaped feature. This dune row showed a large variation in changed elevation between +0.5 m and +7 m. The largest elevation increases were

found at landward facing arches (e.g. X =1400, 1600, 3700 and 4400 m). These positive elevation values could indicate 1) a height increase of the 2013 dune crest and/or 2) a landward shift of the dune. In Figure 19 the four NW-SE transects through blowout systems (including beach and hinterland) with significant elevation change are presented for the years 2013, 2016 and 2019. The blowouts varied in length and height dimensions. The location of the four cross-sections are indicated in Figure 17 and 18.

As also seen in Figure 17c the transects showed insignificant change at the beach and vegetated hinterland (thin lines) with a few exceptions. In 2013 at transect 1 at X = 120 m a small dune-like feature was present, this feature disappeared in the following year to never return at this location. In addition, at the second transect at X = 85 m another small dune was present at 2013 to disappear in the following year and never return. In the fourth transect, the foredune crest shifted 15 meters towards the beach at X = 70 m.

All cross-sections showed a landward (SE) shift of the second dune row, with erosion on the dune's stoss side and accumulation at the lee side. The shape of the morphological change differed per blowout. Comparing the changes in crests, at cross-section 1 and 3 the crests increased in height with respectively 1.8 m and 2.7 m, where the crest at 2 remained the same height and at 4 dropped 1.7 m. On the horizontal dimension, the crest location of transect 3 and 4 shifted 6 m and 3 m landward respectively, where the crest of 1 and 2 remained at the same position.

The amount and length of sand accumulation at the lee side was different per location. Figure 17c and 18 showed more accumulation at the transects with long erosional areas on the stoss side. At transect 1 there was only observed erosion at the dunefoot over a length of 30 m, where for 2-4 the stoss side eroded over approx. 100 m. The erosion of the stoss side resulted in an increase in the dune valley's surface area and a more uniform bed elevation of the valley in 2019 compared to the 2013 DEM. Along the transects 2-4, the valley basin eroded between 3-4 m on average with maximum values of 6 m at the seaward side of the fourth transect. For all four blowouts the erosional trend of the basin showed similar trends over the six-year period (Appendix 4). From 2013 till 2016 the erosional rates were larger than from 2016 till 2019 with 1 m/year to 0.3 m/year (transects 2 and 4), for transects 1 and 3 the change in annual erosional rate were less distinct changing only several centimetres but still showed less erosion in the latter period.

In contrast to the erosion rates in the basin, the accretion rates on the lee side were more constant over time and spread equally over the length of the lee side slope. The new sand layer seemed to follow the 2013 relief. For the years 2013-2018, the annual sand layers coincided at a certain landward point of no elevation increase. For transect 2 and 4, the new sand layer for 2019 exceeded this point to shift the lobe more landward.

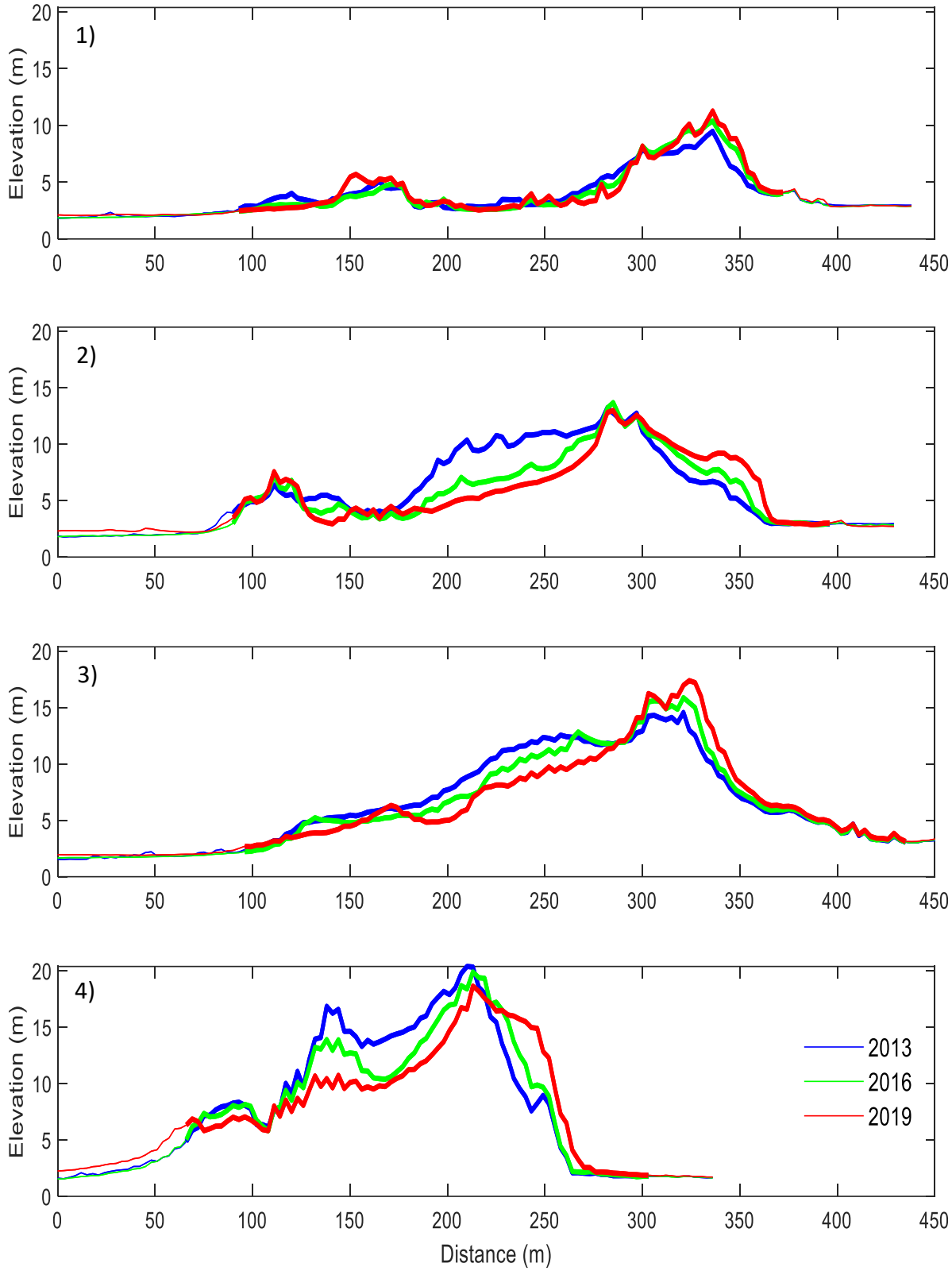


*Figure 19 – Transects based on four blowouts, indicated in the alongshore profile in Figure 18. Bold lines represent the dune area, left is the beach, right hinterland. Location of transects are displayed in Figure 17.*

### 5.1.2 Annual volume change

*Total study area*

Instead of looking at the two-dimensional change in the previous paragraph three dimensional data could be produced in the form of volume change. Furthermore, previously only the start (2013) and end (2019) conditions were compared. To find out if there is a trend of change the annual change in height over the total study area is presented in Figure 20. The changes in volume are directly derived from the change in height by multiplying it by the pixel size (9 $m^2$).

For all years applied a positive elevation change along the borders of the dune area as defined in the methodology. The largest changes at the fore- and back dune row occurred from 2014-2016 and 2017-2018. Also between 2014-2016, the largest erosional patterns within the valleys were found. The change map of 2017-2018 showed a large elevation increase over almost the complete study areas, except for some locations within the valley. Compared to the other years, the area suffering valley erosion was less. Comparing the maps 2017-2018 to 2018-2019 for the western part of the hinterland shows an inverse change. After an elevation increase of 0.50 m in 17/18 roughly the same land surface dropped in elevation with 0.50 m again to counter the change, which is unexpected. This suggests that there could be a measurement error within the 2018 LiDAR data.

Shoreward of the foredune row at X = 1900 m, Y = 900 m a local elevation increase of 6m was found. This change was due to the construction of a restaurant in 2015.

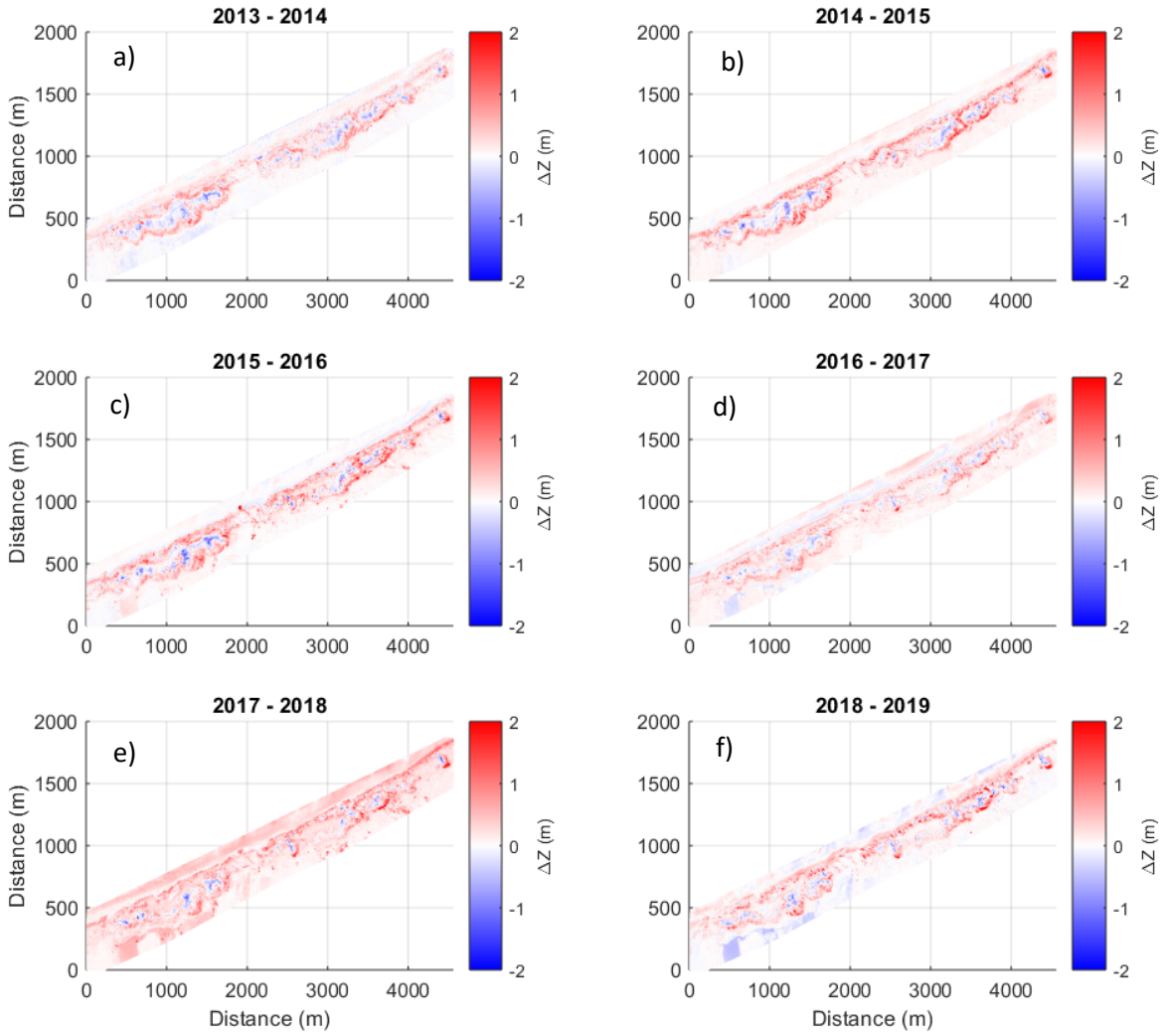


*Figure 20 - Annual elevation differences for the total study area $Z_{Current\ year} - Z_{Previous\ year}$.*

In Figure 21 the annual volume changes and the trend of the total area volume are presented. Between 2013 and 2019 the total sand volume of in the area increased with 4.65 x$10^5$ $m^3$. As seen in Figure 21b the total volume did not increase linearly over the years. Contrary, from the first year the total area volume decreased with 0.90 x$10^5$ $m^3$ and increased the next year with 1.0 x$10^5$ $m^3$. In the two consecutive years the total study area still increased in volume but with a lower amount, 0.65 x$10^5$ $m^3$ and 0.41 x$10^5$ $m^3$. This was followed by a striking increase of 3.75 x$10^5$ $m^3$ between 2017 and 2018, which could be seen in Figure 20e. During the last year interval, the total volume dropped with 0.28 x$10^5$ $m^3$. In Figure 21c the annual volume change rates are presented which correspond with the annual volume change. The average volume change rate over the six-year period amounted 18.5 $m^3$/m/year with a large standard deviation of 35.0 $m^3$/m/year.

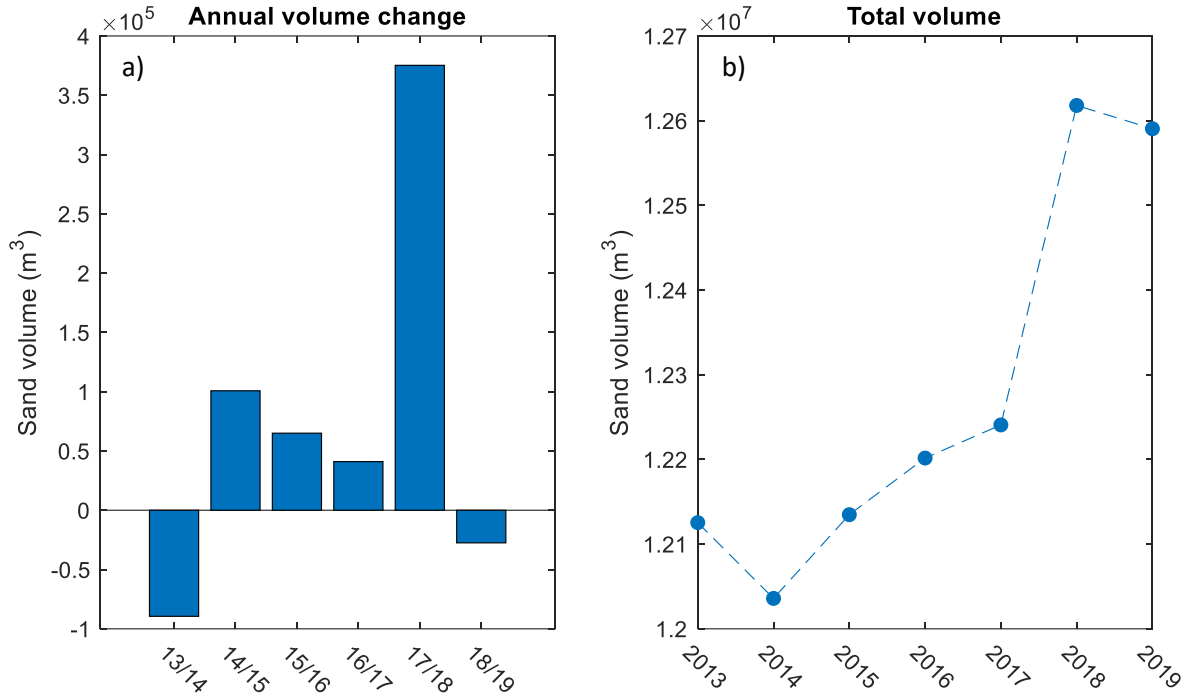


| c) | 13/14 | 14/15 | 15/16 | 16/17 | 17/18 | 18/19 | Avg. |
|---|---|---|---|---|---|---|---|
| **$m^3$/m/year** | -21.3 | 24.0 | 15.5 | 9.8 | 89.3 | -6.5 | 18.5 |

*Figure 21 - a) Annual volume change for the total study area, b) total volume change for the total study area. The dots are connected by a broken line to indicated that the volume change is not linear within a year. Note the different scale on the axis. c) The volume change rates per year. The annual volume changes divided by the beach length = 4200 m.*

### *Districts subdivided*

As the three districts have different landcover properties the transport and volume change could be different. To gain inside in the distribution of the change in sand volume the area is again subdivided into the three districts. The dimensions of the three districts are presented in Figure 15b. Figure 22a presents the absolute volume change and 22b presents the relative volume change per district and how it behaves compared to the total area. At 13/14 the three districts showed similar volume loss per $m^2$, around 0.036 m. For the next year, the districts showed less similarity although all districts increase in volume. For example, the dune area gained 4.5 times more sand volume than the vegetated hinterland. At the years 15/16 and 18/19, the direction of volume change of a district diverges from the total area change, signalizing that it is important to subdivide the area.

The vegetated hinterland showed the most constant trend of the three districts, with an increase of 0.01 m between 2014 and 2017. Moreover, it constantly showed the least change with an exception

in the last year with a steep drop contrary to the other two districts. The opposite was the volume change on the beach, deviating the most through time. Experiencing two times a volume decrease and in 17/18 an excessive volume change of 0.27 m which increased the sand volume of the beach with 12.8% (0.146 x$10^6$ $m^3$) (Figure 23). Even though the fluctuations the beach remained to have the most constant sand volume till 2017. The dunes showed roughly the same trend as the vegetated hinterland only with a constantly larger volume increase. In the period 2014-2016, the largest relative and absolute volume changes were found at this district.

Focusing on the striking volume change in 17/18 all districts experience their largest increase. The relative distribution of volume change was distributed similarly compared to the previous year. However, the amount of volume increase per $m^2$ was significantly larger than compared to the previous years and succeeded by a year showing incomparable trends. The decrease of volume of the vegetated hinterland was such that it overruled the dunes and beach. This resulted in a net volume decrease of the total study area. Overall, for all districts the volume in 2019 has increased compared to 2013 as was already found for the total study area in Figure 21b.

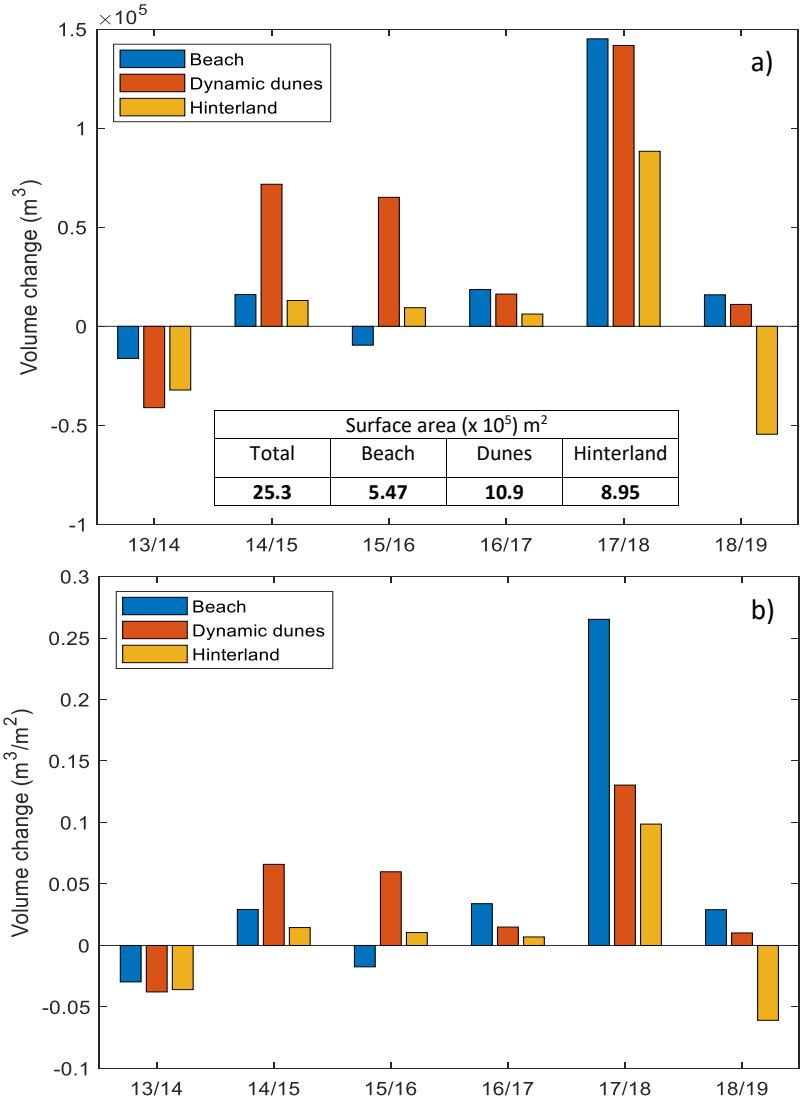


*Figure 22 – a) Annual volume change for the three area districts, cumulative it results in Figure 21a. b) When dividing the volume by the surface area of the corresponding district the relative volume change per $m^2$ is found.*

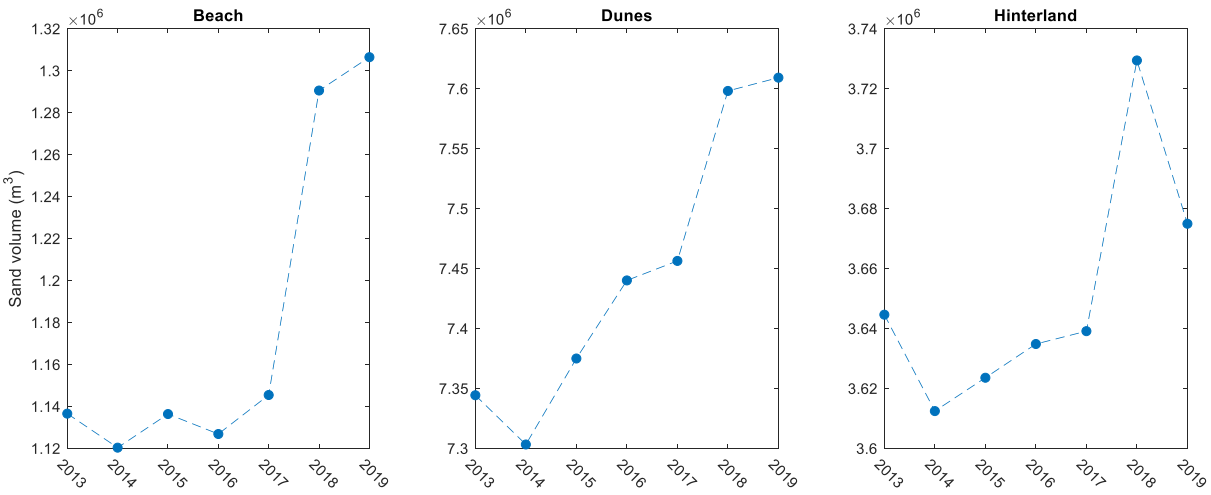


*Figure 23 - Absolute sand volume change for the three area districts. The dots are connected by a broken line to indicated that the volume change is not linear within a year. Note the differences in scale on the y-axis.*

### *Notches*

Based on the DEM 2013 map and the foredune alongshore profile (Figure 18) the location of eight foredune notches were identified (Figure 15c). The surface area was different for each notch and presented in Table 6. The morphological change of the notches will be expressed in volume change per cubic meter to find out which notch undergoes relatively the most annual (Figure 24a) and cumulative change through time 24b.

The first observation was that notches 1, 2, 3, 5 and 7 filled up over the study period. Notches 4 and 6 remained rather constant and notch 8 is the only selected notch that lost a significant amount of sand over the six years (8769 $m^3$). Considering the accretion/erosion trends, notches 1, 2, 5 showed a similar trend and change in elevation, these notches were continuously accreting and increasing in volume. These three notches experienced an elevation increase of 1.5 m per square meter. Notch 7 also shows a similar trend but deviates in the first year when it suffered erosion of -0.12 m instead of a height increase. The year of the largest accretion values was found at 15/16 and the least increase in 18/19 for the three similar notches. This lowest value corresponded with the decrease in volume increase seen in Figure 22 for the dunes. This decline in volume gain applied for all notches except for notch 3. Notches 3, 4, 6, 7 and 8 started with a decrease in volume, suffering erosion. Notches 3 and 7 already showed positive volume changes after the first year, where notch 4 and 6 gained sand for the first time from the year 17/18. Compared to all other notches, notch 3 showed a rather constant increase from 14/15 onward with an extra 0.05 m each year. Notch 8 showed the most striking notch evolution. It showed continuous erosion with the lowest value in 15/16 of -0.21 m and the highest of -0.54 m in 18/19. Therefore, it is the only notch that does not partly fill up. Transect four in Figure 19 crosses this notch and shows an average elevation decrease between X = 70-100 m of 1.8 m, which is less than found in Figure 24b with -2.1 m. Overall, the notches have filled up over the six-year period with exceptions of notch 6 and 8. Comparing the first and last year for notch 4 and 6 shows that the volume hardly changes with only 0.03 and -0.12 m in total. So these two notches show the least morphological activity based on volume change. Table 7 contains the absolute volume gain/loss per notch.

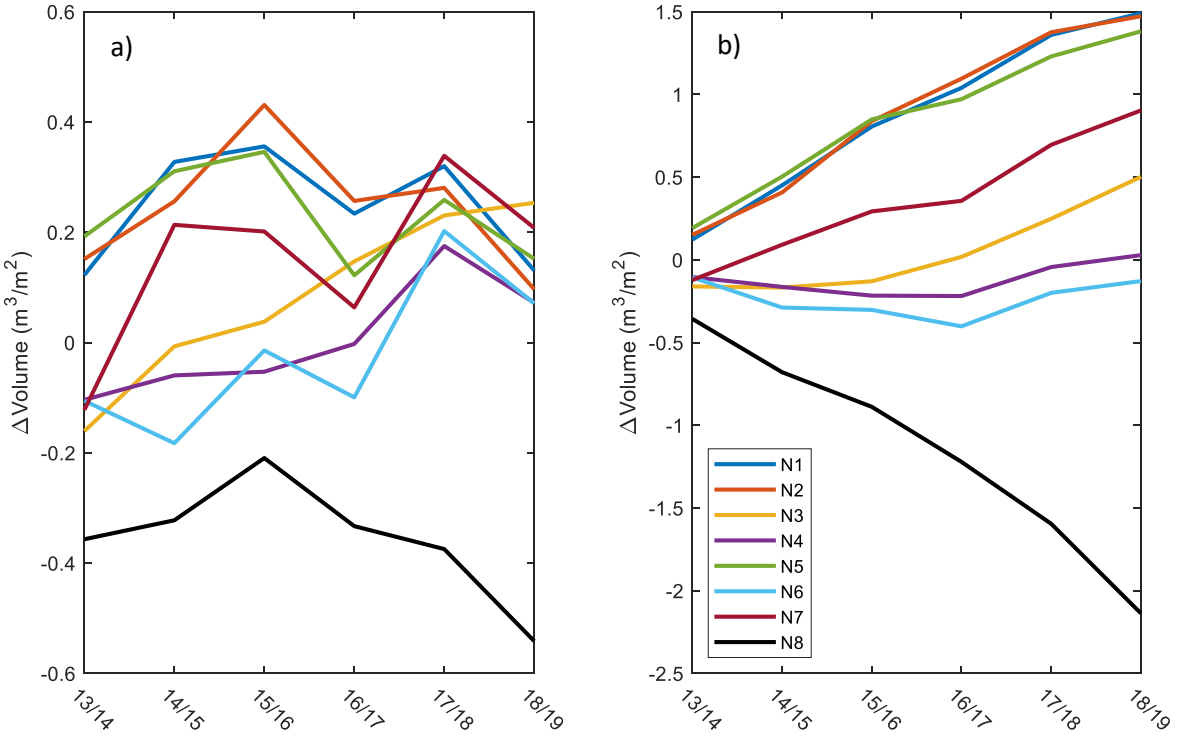


*Figure 24 - a) Annual volume change per surface area per notch. b) Cumulative volume change per surface area over the study period. Both graphs are normalized by dividing the notch volume change by its corresponding surface area.*

*Table 7 - Surface area and absolute volume gain/loss of notches over the study period.*

| Notch | Surface area ($m^2$) | Absolute volume gain ($m^3$) |
|---|---|---|
| 1 | 2511 | 3744 |
| 2 | 1350 | 2286 |
| 3 | 3591 | 1803 |
| 4 | 4374 | 127 |
| 5 | 2322 | 3209 |
| 6 | 2403 | -307 |
| 7 | 2529 | 1988 |
| 8 | 4104 | -8769 |

## 5.2 PlanetScope spectral data

### 5.2.1 Landcover area

As described in section 4.3.2, the area was classified into a total of four classes of which vegetation and sand filled up the majority of the total 2.53 $km^2$. In Figure 25 the landcover surface area change through the study period is presented.

The area of both landcover classes showed an oscillating trend through the study period. The amount of landcover area change within a year was not constant. From autumn 2016 to spring 2017 it amounted ~0.2 $km^2$. For the succeeding years the change over the same time period amounted ~0.35 $km^2$. The landcover areas showed distinct peaks at roughly the same period of the year for the total study period. Furthermore, the oscillating trend of vegetation and sand surface area varied out-of-phase. Considering vegetation, the maximum landcover areas were found at 26-11-2016, 15-10-2017 and 31-10-2018 ((early) autumn) increasing each year in surface area with respectively 0.051 $km^2$ and 0.064 $km^2$. As the sand area showed a direct response on the changing vegetation area – and vice versa – the minimum area coverage for sand was found at the same dates and showed a decreasing trend. The maximum sand area coverage peaks showed a different trend than for maximum vegetation and were recorded at 22-03-2017, 06-04-2018 and 30-03-2019 (early spring). There was no continuous increase/decrease measured. The second sand area peak (06-04-2018) covered the largest area of sand, 1.41 $km^2$, where the first and third peak showed area coverage of ~1.35 $km^2$.

For the largest period, the landcover classes showed a relatively smooth transition over the years. Only between June and August 2018 and February and April 2019, the trend showed some disturbances of very quick alternation of landcover area. These were unexpected changes while comparing to the other years. It was expected that these alternations are not seen in the field and were caused by disturbances during data collection by the CubeSats.

So overall, the vegetation and sand in the area showed an inversed trend over the three years. The vegetation surface area reaches its maximum extent halfway/early autumn (end of growth season) and the sand during early spring (start of growth season). Moreover, the vegetation surface area increases during these peak periods by 0.115 $km^2$.

The total amount of area that was classified as vegetation or sand increased through time. This was not caused by area expansion, instead, the pixels that were first classified as *No Change* "learned" their true entity as more scenes passed by. At the first scene on September 21$^{st}$ 2016, 98,68% of the pixels were classified as vegetation or sand. One year later at scene 14 (04-09-2017), 99,95% was classified as one of the landcover classes. From scene 30 (14-05-2018) onwards the classification did not drop below 99,99% classification but never reached the full 100% landcover classification. In the last scene, only 9 pixels (81 $m^2$) were not classified as vegetation or sand.

Figure 26 illustrates the NDVI-value of the study area at the discussed landcover surface area peaks. At Figure 26a-c the dates with maximum vegetation landcover are presented. Over the three-year period it was clearly visible that NDVI values within the dune area had increased. Green patches have expanded through time. At the beach and hinterland, district values remained rather constant over the three-year period. For the maximum sand surface area (Fig. 26d-f) the changes over time were less distinct. Over the total study area NDVI values showed lower values at these dates. One striking observation in Fig. 26e was that three patches at the hinterland district had NDVI values close to zero, these patches are circled. In the visual PlanetScope images these patches were much darker than the surrounding area, hinting that the landcover changed from grass-like into a more woody vegetation

type. These dark patches were visible between 17-12-2017 and 24-07-2018 before changing back into more grass-like landcover with higher NDVI values.

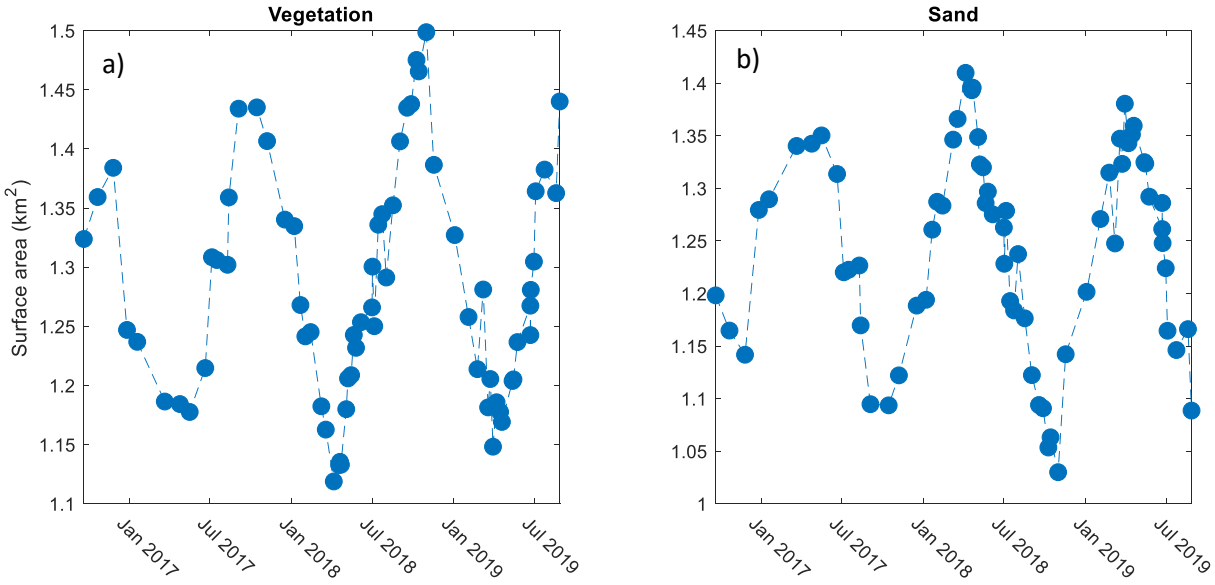


*Figure 25 - Landcover surface area change during the study period for a) Vegetation and b) Sand.*

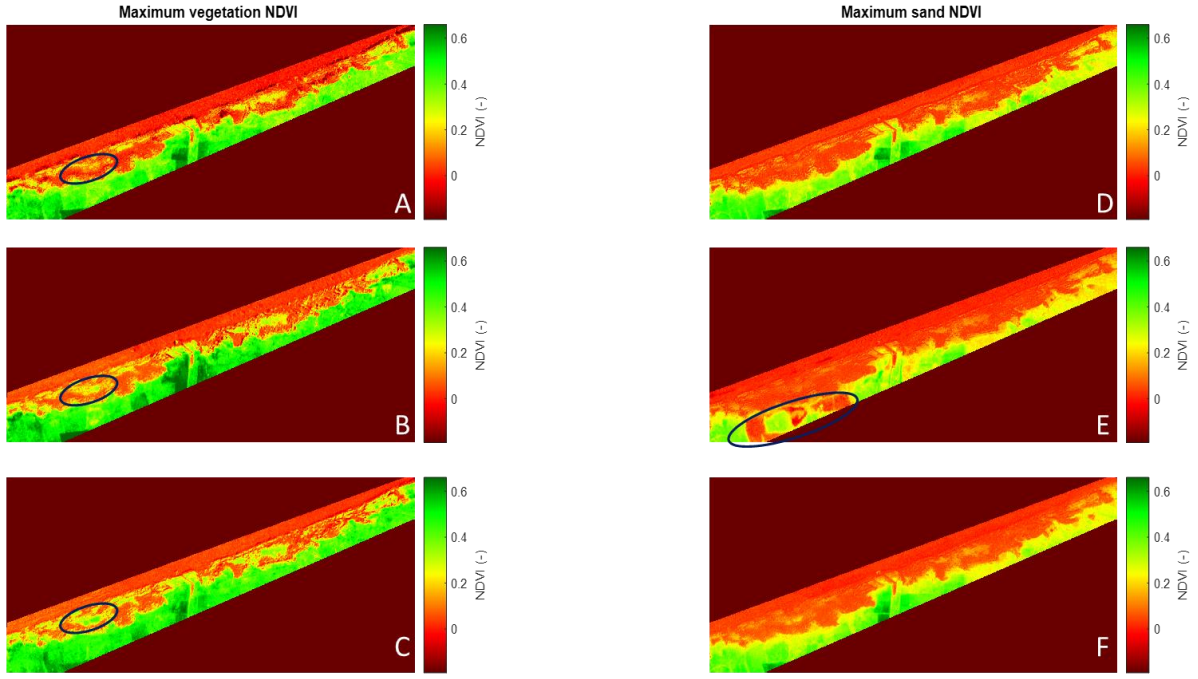


*Figure 26 - NDVI-map for study area during landcover peaks, a-c) Vegetation 2016-2018 and d-f) Sand 2017-2019. In a-c an area of large NDVI change is highlighted. In e the deviant NDVI values in the hinterland are highlighted.*

### 5.2.2 Seasonal NDVI change

As discussed in section 4.3.2 the landcover classification predominantly relies on a division on NDVI values. Therefore, NDVI maps are of good use to investigate the vegetation evolution at the blowout area on an annual scale. Figures 27-29 zoom in to the dune area as here the most relevant changes took place. Each figure represents the annual seasonal cycle starting in autumn (October) and continuous in chronological order.

For all three years, roughly the same trend was visible. In autumn, as in agreement with Figure 26, the overall NDVI values were highest to strongly decrease in winter. The following spring the values had slightly increased. In summer the green patches emerged again along the border and within the blowout area. Note that for the winter images shadow might be present in the collected scenes. A property of shadow is that it results in significant low NDVI values (NDVI << 0). That may explain the low mean winter values as presented in Table 8.

Considering the three figures and Table 8, it showed that only in autumn the mean NDVI values rose. In summer the values dropped slightly after 2017 to remain constant over 2018 and 2019. The most striking deviation was found in spring 2018. Here the mean NDVI value was almost half of the value as the surrounding years. Additional data shows that before the 22$^{nd}$ of April 2018 comparable low values were measured, where the next date (04-05-2018) contains a more expected value of 0.12.

Even though the values found for autumn and summer were relatively similar, the amount of surface area classified as vegetation showed large differences as presented in Figure 25. Considering Figures 28 and 29, autumn contained more and more vibrant green patches. The areas around the patches showed darker red, representing lower NDVI values, which resulted in a lower mean NDVI value for autumn than summer.

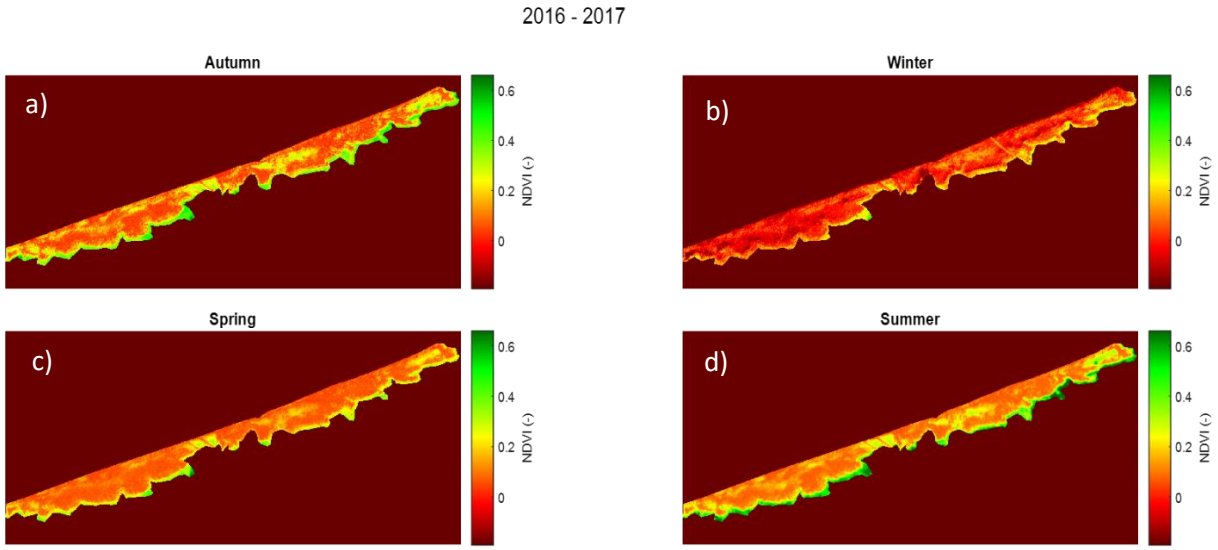


*Figure 27 - Seasonal NDVI-maps zoomed in to the dunes district for 2016-2017, a) 22-10-2016, b) 19-01-2017, c) 25-04-2017, d) 17-07-2017.*

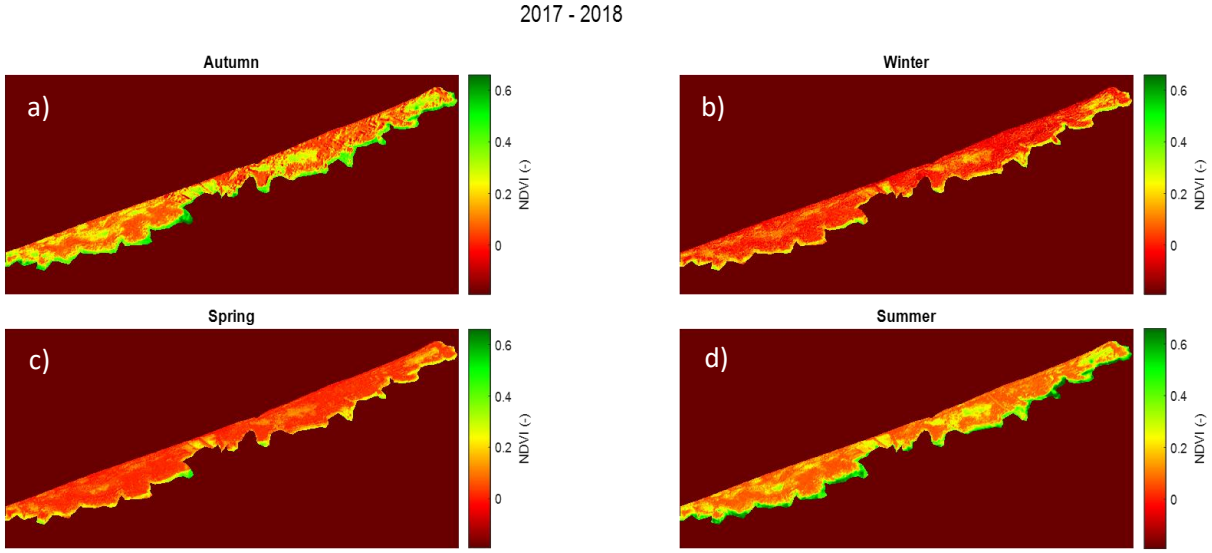


*Figure 28 -Seasonal NDVI-maps zoomed in to the dunes district for 2017-2018, a) 15-10-2017, b) 21-01-2018, c) 22-04-2018, d) 15-07-2018.*

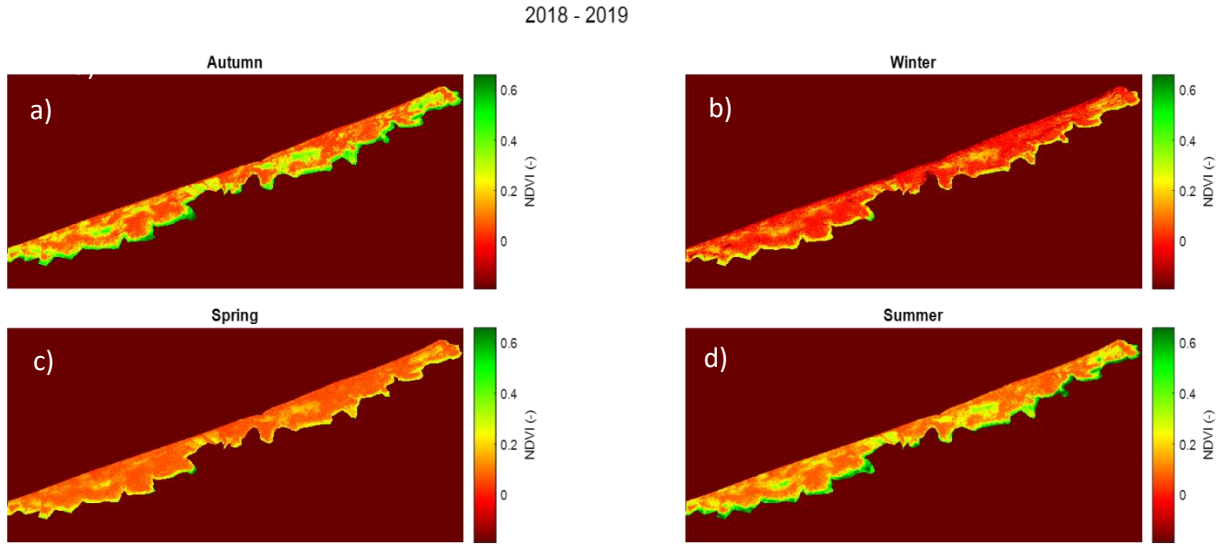


*Figure 29 - Seasonal NDVI-maps zoomed in to the dunes district for 2018-2019, a) 14-10-2018, b) 03-02-2019, c) 19-04-2019, d) 24-07-2019.*

*Table 8 - Mean NDVI values per season for the dune district.*

| **Season** / **Year** | Autumn | Winter | Spring | Summer |
|---|---|---|---|---|
| 2016 – 2017 | 0.16 | 0.014 | 0.12 | 0.21 |
| 2017 – 2018 | 0.18 | 0.059 | 0.069 | 0.19 |
| 2018 – 2019 | 0.19 | 0.057 | 0.11 | 0.19 |

### 5.2.3 Seasonal landcover change

Figures 30-33 represent the three-year landcover change per each season. For each season, three landcover classified scenes, taken at roughly the same day of the year are compared. The used dates are presented in Table 5. For all seasons applied that at the districts beach and hinterland little to no landcover change has occurred. In Table 9 the absolute surface area changes for the four seasons are summarized and compared.

#### Seasonal change characteristics

Starting in autumn (Figure 30), the most striking characteristic was the emerging of large (light) green areas. In the western part (X = 0-1800 m) a chain of vegetation had developed within the dune valley. In the eastern part, less change has occurred. It seems that new vegetation areas are bound to already existing vegetation patches, seen in dark blue. Besides the new vegetation areas in the middle of the dunes district, additional change was found along the border between the dune and hinterland districts where a strip of alternating landcover was present. In the western part, the change of sand into vegetation cover was dominating, where east of X = 3200 m the main change here was vegetation into sand.

Keeping this in mind, for the winter and spring seasons (Fig. 31-32) almost only the change of vegetation into sand was experienced along this border. At X = 1800 m/Y = 600 m both maps showed a large area changing into sand area, with the most recent change (orange), most landward protruding in to the hinterland. The difference between winter and spring was that in winter more vegetation emerges than in spring, mainly located inside the dune complex. In general, hardly any change within the dunes was found during spring, represented by the area coloured yellow. Continuing with summer, sand changed into vegetation, mainly in the western part showing similarities with the change in autumn. In the eastern part, especially in 18/19, there was a change from vegetation to sand along the landward edge of the dune district.

Applicable to all the seasons was that in 17/18 (16/17 for autumn) more area change occurred for both vegetation as sand than in the continued year (Table 9). Except for spring, when the sand into vegetation was two times larger for 18/19 than for 17/18 (Table 9). Moreover, although the landcover changes were calculated per season two important changes were present at all individual four maps. The first was the expanding new vegetation patches at X = 1000 m/Y = 400 m and X = 3000 m/Y = 1200 m. These areas were found to change from sand into vegetation after the first year during every season. So, this implied that these areas did not turn back into sand during winter or spring and remained vegetation all year round in contrast to multiple other new vegetation areas present at the autumn change map. The second change that returned in every individual season were the new sand areas along the dunes/hinterland border. These areas were landward extensions into the hinterland occurring continuously over the year although the size of landward extension was seasonal depended as described previously.

*Notches*

Considering area around the foredune notches, no clear changes are visible here. Most of the notches were located in the area of no change sand. In autumn small areas (pixel-sized) were found around the edges of the notches, as selected in Figure 15c. An exception was notch 8, here change around the edges was visible in all of the four seasons. In autumn and winter, a light green strip was visible on the western edge. Landward brown and orange areas were present that changed into sand. In spring and summer, these brown and orange areas were larger and also found on the eastern edge, with no presence of green.

## Change activity

Besides the landcover changes, the surface area of the no-change areas was also assigned and variates between the seasons. If there was a large area of no change, fewer pixels could have changed over the three years, indicating a less dynamic season. Furthermore, the division between no change vegetation and no change sand was typical per season as could be expected according to the change presented in Figure 25. Presented in Table 9, spring contains the most no change sand and least no change vegetation surface area. Furthermore, the total no-change area in spring is the largest with 2.4 $x10^6$ $m^2$. This area was 0.09 $x10^6$ $m^2$ larger than the no-change area assigned at summer, which was the season with the least no-change area. The no-change division and total area for all four seasons are presented in Table 9.

Then consider the amount of change per season. Starting with sand to vegetation, for both period the most change took place in autumn 102 and 57 $x10^3$ $m^2$ respectively. The least amount of change occurred during spring with only 14 and 29 $x10^3$ $m^2$. This difference was clearly visible comparing Figure 30 and 32. Then consider the vegetation into sand area, here summer was the season with the least change: 24 and 12 $x10^3$ $m^2$. The largest area changed into sand for 17/18 occurred in spring with 65 $x10^3$ $m^2$, where in the next period the largest changes were found in winter: 35 $x10^3$ $m^2$.

From the collected data in Table 9, for every season the amount of net gain vegetation surface area was calculated. In autumn the most change into vegetation surface area was found, it showed an increase of +116 $x10^3$ $m^2$ over the study period. Winter and summer also showed an area increase of +35 and +80 $x10^3$ $m^2$ respectively. Only in spring a decrease in vegetation surface area, or increase of sand surface area, was found of -39 $x10^3$ $m^2$.

As the landcover change maps were designed for annual season comparison it is not possible to calculate the total vegetation surface area increase for the three-year period. This is due to the fact that pixels could be assigned the same change value for multiple seasons, as for example was visible for the large new sand area at X = 1800 m/Y = 600 m at the winter and spring change map.

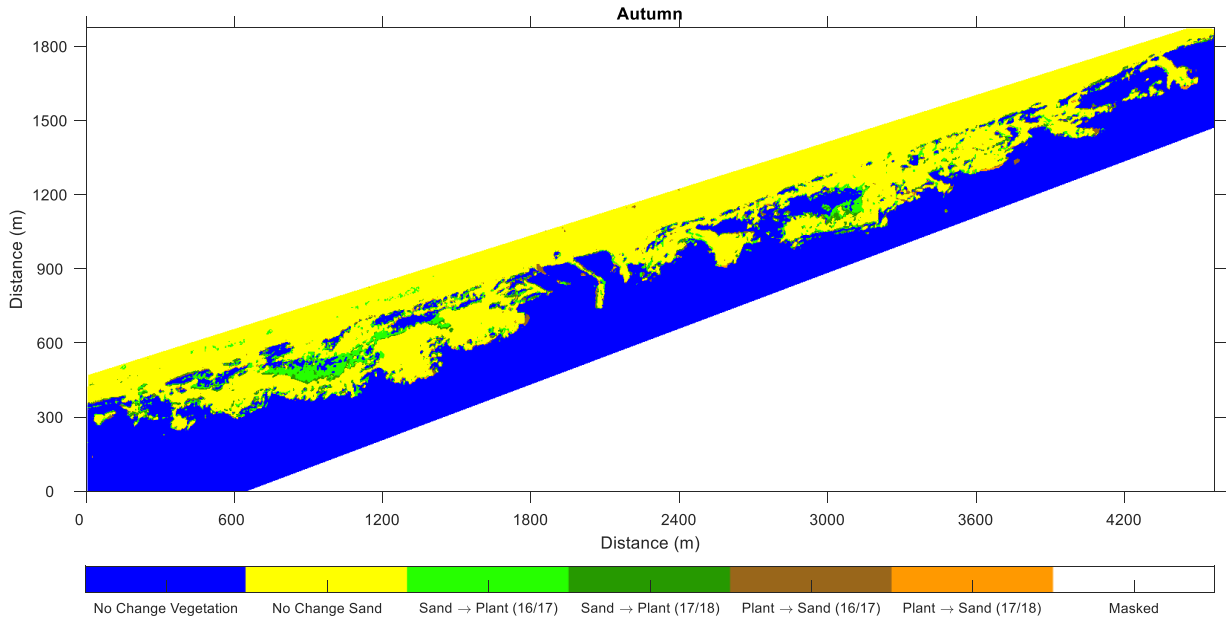


*Figure 30 - Landcover change map for Autumn 2016-2018. Landcover change of sand into vegetation or vegetation into sand is presented with the according year the change took place. Dates are the same as used for NDVI maps in Figures 27-29.*

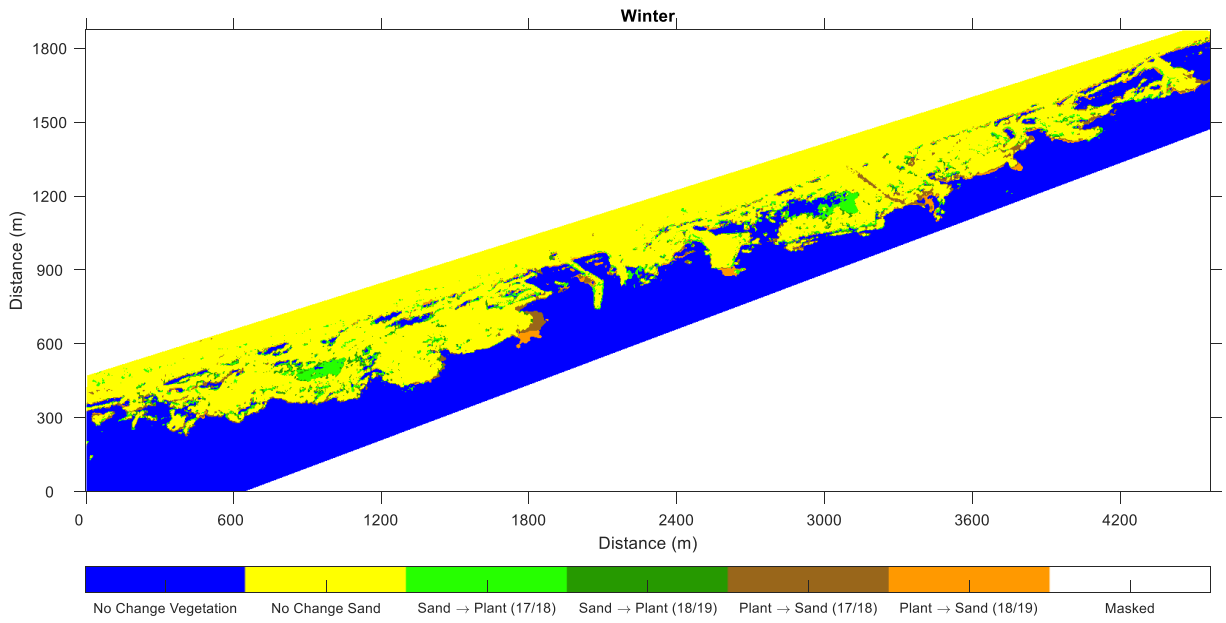


*Figure 31 - Landcover change map for Winter 2017-2019. Landcover change of sand into vegetation or vegetation into sand is presented with the according year the change took place. Dates are the same as used for NDVI maps in Figures 27-29.*

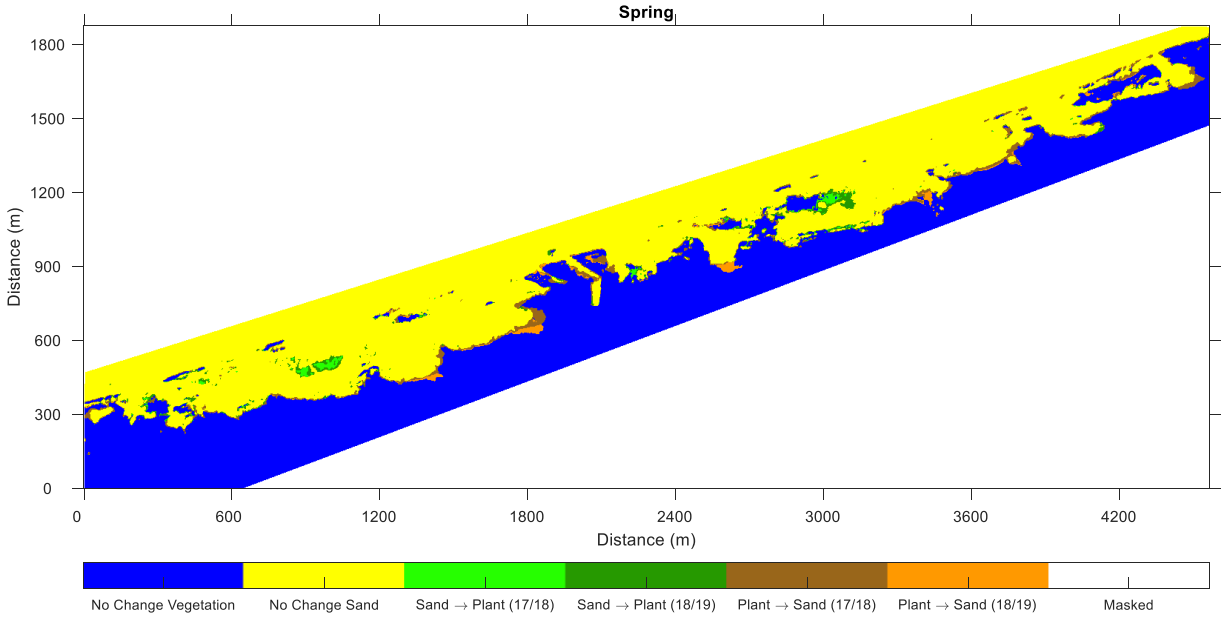


*Figure 32 - Landcover change map for Spring 2017-2019. Landcover change of sand into vegetation or vegetation into sand is presented with the according year the change took place. Dates are the same as used for NDVI maps in Figures 27-29.*

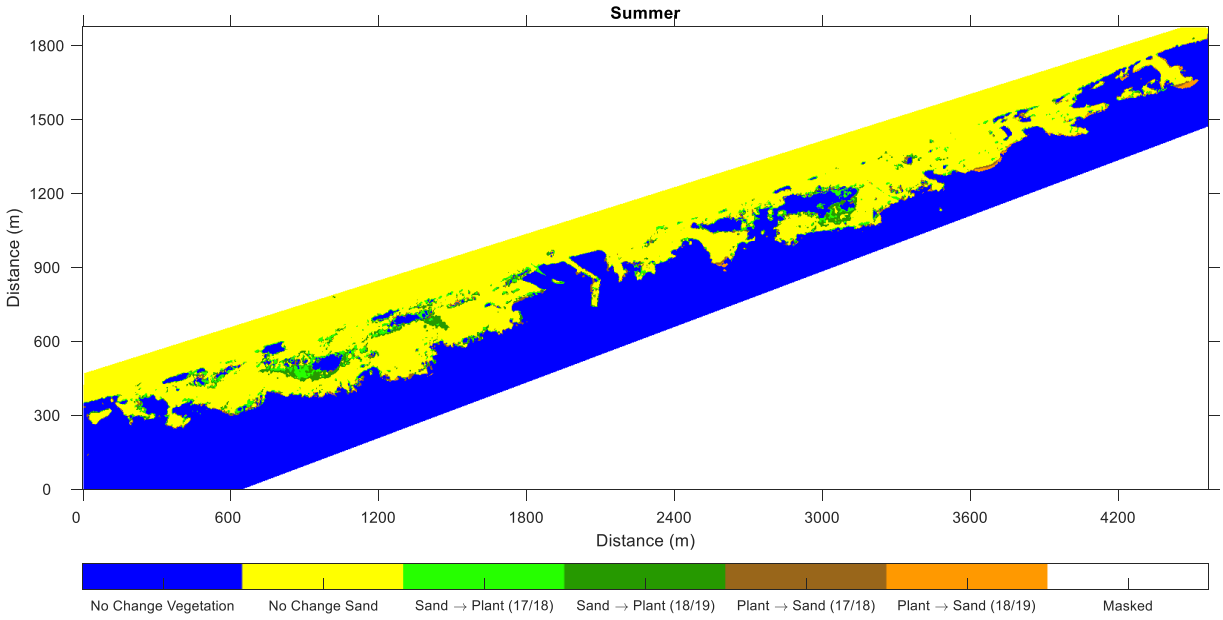


*Figure 33 - Landcover change map for Summer 2017-2019. Landcover change of sand into vegetation or vegetation into sand is presented with the according year the change took place. Dates are the same as used for NDVI maps in Figures 27-29.*

*Table 9 - Surface area of change per season over a year, divided for the changes plant to sand and sand to plant. The largest affected surface area per change unit is displayed in bold and smallest italic. The surface area is presented in $m^2$ x$10^3$.*

| **Season** / **Landcover ($m^2$ x$10^3$)** | Autumn | Winter | Spring | Summer |
|---|---|---|---|---|
| No change vegetation | 1316 | 1145 | 1103 | 1270 |
| No change sand | 1007 | 1163 | 1301 | 1107 |
| Total no-change area | 2323 | *2308* | **2404** | 2377 |
| **Landcover change ($m^2$ x$10^3$)** | | | | |
| Sand → Plant (17/18) | **102** | 88 | *14* | 63 |
| Sand → Plant (18/19) | **57** | 40 | *29* | 53 |
| Total change vegetation | 159 | 128 | 43 | 116 |
| Plant → Sand (17/18) | 30 | 58 | **65** | *24* |
| Plant → Sand (18/19) | 14 | **35** | 17 | *12* |
| Total change sand | 43 | 93 | 82 | 36 |
| Net change: Vegetation - Sand | +116 | +35 | -39 | +80 |

## 5.3 Meteorological data

### 5.3.1 Wind speed and direction

To discover a trend in the behaviour of the wind characteristics, the monthly averaged wind speed and direction are plotted in Figure 34. The X-axis starts at March as this agrees with the seasonal division and second it coincides with the date the LiDAR data was retrieved so it represents the period displayed in the elevation change maps (Figure 20).

For the years 2013 – 2017 the monthly averaged wind speeds show similar trends. The highest averaged wind speeds (> 6 m/s) were found in the winter months (Dec – Feb) and occasionally in November. Contrary, in 2018 the highest average wind speeds were measured during late summer and autumn and decreased during the winter months. For all years applied that in late spring and summer the wind speeds were lowest and hardly exceed 6 m/s.

The wind direction average for each year showed little similarities between the years. Within a year there was a large variation. However, the annual average wind directions were rather similar, shifting between 190° and 208°, representing SSW winds. This agreed with the wind rose presented in Figure 11 over the period 1997-2019.

*Specifying wind data*

The average wind direction was from the SSW, while the blowout complex is oriented in an NW direction. In Figure 35 the wind data was filtered according to the conditions stated in section 4.3.4. The results are presented as the number of days the combination occurred and were subdivided into seasons per year accompanied by the yearly sum of days.

In 2017, 57 days had an average wind speed of at least 6 m/s directed from the requested direction which is the most during the study period. This year is followed by 2015 with 45 days. 2013 had the least days which met the criteria: 31. In total 253 days over the total study period met the favoured criteria, which is 11.5% of the total days (2191). On the seasonal scale, the trend showed that the number of days was rather evenly distributed. Only in summer significant fewer wind days were found. The number of days per season fluctuated year to year. Autumn showed the most fluctuation with for example only four days in 2016 followed by 21 days in 2017 (of which 19 out of 21 even exceeded a wind speed of 7 m/s). These 21 days were the most days found within one season for the total dataset. Summer was the most constant season averaging on nine days a year.

In Table 10 the distribution of days over the season are presented. Most days had occurred during winter (68), which is 26.9% of the total days that met the requirements. The least amount of days were found in summer (53) which only made up 20.9% of the total. It showed that the wind climate was relatively constant for Terschelling, with these thresholds. In the third row, the number of days per season was divided by the total amount of days within the particular season over the six-year span. This shows the occurrence rate within the season instead. For example, over the total study period 12.6% of the days in winter met the wind speed and direction criteria, which represented roughly 11 days within a season.

When raising the wind speed threshold the days in spring and summer rapidly decreased and a larger percentage of the days will be concentrated in winter.

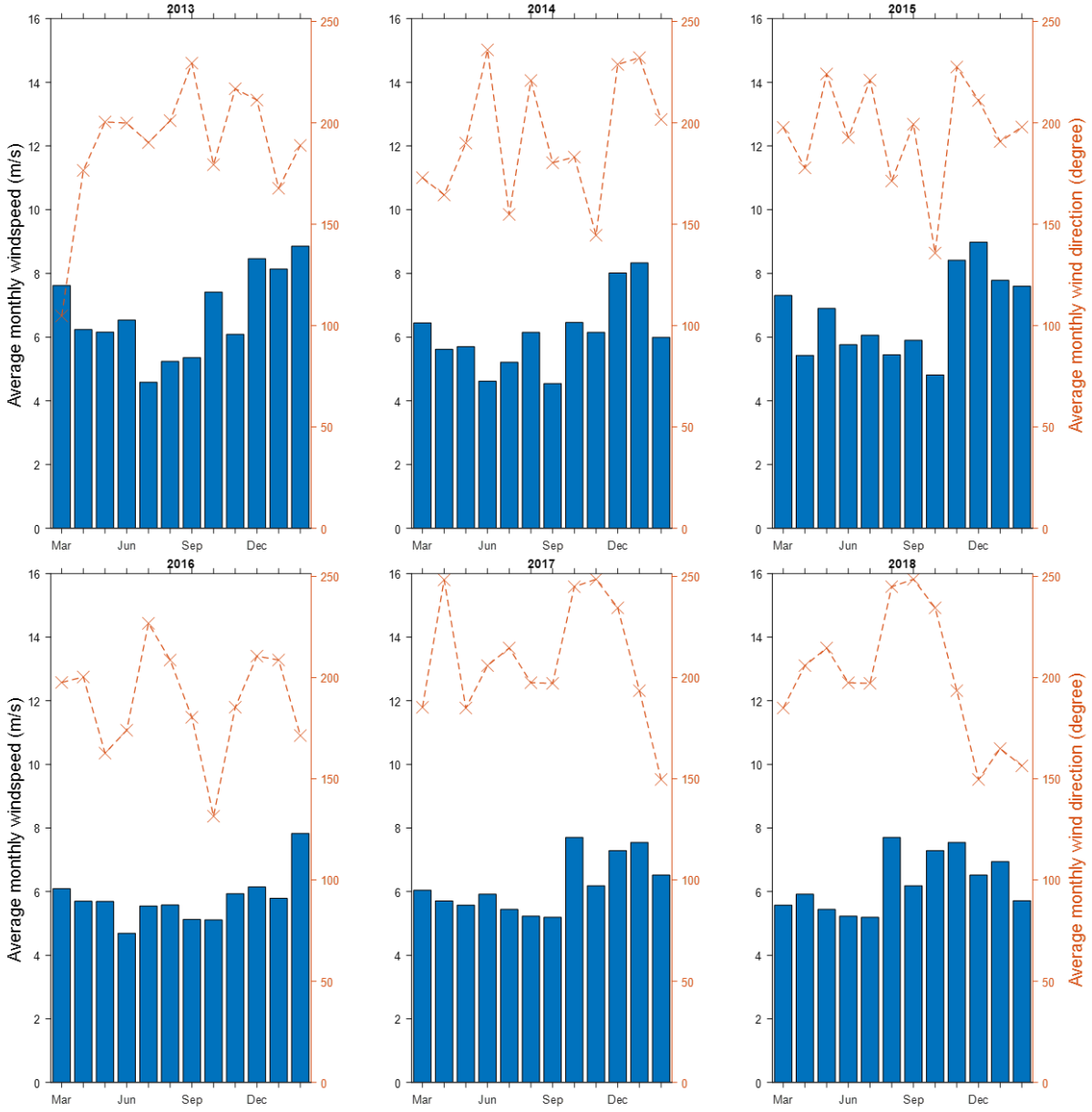


*Figure 34 - Average monthly wind speed (m/s) and average monthly wind direction (degree). Daily data from the weather station in Hoorn (Terschelling) was converted into monthly data, starting in spring (March-February).*

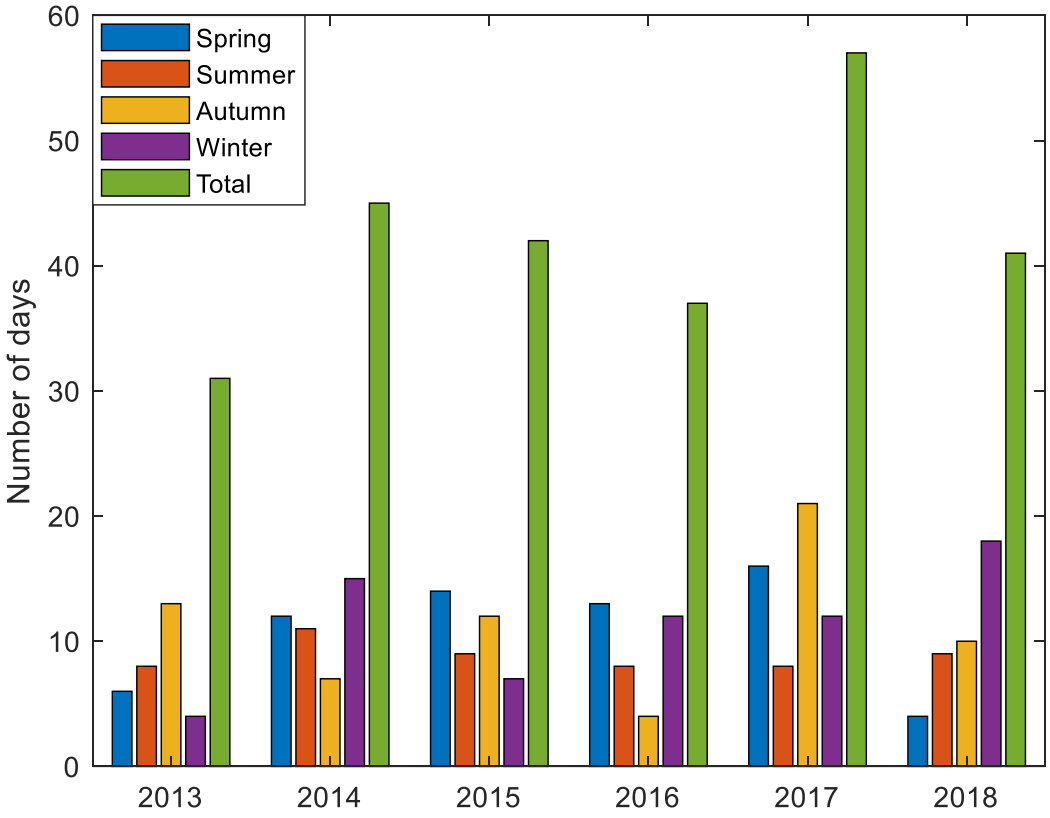


*Figure 35 - Number of days per season wind meets the two criteria: wind speed > 6 m/s and wind direction = 270° - 20°.*

*Table 10 – Total number of days with strong winds (>6m/s) and favoured direction (270° - 20°) per season. 01-03-2013 till 28-02-2019. In between brackets the distribution over the ideal wind days*

| | Spring | Summer | Autumn | Winter* | Total days |
|---|---|---|---|---|---|
| Total days per season | 65 (25.7%) | 53 (20.9%) | 67 (26.5%) | 68 (26.9%) | **253** |
| Percentage of total days | 65/552 (11.6%) | 53/552 (9.6%) | 67/546 (12.3%) | 68/541 (12.6%) | **253/2191 (6.8%)** |

**Winter starts at December till February 28th next year*

### 5.3.2 Precipitation, Temperature and Solar radiation

In Figure 10, the monthly sum of precipitation and the average temperature is presented. Considering the average temperature, it showed a constant annual trend with the lowest temperatures in winter and highest in summer. However, precipitation showed a less constant trend varying from year to year. In Figure 36 the precipitation, temperature and solar radiation are presented on a seasonal scale.

Corresponding with the monthly precipitation sum, the seasonal sum also varied annually. Generally, the largest precipitation sum was measured during autumn and the least in spring. 2017 was the wettest year with a total sum of 907 mm precipitation. This was followed by the driest year with a total amount of only 567 mm. That is 117 mm less than in 2013 which is the next least precipitation year. Overall, 2018 was marked as a drought year in The Netherlands, resulting in large water deficits around the country (KNMI, 2019).

Temperature and solar radiation remain rather constant over time. For the temperature, the only significant change occurs in summer 2018 and 2019 when the temperature increased with 1 °C compared with previous years. Overall, temperatures were lowest in winter, followed by spring and

autumn. The difference in annual trend for solar radiation and the temperature was that the solar radiation was high in spring (170 W/m$^2$) and significantly lower in autumn (80 W/m$^2$). Season based, the solar radiation was constant over the study period with a slight increase (+10 W/m$^2$) in summer 2018 and 2019.

As mentioned in the background relative humidity is an important driver to determine the amount of possible sediment transport. Even though these measurements were not available we could assume the following findings in Bauer et al. (2009): The relative humidity is often inverse to temperature and increases with larger precipitation sum.

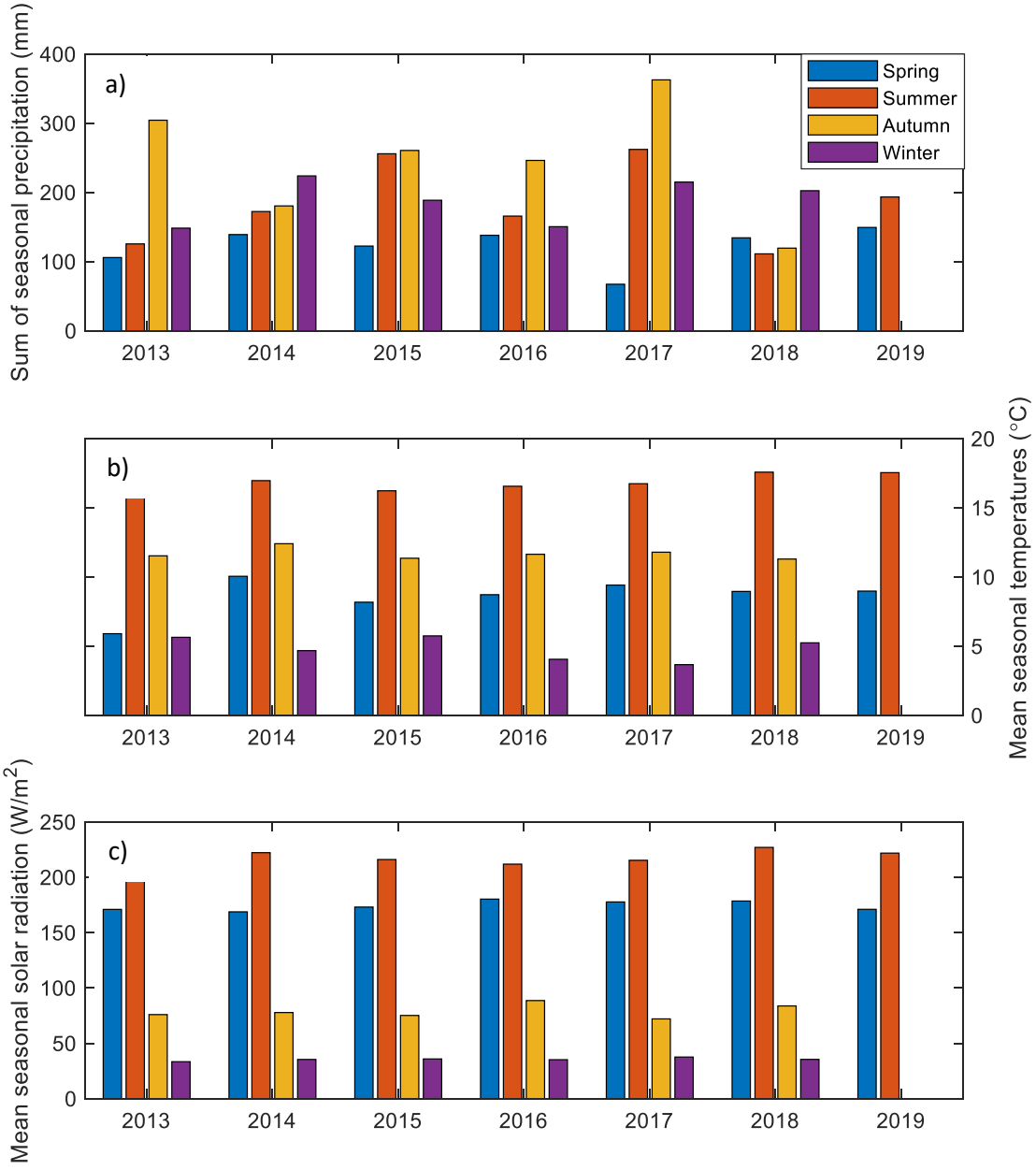


*Figure 36 - Seasonal averaged meteorological data, a) sum of precipitation, b) mean temperature, c) mean solar radiation.*

# 6. Discussion

The different abiotic and biotic morphological aspects present in the blowout complex are still experiencing significant changes on seasonal and annual time scales. The dune area is still net gaining sand over the study period as was also the case during the preceding period from initiation onwards as described by Arens, Slings, et al. (2013). On biotic scale vegetated areas were regaining large surface areas and remained present year-round. By separately discussing the 3-dimensional abiotic (sand volume) and 2-dimensional (landcover) development behaviour on the first hand, the most significant findings will be clarified. Combining both data sets with the filtered climate data, the aim is to eventually couple the abiotic and biotic data to discuss the area's position within in bio-geomorphological development cycle.

## 6.1 Sediment transport over the blowout complex

The processed LiDAR data maps as presented in Figures 17c and 20 showed that the area is morphological active, with on the first sight no significant signs of decreasing dynamic activity. Changes in height and sand volume were present and widely distributed over the total area. Along the landward border between the blowout complex and the vegetated hinterland, a clear division in morphological activity was visible.

### 6.1.1 Dune mobility

The net elevation change over the period 2013 – 2019 (Figure 17c) showed the general pattern of accretion at the locations of the foredunes and back dunes and depletion at the valley in between. The height increase per location did not simply imply an increase at that particular location as the blowout complex migrates landward as found with the four cross-shore transects (Figure 19). The landward migration is in line with the previous observations in Arens et al. (2007) and Rijkswaterstaat et al. (2014). In the latter report, a landward migration between 50 and 200 m was measured for the period 1995 – 2013 what averages to 7 m/year and was described as a transgressive dune field. The average annual migration of the dunes for the period 2013 – 2019 was found to be 2-3 m/year, which is significantly lower than the rate found averaged over the preceding period. Within the study period, no clear change in migration trend was found. The significant difference between the two periods indicates a decline in the dune mobility and that the back dune row may start to become fixed. Another indication for this is the changing shape of the back dune row. From 2013 till 2019 the transgressive dune row has developed into an interconnected chain with a more U-(parabolic) shape. The formation of the parabolic shape is an important indication for a stabilizing blowout (Carter et al., 1990; Duran & Moore, 2013; Hesp, 2002). In general, the formation of this shape is mainly initiated by the decrease of sediment erosion over the deflation basin and the coupled regrowth of vegetation along the borders, so similar to the blowout evolution (Duran & Moore, 2013; Hesp, 2012).

To label the back dune row as parabolic dunes is for further discussion as the study area's morphology slight differs with the general morphology expected by the formation of parabolic dunes. In the study area no clear defined elongated deflation basin and depositional lobe from the notch towards the back dunes could be defined from the DEM as described in the literature (e.g. Hesp, 2002, 2012; Pye and Tsoar, 2008). However, seaward of the parabolic shape, erosion of the valley floor has occurred as seen in Figure 17c and the transects in Figure 20. The width of the erosional area does match the width of the parabolic curvature (400-500 m) much better than the width of the foredune trough notches (~50 m). It seems that the curvature is not one-by-one correlated with the notches, as more foredune notches are present than parabolic shapes, but with the erosional area in the valley. Therefore, this parabolic shape seems to result from aeolian activity within the region rather than be forced from the initial trough blowouts. Moreover, the width could be possibly explained by the average direction of the blowout axis (320°) in combination with the changing wind directions (Figure 11 & 34). An

elongated parabolic dune will form in the direction of the prevailing wind direction. If the wind direction is varying, shapes could become less pronounced as the jet flow is minimized (Hesp, 2012). As the blowout complex is not orientated in the direction of the prevailing wind direction (SW), it is expected to find a less textbook defined shaped feature. In addition, vegetation type and density play a vital role in the stabilization process. On the visual PlanetScope scenes, it is visible that vegetation has settled around the edges of the convex shape. Moreover, the type of vegetation cover seen at the horns shows a different spectral signal than at the landward facing bays. This vegetation type might be more resistant to burial and will therefore keep the sand in place (Maun, 1998). This eventually results in the parabolic shape to become more pronounced over time (Pye & Tsoar, 2008).

On average the foredunes increased in elevation and widened in the seaward direction. In contrast to the back dunes, the amount of foredune migration varied per location instead of a joint migration seen at the back dunes. In the eastern part (X: 2850 – 3650 m) the foredune showed a slight landward shift. The difference between this part and the western part based on visual imagery is the vegetation cover at the foredune's crest. The same issue applies to the difference between de fore- and back dunes. According to Tsoar (2005), dune mobility is determined by a hysteresis between vegetation cover and wind power (Figure 8). As the wind power could be assumed the same for fore- and back dunes the vegetation cover is decisive for the difference in mobility.

So overall, the transgressive dune field behind the foredunes shows signs of a decreasing abiotic activity as the dune migration rate decreased compared to the preceding years. This process could be caused by the increased foredune volume and the (re)-emergence of vegetation. This abiotic and biotic evolutions are catching-in sand and prevent it to be transported further into the valley and back dunes, resulting in less dynamic back dunes.

### 6.1.2 Changes in sand volumes

Over the six-year study period, the total study area increased in volume as was in line with the beforehand expected and hoped results of the remobilization project (Arens et al., 2007). The total volume increased with 4.65 $x10^5$ $m^3$ or 18.5 $m^3$/m/year. In the preceding period (1997-2013) Rijkswaterstaat monitored the volume change in the western area between pole 15.5 and 18. This area is roughly half the size of this studies research area. They measured the volume every five years and found an average volume increase of 1.80 $x10^5$ $m^3$ over five years or 15.6 $m^3$/m/year, without major differences in volume change among the five years. Moreover, Keijsers et al. (2014) measured the dune volume change on Terschelling just west of the study area, between pole 9 – 16. Here the foredune row has remained fixed, resulting in sand deposition on the seaward side of the foredunes. They measured dune volume change rates in the order of ~15 $m^3$/m/year, corresponding rather well with the results of this study and the measurements by Rijkswaterstaat et al. (2014). The slightly higher volume change rate found in this study may possibly be caused by a large sand wave that migrated along the coast in the eastern direction. In 2014 it was located near pole 16, in the western part of the study area (Rijkswaterstaat et al., 2014). Its presence resulted in a ca. 7 m/year seaward expansion of the beach (MKL-trend). This increased the wave energy absorption ability of the beach resulting in an increase of actual sand volume that could be transported into the dunes. Although the actual sand volume increased and the beach widened (increasing water safety) it does not automatically result in an increase in volume change rates as was presented in Keijsers et al. (2014). For beaches exceeding widths of 200 m the volume change rates remained constant at Terschelling (~15 $m^3$/m/year). For reference, the beach at the study area has a width of approx. 250 m.

That the volume change rates are almost independent to beach width could for a large extend be accounted to meteorological variables. The most important driver to transport new sand into the dunes is the wind when exceeding a certain threshold and blows from the desired direction (here: 270°

- 20°) (e.g. Gares & Nordstrom, 1995; Hesp, 2002; Hesp & Hyde, 1996; Liu et al., 2005). This threshold is mainly determined by the soil moisture content of the beach, which is controlled by tides, waves, precipitation and temperature (Bauer et al., 2009; Delgado-Fernandez & Davidson-Arnott, 2011). Comparing the unrealistic volume increase encountered between spring 17/18 (89.3 $m^3$/m/year) with the corresponding precipitation and temperature data in Figure 36, it shows an unexpected relation. 2017 was the wettest year during the study period and temperature was similar to the preceding years. Furthermore, although the favoured wind events in 2017 were maximum, the difference with the surrounding years was not larger enough to be responsible for the sand volume increase in combination with the large amounts of precipitation. With this combination of meteorological factors it is not expected that the volume change rate at 17/18 would be seven times larger than the volume change the year before. This strengthens the assumption that the 2018 elevation data includes a significant measurement error as the volume change rate of 89.3 $m^3$/m/year is physically impossible with the local meteorological conditions.

Based on the volume change rates found in Rijkswaterstaat et al. (2014) and Keijsers et al. (2014) the expected total volume increase over the study period would be approx. 3.75 x$10^5$ $m^3$ instead of the found 4.65 x$10^5$ $m^3$ (18.5 $m^3$/m/year). Therefore, the measurement error over the total study period amounted ~+0.9 x$10^5$ $m^3$ or ~+0.04 m, which is more than double the amount of allowed error margin of the LiDAR altimetry data (0.015 m) (Rijkwaterstaat Kwaliteitsdocument laseraltimetrie, 2013).

### *Volume change district correlation*

The volume change in the first year (13/14) deviates from the preceding years as the volume change for all three districts were negative. This was unexpected considering the positive volume growth trend of the previous years. This unexpected volume loss could be explained by one extreme surge event, the “Sinterklaasstorm” which occurred December 5th and 6th. During this event wind speeds over 30 m/s or 11-12 Bft, directed out of the northwest were measured. The peak water level was 2.66 m +NAP, submerging the total beach and caused erosion along the foredunes (RWS WaterInfo, 2020). The storm removed the embryo dunes along the entire study area’s coastline and the dune valley was partly inundated preventing aeolian transport (Rijkswaterstaat et al., 2014).

For the first three years, the volume gain or loss within the dunes exceeded the volume gain or loss on the beach, from 16/17 onwards this reversed (Figure 22). Moreover, the differences in volume change between the beach and dunes became roughly 10 times smaller regardless of the total change. An explanation for this reversal could be the re-emerging of embryo dunes in front of the foredunes which were removed in 2013. The embryo dunes retain sand that otherwise would be transported into the dunes. The elevation increase seen over the last three years in front of the foredunes may therefore be assigned to the formation of embryo dunes (Figure 37). This corresponds with the evolution process found in section 6.1.1.

The hinterland elevation change was expected to be minimal. This was found for all years except 17/18 and 18/19, where the changes almost cancel each other out. This unexpected change will be accounted to the measurement error discussed above.

*Notches*

Only one out of the eight selected notches (N8) showed significant erosion. With a rate of 1462 $m^3$/year the notch becomes deeper and wider. The axis of this notch is the most westward orientated of all notches, experiencing the most effective winds. All other notches seem the fill-up and losing the defined V/U-shape, possibly resulting in a reduced jet flow. Oblique incoming winds become less efficient to transport sand into the dunes supporting this negative feedback mechanism (Hesp & Hyde, 1996). Therefore, it is expected that most of the notches will slowly become less effective and

eventually close up or merge, with the help of returning vegetation as already could be seen on the foredune crests. If the notches close sand will be transported to a lesser extent into the dunes, reducing the positive volume change. This trend is already visible in the area when excluding the 17/18 volume change, compared to the 1995 – 2013 period.

*Correlation with wind data and limitations*

The in Figure 35 presented amount of days per year that according to literature would result in sediment transport into and over the dunes matches the trend in volume change relatively well. This in combination with the results in Jungerius et al. (1991) that average wind speeds, in direction of the blowouts axis, will cause the most long term changes to the system, strengthens the relationship between the filtered wind results and volume change. Per definition, the wind conditions are not the only force explaining volume change as mentioned in the background. The largest transport rates could be expected in winter and spring when the air temperatures are lowest, precipitation is least and vegetation density is lowest (Figure 36). Colder air has a larger transport potential than warm humid air (Bagnold, 1941).

The limiting factor in correlating the abiotic morphological evolution with weather data could be accounted to the data availability of the LiDAR data (once per year). Within a year the weather is highly variable and alters the landscape in a non-linear way, this could not be seen when comparing annual DEM's. An additional but smaller limitation is the pixel size conversion. To compare the LiDAR data with the PlanetScope scenes the data points were averaged to form the 3x3 m pixel size. This had mainly consequences for the detection of embryo dunes, which are often smaller than 9 $m^2$ and would therefore not be detected as an object.

## 6.2 Landcover changes and seasonal variability

The amount of vegetation cover showed large seasonal variability throughout the three years (Sept 2016 – Aug 2019). The peaks in vegetation surface area all appeared halfway autumn followed by a rapid decline till mid-spring. Each year the vegetated area in autumn increases compared to the previous year with ~60.000 $m^2$ (~4%). The regrowth of vegetation is determined by mostly abiotic climate effects and the plant's ability to survive under changing dynamic conditions (e.g. Maun, 1998; Schwarz et al., 2018). The location of the regrowth is mainly concentrated inside the dune valley as is circled in Figure 37. Below the surface of the valley, a large freshwater bubble has developed and nutrients were deposited by the sand spray from the beach, favouring vegetation regrowth and reducing soil erosion (Barchyn & Hugenholtz, 2013; Pye et al., 2014; RWS & SBB, 2015).

### 6.2.1 Seasonal vegetation regrowth

The total landcover surface area change for autumn, winter and summer in 17/18 significantly exceeded the change found between 18/19. Furthermore, a larger area had changed from sand into vegetation than reversed. This indicates an increasing regrowth of vegetation relative to the sediment transport. Large vegetation growth rates are expected by a combination of the following factors: average low wind speeds, high precipitation, long growing season and sufficient nutrient availability (Pye et al., 2014). This combination will eventually result in a stabilizing blowout. The winters of 17/18 and 18/19 were labelled as mild winters, relatively warm and wet by the KNMI. Such mild winters allow the majority of the vegetation to survive and increase the length of the growing season. Considering year-round precipitation the year 2017 peaked with 907 mm. In contrast, 2018 was marked as a drought year with a precipitation sum below the long-term average (567 mm). This accompanied with average 1°C higher temperatures. Furthermore, the number of days with strong winds peaked in 2017 (57), mainly concentrated in autumn (21), when vegetation resilience is largest. In 2018 the peaks of strong winds were in winter (18). Combining these mentioned abiotic climate characteristics draws the

conclusion that the year 2017 was more favourable for vegetation regrowth than 2018, which supports the findings in the seasonal landcover change maps. The wind characteristics are less important as was found that most vegetation increases concentrated inside the dune valley, isolated from open wind fields.

Contrary to the other seasons, in spring the dominating landcover change was from vegetation into sand. In spring the vegetation area was minimal as the growing season still needs to start. So, vegetation is less resilient to abiotic forcing (Schwarz et al., 2018). Therefore, strong winds have a larger effect during spring/end of winter than during the other seasons, resulting in more deposition. Therefore, it is assumed that dominating landcover change in the area could be linked to the vegetation growth cycle.

So, the re-emergence of vegetation seems to reduce the aeolian transport activity in the blowout complex. This could be seen when comparing the 17/18 to the 18/19 vegetation in to plant change area. Even though 2018 was theoretically a more favourable year for aeolian sand transport than 2017, the area changed into sand was less than in 2017, probably due to the increased vegetation cover.

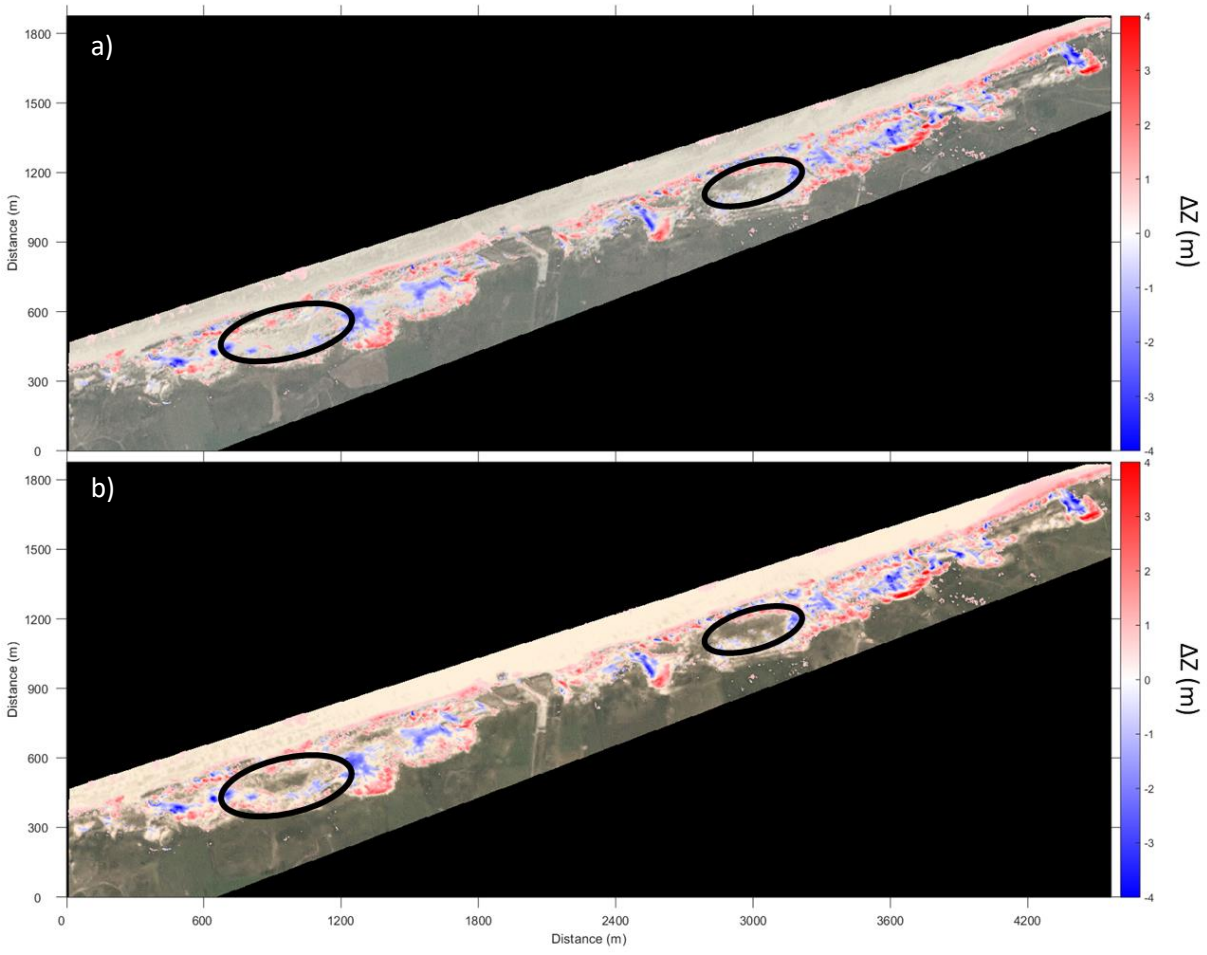


*Figure 37 - Comparison of vegetation cover for a) the first available image (16-09-2016) and b) the last available image (28-08-2019) combined with elevation change over the study period ($\Delta Z_{2019}$ - $\Delta Z_{2016}$). ΔZ ±0.5 m is not shown for clarity.*

### 6.2.2 Vegetation regrowth at notches and model limitations

The used classification model with a pixel resolution of 3x3 m found no significant increase of vegetation regrowth around or inside the foredune notches. By further visual inspection, small patches of vegetation seemed to return within the notches, at least in summer and autumn. The regrowth of

vegetation inside or on the edge of the deflation basin is another indication for blowout closure (Hesp, 2002). The filling up of the notches and the decrease of the jet flow, except for N8, presumably passed a certain threshold for the local vegetation species to start colonizing the deflation basin.

The difference in observations by the classification model created maps and visual inspection shows an important model limitation. The newly emerging vegetation patches were less dense and often smaller than the 9 $m^2$ pixel size are therefore harder to detect based on its spectral signal. The average spectral signal may show a closer correlation with the mean spectral signal of sand than vegetation, resulting in a misinterpretation by the model. Therefore, the amount of vegetation could have been underestimated by the classification model. To decrease this error, for further research it is advised to add an additional landcover class, rather than only vegetation and sand. Furthermore, the visual quality of the image plays an important role (e.g. illumination, viewing angle) in the quality of classification. With low illumination the spectral signals of the landcover classes are less distinct resulting in a larger chance of wrong classification. In this light, the quality of the classifications for the winter imagery should be considered less viable than for the other seasons. This also coincides with the fact that in winter the image density is much lower than across the other seasons.

## 6.3 Change in bio-geomorphologic stage

By combining the effects of abiotic and biotic changes in the blowout complex as described in part 6.1 and 6.2 it is possible to position the study area within the blowout development cycle as presented by Schwarz et al. (2018). In part 6.2 it turned out that the regrowth of vegetation is the leading process for at least the last three years. An important indicator to investigate the relation between the return of vegetation and the abiotic sand transport is the burial rate of vegetation.

### 6.3.1 Vegetation return versus accretion rate

The cross-shore transect 1 (Figure 19) crosses the large returning vegetational area indicated in the western part in Figure 37. Between 190 – 240 m the bed-elevation develops from a slightly alternating bed into a more smooth plane. The elevation changes between 2013 – 2016 are larger than for the period 2016 – 2019 which is presumably linked to the return of the vegetation seen in Figure 37. To investigate this into more detail the landcover change maps and LiDAR elevation maps will be combined to be able to investigate this on centimetre scale.

This centimetre scale is important regarding the burial tolerance of vegetation. Recent personal field observations (01-02-2020) found that the dominating returning vegetation type is European Marram grass (*Ammophila Arenaria*), wherein the valleys a wider variety of vegetation types were found. *Ammophila Arenaria* has two important characteristics considering aeolian sand deposition: 1) a high burial tolerance and 2) a positive feedback on growth with sand burial (Nolet, van Puijenbroek, Suomalainen, Limpens, & Riksen, 2018). It could survive burial rates maximizing 0.9 m per growing season (Nolet et al., 2018; Ranwell, 1958). In Figure 38 the landcover and elevation change maps were combined and indicate the amount of sand deposition at a certain landcover change. It is seen that at the vegetation regrowth areas deposition hardly exceeds 0.2 m over the two year period. Furthermore, Nolet et al. (2018) found that the ideal deposition rate for *Ammophila Arenaria* growth is around 0.3 m/growth season, being much larger than found in the area. Along the borders of the new vegetation areas, the sand deposition often exceeds 0.5 m, which could support the expansion of the *Ammophila Arenaria* in the future.

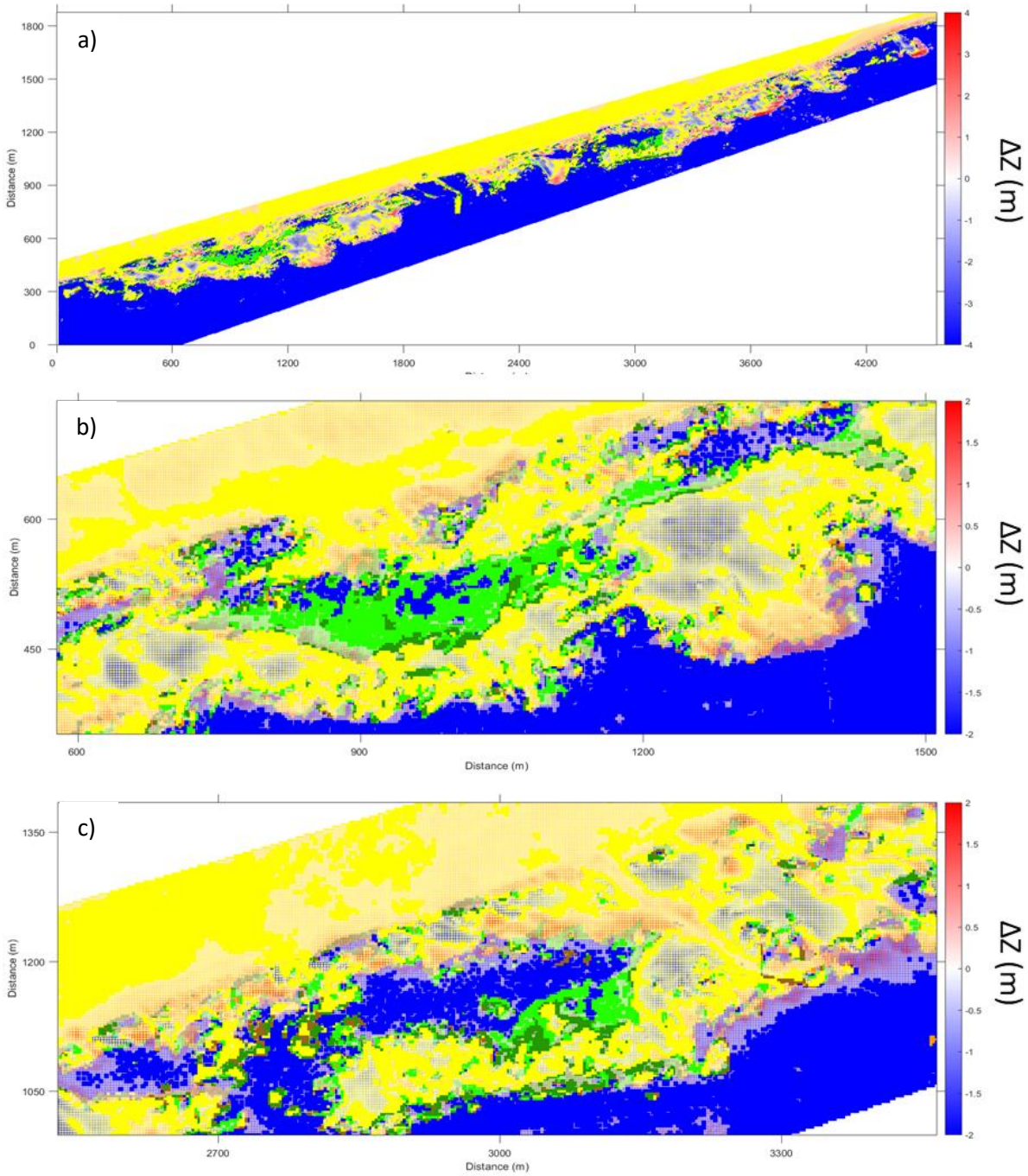


*Figure 38 - Combination of the 2D (landcover change) and 3D (bed-elevation change) for the period autumn 2017 -2019. a) An overview of the total study area, ΔZ ±0.5 m is not shown for clarity. b) and c) are zoomed in to the largest vegetation regrowth locations circled in Figure 38. Here ΔZ +0.2 m - -0.05 m is not shown for clarity. Note that the scale for a) is different than for b) and c). For the legend of the landcover map, the reader is referred to Figures 30 – 33.*

On the zoomed figures it is striking that on the seaward side of the large vegetation areas sand is accreting where on the landward side more erosion takes place. This could be explained by the fact that due to the appearance of vegetation drag increases and forces the sand to be deposited (Bagnold, 1941). This again probably promotes the marram grass to expand. When the wind passed the vegetated area the drag decreases and is able to accelerate, increasing ability to transport the sand landward.

From Figure 38 and the study by Nolet et al. (2018), it is highly presumable that the *Ammophila Arenaria* will survive and recolonize its surroundings. Other dune vegetation is often less burial tolerant and will be able to settle with burial rates between 0.01 – 0.1 m (Maun, 1998). In Table 11 the average deposition per landcover change area (17/18 & 18/19) is presented for autumn. Despite the overestimated elevation data of 17/18, the depositional rates seem also be favourable for less burial tolerant species to settle.

*Table 11 - Mean elevation change (ΔZ (m)) per year split per classified change area as presented in Table 9 for the dune area. The fourth column is the sum of elevation change over the two years. Note that the 17/18 elevation data is overestimated as discussed in section 6.1.*

| **Burrow threshold (m)** | **Autumn** | | |
|---|---|---|---|
| | *17/18* | *18/19* | *17 – 19* |
| **No change vegetation** | 0,20 | 0,05 | 0,26 |
| **Sand → Plant (17/18)** | 0,22 | 0,04 | 0,25 |
| **Sand → Plant (18/19)** | 0,22 | 0,05 | 0,27 |
| **New plant area** | 0,22 | 0,04 | 0,25 |
| **New sand area** | 0,29 | 0,13 | 0,41 |
| **Difference elevation change sand – plant area** | 0,06 | 0,09 | 0,16 |

### *Vegetation versus sand*

At the areas that changed into sand the mean elevation increased 0.16 m more than the areas that changed into vegetation. This is in line with findings in e.g. Gares & Nordstrom (1995), Hesp (2002). They presented that at areas where vegetation is returning the increment of the sand should be below a certain threshold so plants are able to settle. The other way around, at locations where vegetation landcover is changing into sand the aeolian transport should exceed that certain threshold. With the currently available data, it remains hard to assign a fixed threshold range for the blowout complex. As the biodiversity in the dunes increases, multiple types of vegetation appear, desiring different conditions to flourish. For further research it would be interesting to focus solely at the large new vegetation patches, this will result in a more reliable result as extremes are filtered out. For example pioneer vegetation on top of embryo dunes which often experiences much larger burial rates than vegetation within the valley. Moreover, for such research it would be desired to use elevation data that was collected at dates corresponding with the dates used for the change maps.

Overall, the accretion rates found for 2016 till 2019 agree with rates mentioned by Maun (1998), to support the regrowth of vegetation. The burial tolerant species as *Ammophila Arenaria* should have survived the accounted elevation changes. Closer to the centre of the vegetation patches elevation decrease is close to zero. This supports even burial-intolerant species to reproduce and increasing the biodiversity.

Now there are an increasing amount of indications that the intensity of biologic interactions intensify and overrule the effect of the abiotic forces. This indicates that the Terschelling blowout complex is developing more and more towards the ecological development stage and decreasing the strength of bio-geomorphological interactions. This could be explained as a shift towards the ecological phase as was conceptually described by Corenblit et al. (2015) and presented in Figure 5.

# 7. Conclusions

This study was conducted to get more insight on recent morphological and vegetational change of the large blowout complex at Terschelling that was initiated in 1995 to remobilize the foredunes. Combining daily to seasonal multispectral and annual altimetry data made it possible to couple the abiotic and biotic mechanisms and learn their relative importance as the driving force on the ever-changing morphology.

The largest morphological changes have, as expected, occurred within the dune area where the extremes in elevation intensified. Both the fore- and back dunes showed indications of stabilisation, an increase in elevation and a decrease in landward migration. The valley in between the dunes had become wider and deeper at locations where vegetation was absent. Over the years 2016 – 2019 the beach increased in volume, which could largely be accounted to the formation of embryo dunes on the seaward side of the foredunes. The net volume for the vegetated hinterland only slightly increased. Over the six-year study period, the total area experienced a net volume increase of 4.65 $x10^5$ $m^3$ of which the largest part could be assigned to the dune area (2.65 $x10^5$ $m^3$). This indicates that the effect of the foredune excavation is still significant for remobilizing the back dunes. An important side note to the total volume increase is the staggering and unexpected volume increase of 3.75 $x10^5$ $m^3$ between spring 2017 and 2018. As there was no clear documentation available of its origin it should be interpreted with great care and a measuring error could not be excluded. Assuming the volume change rates presented in additional studies the net volume change would have been approx. 3.75 $x10^5$ $m^3$ instead of 4.65 $x10^5$ $m^3$.

At the time that dunes showed strong indications of reduced abiotic activity the area of the vegetated surface increased. The regrowth of vegetation shows seasonal behaviour with increasing peaks in autumn with a total increase of 116.000 $m^2$ between 2016 – 2018. The amount of emerged vegetation per season shows a correlation with the local weather conditions. The largest vegetational regrowth areas had arisen during the year with the largest seasonal precipitation sums and average temperatures. When vegetation emerged within the valley, erosion/deposition rates dropped to almost zero. In contrast, at the foredunes the accretion rates increased at the time vegetation resettled. At the same time, the majority of the excavated notches started to fill in although a strong correlation with the regrowth of vegetation was not found. Despite this, the indications of decreasing abiotic morphologic activity and the intensified biologic interactions in the system, indicate a shift within the bio-geomorphological succession on blowout development. Over six years the system shifted more and more towards the ecological development phase resulting in a decrease in dynamic activity.

Despite the shift towards a more ecological development phase, the blowout complex is currently still expanding landward and showing a positive volume change. In addition, due to the widening of the beach, the hinterland becomes less prone to erosion during future storm events. Overall, the morphological changes have increased the water safety during the study period, taking away concerns of the *Eilanders*. Therefore, it could be concluded that the morphological change due to dune remobilization still results in more advantages than challenges, even 25 years after initiation.

# References


Arens, S. M., Loffler, M. A. M., & Nuijen, E. M. (2007). *Evaluatie dynamisch kustbeheer Friese Waddeneilanden*.

Arens, S.M., Slings, Q., & de Vries, C. N. (2004). Mobility of a remobilised parabolic dune in Kennemerland, The Netherlands. *Geomorphology*, *59*(1–4), 175–188. https://doi.org/10.1016/j.geomorph.2003.09.014

Arens, S. M., Mulder, J. P. M., Slings, Q. L., Geelen, L. H. W. T., & Damsma, P. (2013). Dynamic dune management, integrating objectives of nature development and coastal safety: Examples from the Netherlands. *Geomorphology*, *199*, 205–213. https://doi.org/10.1016/j.geomorph.2012.10.034

Arens, S. M., Slings, Q. L., Geelen, L. H. W. T., & Van der Hagen, H. G. J. M. (2013). *Restoration of Coastal Dunes in The Netherlands*. (M. L. Martínez, J. B. Gallego-Fernández, & P. A. Hesp, Eds.), *Restoration of Coastal Dunes*. Berlin, Heidelberg: Springer Berlin Heidelberg. https://doi.org/10.1007/978-3-642-33445-0

Bagnold, R. A. (1941). The physics of blown sand and desert dunes: New York. *William Morrow & Company*.

Barchyn, T. E., & Hugenholtz, C. H. (2013). Reactivation of supply-limited dune fields from blowouts: A conceptual framework for state characterization. *Geomorphology*, *201*, 172–182. https://doi.org/10.1016/j.geomorph.2013.06.019

Bauer, B. O., Davidson-Arnott, R. G. D., Hesp, P. A., Namikas, S. L., Ollerhead, J., & Walker, I. J. (2009). Aeolian sediment transport on a beach: Surface moisture, wind fetch, and mean transport. *Geomorphology*, *105*(1–2), 106–116. https://doi.org/10.1016/j.geomorph.2008.02.016

Byrne, M. L. (1997). Seasonal sand transport through a trough blowout at Pinery Provincial Park, Ontario. *Canadian Journal of Earth Sciences*, *34*(11), 1460–1466. https://doi.org/10.1139/e17-118

Carter, R., Hesp, P., & Nordstrom, K. (1990). Erosional landforms in coastal dunes. In *Coastal Dunes: Form and process* (pp. 217–250).

Cheplick, G. P., & Grandstaff, K. (1997). Effects of sand burial on purple sandgrass (Triplasis purpurea): The significance of seed heteromorphism. *Plant Ecology*, *133*(1), 79–89. https://doi.org/10.1023/A:1009733128430

Clemmensen, L. B., Hansen, K. W. T., & Kroon, A. (2014). Storminess variation at Skagen, northern Denmark since AD 1860: Relations to climate change and implications for coastal dunes. *Aeolian Research*, *15*, 101–112. https://doi.org/10.1016/j.aeolia.2014.09.001

Corenblit, D., Baas, A., Balke, T., Bouma, T., Fromard, F., Garófano-Gómez, V., … Walcker, R. (2015). Engineer pioneer plants respond to and affect geomorphic constraints similarly along water-terrestrial interfaces world-wide. *Global Ecology and Biogeography*, *24*(12), 1363–1376. https://doi.org/10.1111/geb.12373

Davidson-Arnott, R. G. D., & Law, M. N. (1996). Measurement and Prediction of Long-Term Sed Supply to Coastal Foredunes. *Journal of Coastal Research*, *12*(123), 654–663. Retrieved from http://www.jstor.org/stable/4298513%0Ahttp://about.jstor.org/terms

Delgado-Fernandez, I., & Davidson-Arnott, R. (2011). Meso-scale aeolian sediment input to coastal dunes: The nature of aeolian transport events. *Geomorphology*, *126*(1–2), 217–232.

https://doi.org/10.1016/j.geomorph.2010.11.005

Duran, O., & Moore, L. J. (2013). Vegetation controls on the maximum size of coastal dunes. *Proceedings of the National Academy of Sciences*, *110*(43), 17217–17222. https://doi.org/10.1073/pnas.1307580110

Earth Observing System, 30 August 2019. NDVI FAQ: ALL YOU NEED TO KNOW ABOUT NDVI. Retrieved 5 January 2020, from https://eos.com/blog/ndvi-faq-all-you-need-to-know-about-ndvi/

Gares, P. A., & Nordstrom, K. F. (1995). A Cyclic Model of Foredune Blowout Evolution for a Leeward Coast : Island Beach , New Jersey All use subject to https://about.jstor.org/terms A Cyclic Model of Foredune Blowout Evolution for a Leeward Coast : Island Beach , New Jersey. *Annals of the Association of Amercan Geographers*, *85*(1), 1–20.

Gonzalez-Villanueva, R., Costas, S., Duarte, H., Perez-Arlucea, M., & Alejo, I. (2011). Blowout evolution in a coastal dune: using GPR, aerial imagery and core records. *Journal of Coastal Research*, (64), 278–282.

Hesp, P. (1983). Morphodynamics of Incipient Foredunes in New South Wales, Australia. In *Developments in Sedimentology* (Vol. 38, pp. 325–342). https://doi.org/10.1016/S0070-4571(08)70802-1

Hesp, P. (1989). A review of biological and geomorphological processes involved in the initiation and development of incipient foredunes. *Proceedings of the Royal Society of Edinburgh. Section B. Biological Sciences*, *96*(May), 181–201. https://doi.org/10.1017/s0269727000010927

Hesp, P. (2002). Foredunes and blowouts: initiation, geomorphology and dynamics. *Geomorphology*, *48*(1–3), 245–268. https://doi.org/10.1016/S0169-555X(02)00184-8

Hesp, P. (2012). *Dune Coasts*. *Treatise on Estuarine and Coastal Science* (Vol. 3). Elsevier Inc. https://doi.org/10.1016/B978-0-12-374711-2.00310-7

Hesp, P. A., & Thom, B. G. (1990). Geomorphology and evolution of active transgressive dunefields. In K. F. Nordstrom, N. Psuty, & R. W. G. Carter (Eds.), *Coastal Dunes: Form and process* (pp. 253–288). Wiley, New York.

Hesp, P., & Hyde, R. (1996). Flow dynamics and geomorphology of a trough blowout. *Sedimentology*, *43*(3), 505–525. https://doi.org/10.1046/j.1365-3091.1996.d01-22.x

Jungerius, P. D., & van der Meulen, F. (1989). The development of dune blowouts, as measured with erosion pins and sequential air photos. *Catena*, *16*, 369–376.

Jungerius, P. D., Witter, J. V., & van Boxel, J. H. (1991). The effects of changing wind regimes on the development of blowouts in the coastal dunes of The Netherlands. *Landscape Ecology*, *6*(1–2), 41–48. https://doi.org/10.1007/BF00157743

Keijsers, J. G. S., Poortinga, A., Riksen, M. J. P. M., & Maroulis, J. (2014). Spatio-temporal variability in accretion and erosion of coastal foredunes in the Netherlands: Regional climate and local topography. *PLoS ONE*, *9*(3). https://doi.org/10.1371/journal.pone.0091115

Lithgow, D., Martínez, M. L., Gallego-Fernández, J. B., Hesp, P. A., Flores, P., Gachuz, S., … Álvarez-Molina, L. L. (2013). Linking restoration ecology with coastal dune restoration. *Geomorphology*, *199*, 214–224. https://doi.org/10.1016/j.geomorph.2013.05.007

Liu, L. Y., Skidmore, E., Hasi, E., Wagner, L., & Tatarko, J. (2005). Dune sand transport as influenced by wind directions, speed and frequencies in the Ordos Plateau, China. *Geomorphology*, *67*(3–4), 283–297. https://doi.org/10.1016/j.geomorph.2004.10.005

Löffler, M., Landwijzer, B., Goessen, P., & Hollands, H. (2016). Dynamisch kustbeheer - Kustveiligheid en natuur profiteren van stuivend zand, 1–5.

Martínez, M. L., Gallego-Fernández, J. B., & Hesp, P. A. (2013). *Restoration of Coastal Dunes*. (M. L. Martínez, J. B. Gallego-Fernández, & P. A. Hesp, Eds.), *Water, Air, and Soil Pollution* (Vol. 143). Springer. https://doi.org/10.1023/A:1022808908500

Martínez, M. L., Hesp, P. A., & Gallego-Fernández, J. B. (2013). Coastal Dunes: Human Impact and Need for Restoration. In M. L. Martínez, J. B. Gallego-Fernández, & P. A. Hesp (Eds.), *Restoration of Coastal Dunes* (pp. 1–14). Berlin, Heidelberg: Springer Berlin Heidelberg. https://doi.org/10.1007/978-3-642-33445-0

Maun, M. A. (1994). Adaptations enhancing survival and establishment of seedlings on coast! dune systems. *Vegetatio*, *111*, 59–70.

Maun, M. A. (1998). Adaptations of plants to burial in coastal sand dunes. *Canadian Journal of Botany*, *76*(5), 713–738. https://doi.org/10.1139/b98-058

Mulder, J. P. M., Hommes, S., & Horstman, E. M. (2011). Implementation of coastal erosion management in the Netherlands. *Ocean and Coastal Management*, *54*(12), 888–897. https://doi.org/10.1016/j.ocecoaman.2011.06.009

Nolet, C., van Puijenbroek, M., Suomalainen, J., Limpens, J., & Riksen, M. (2018). UAV-imaging to model growth response of marram grass to sand burial: Implications for coastal dune development. Aeolian Research, 31(October 2017), 50–61. https://doi.org/10.1016/j.aeolia.2017.08.006

Nordstrom, K. F., & Arens, S. M. (1998). The role of human actions in evolution and management of foredunes in The Netherlands and New Jersey, USA. *Journal of Coastal Conservation*, *4*(2), 169–180. https://doi.org/10.1007/BF02806509

Otsu, N. (1979). A Threshold Selection Method from Gray-Level Histograms. *IEEE*, *9*(1), 62–66. https://doi.org/10.1109/TSMC.1979.4310076

Planet Labs Inc. (2019) PLANET IMAGERY PRODUCT SPECIFICATION: PLANETSCOPE & RAPIDEYE. 1–52. Retrieved from: https://www.planet.com/products/satellite-imagery/files/1610.06_Spec%20Sheet_Combined_Imagery_Product_Letter_ENGv1.pdf

Pluis, J. L. A. (1992). Relationships between deflation and near surface wind velocity in a coastal dune blowout. *Earth Surface Processes and Landforms*, *17*(7), 663–673. https://doi.org/10.1002/esp.3290170703

Provoost, S., Jones, M. L. M., & Edmondson, S. E. (2011). Changes in landscape and vegetation of coastal dunes in northwest Europe: a review. *Journal of Coastal Conservation*, *15*(1), 207–226. https://doi.org/10.1007/s11852-009-0068-5

Pye, K., & Blott, S. J. (2016). *Natural Resources Wales Dune Rejuvenation Trials Overview Report*. Solihull.

Pye, K., Blott, S. J., & Howe, M. A. (2014). Coastal dune stabilization in Wales and requirements for rejuvenation. *Journal of Coastal Conservation*, *18*(1), 27–54. https://doi.org/10.1007/s11852-013-0294-8

Pye, Kenneth, & Tsoar, H. (2008). *Aeolian Sand and Sand Dunes*. *Springer*. Berlin, Heidelberg: Springer Berlin Heidelberg. https://doi.org/10.1007/978-3-540-85910-9

Ranwell, D. (1958). Movement of Vegetated Sand Dunes at Newborough Warren, Anglesey. *Journal of Ecology*, *46*(1), 83–100. Retrieved from https://www.jstor.org/stable/2256905

Rijskwaterstaat (2013), Kwaliteitsdocument Laseraltimetrie Rijkswaterstaat.

Rijkswaterstaat, & Staatsbosbeheer. (2015). *Een levend duinlandschap op Terschelling Duurzame bescherming voor mens en natuur*.

Rijkswaterstaat, Staatsbosbeheer, & Vitens. (2014). *Notitie Ontwikkelingen kustvak paal 15-20 op Terschelling*.

Riksen, M. J. P. M., Goossens, D., Huiskes, H. P. J., Krol, J., & Slim, P. A. (2016). Constructing notches in foredunes: Effect on sediment dynamics in the dune hinterland. *Geomorphology*, *253*, 340–352. https://doi.org/10.1016/j.geomorph.2015.10.021

Ruessink, B. G., Arens, S. M., Kuipers, M., & Donker, J. J. A. (2018). Coastal dune dynamics in response to excavated foredune notches. *Aeolian Research*, *31*, 3–17. https://doi.org/10.1016/j.aeolia.2017.07.002

Samapriya Roy. (2019, September 29). samapriya/porder: porder: Simple CLI for Planet ordersV2 API (Version 0.4.8). Zenodo. http://doi.org/10.5281/zenodo.3464574

Schwarz, C., Brinkkemper, J., & Ruessink, G. (2018). Feedbacks between Biotic and Abiotic Processes Governing the Development of Foredune Blowouts: A Review. *Journal of Marine Science and Engineering*, *7*(1), 2. https://doi.org/10.3390/jmse7010002

Sloss, C.S., Hesp P.A., & Shepherd, M.J., 2012. Coastal Dunes: Aeolian Transport. Nature Education Knowledge 3(10):21 http://www.nature.com/scitable/knowledge/library/coastal-dunes-aeolian-transport-88264671

Tsoar, H. (2005). Sand dunes mobility and stability in relation to climate. *Physica A: Statistical Mechanics and Its Applications*, *357*(1), 50–56. https://doi.org/10.1016/j.physa.2005.05.067

Van Boxel, J. H., Jungerius, P. D., Kieffer, N., & Hampele, N. (1997). Ecological effects of reactivation of artificially stabilized blowouts in coastal dunes. *Journal of Coastal Conservation*, *3*(1), 57–62. https://doi.org/10.1007/BF02908179

Van der Valk, L., Reinders, J., van der Spek, A. J. F., & Gelder-Maas, C. van. (2013). *Voorbeelden van dynamisch kustbeheer Een inventarisatie van dynamisch kustbeheer- Voorbeelden van Dynamisch*.

Weier, J., & Herring, D., 2000. Measuring Vegetation (NDVI & EVI). Retrieved 5 January 2020, from https://earthobservatory.nasa.gov/features/MeasuringVegetation/measuring_vegetation_1.php

Zarnetske, P. L., Ruggiero, P., Seabloom, E. W., & Hacker, S. D. (2015). Coastal foredune evolution: the relative influence of vegetation and sand supply in the US Pacific Northwest. *Journal of The Royal Society Interface*, *12*(106), 20150017–20150017. https://doi.org/10.1098/rsif.2015.0017

Zhang, J., & Maun, M. A. (1990). Effects of sand burial on seed germination, seedling emergence, survival, and growth of Agropyron psammophilum. *Canadian Journal of Botany*, *68*(2), 304–310. https://doi.org/10.1139/b90-041

**Websites:**

KNMI, 2019. Klimatologie, Daggegevens van het weer in Nederland – Download. Retrieved 14 October 2019, from http://projects.knmi.nl/klimatologie/daggegevens/selectie.cgi

KNMI, Summary on seasonal weather. Retrieved from: https://www.knmi.nl/nederland-nu/klimatologie/maand-en-seizoensoverzichten/

MathWorks, 2019. MATLAB Documentation (Help). From https://nl.mathworks.com/help/matlab/

Rapidlasso GmbH, 2019. Retrieved 5 November 2019, from: https://rapidlasso.com/lastools/

Rijkswaterstaat, 2020. Waterinfo. Retrieved 18 January 2020, from: https://waterinfo.rws.nl/#!/nav/bulkdownload/periode-selectie/

# Appendices

## Appendix 1

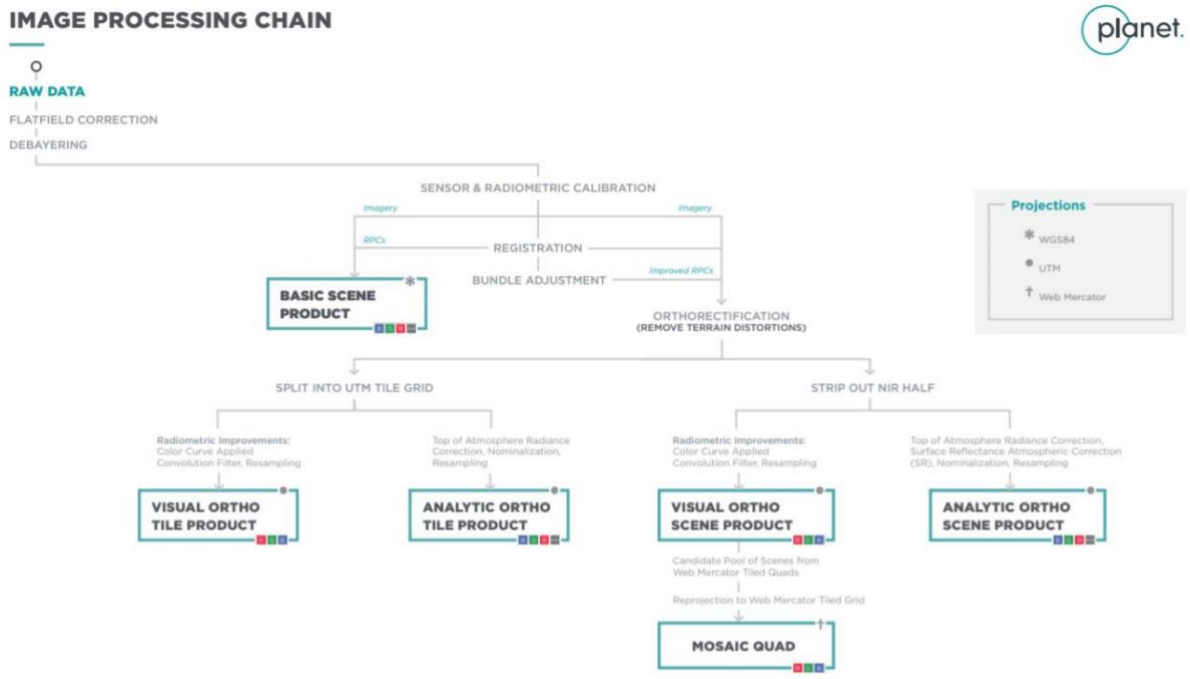


The PlanetScope image processing chain. For this study the Visual and Analytic ortho scene product were used. Retrieved September 2019, from: https://www.planet.com/products/satellite-imagery/files/1610.06_Spec%20Sheet_Combined_Imagery_Product_Letter_ENGv1.pdf (page 26).

## Appendix 2

The used image processing workflow, created in corporation with L.M. Schemmekes. This workflow presents the steps from raw spectral data to a classified image.

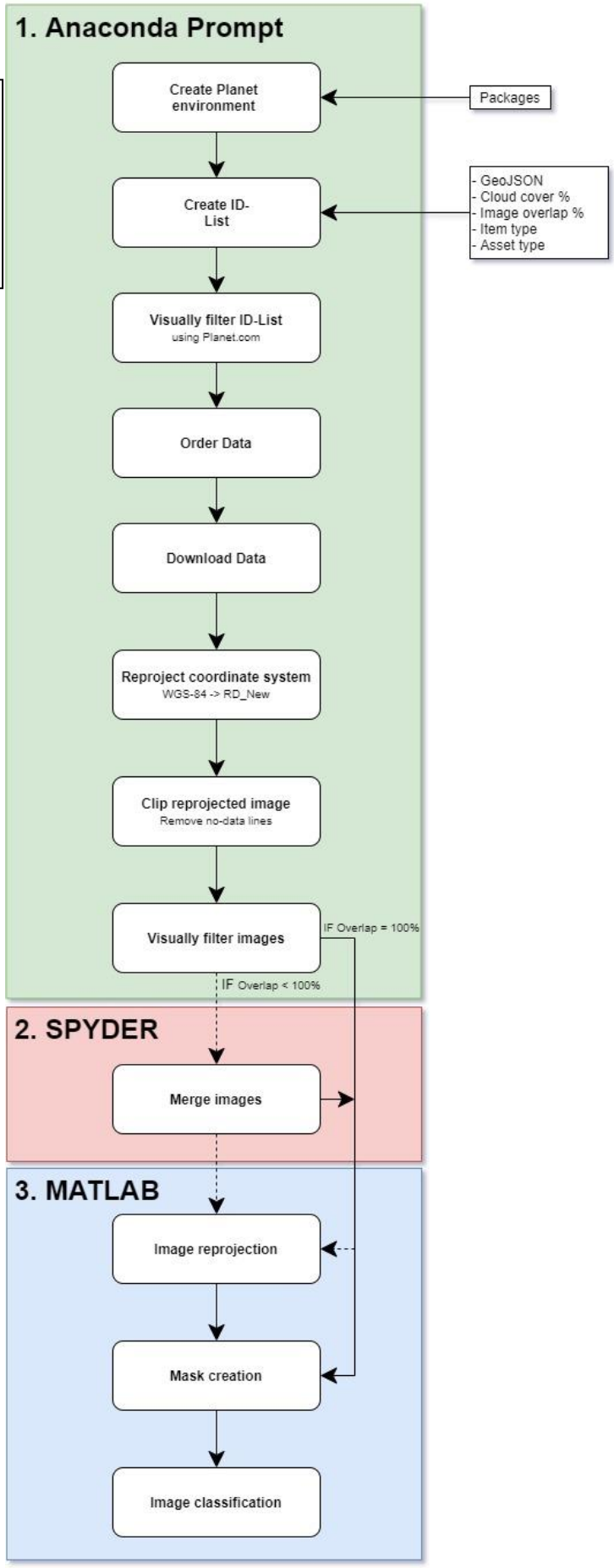

## Appendix 3

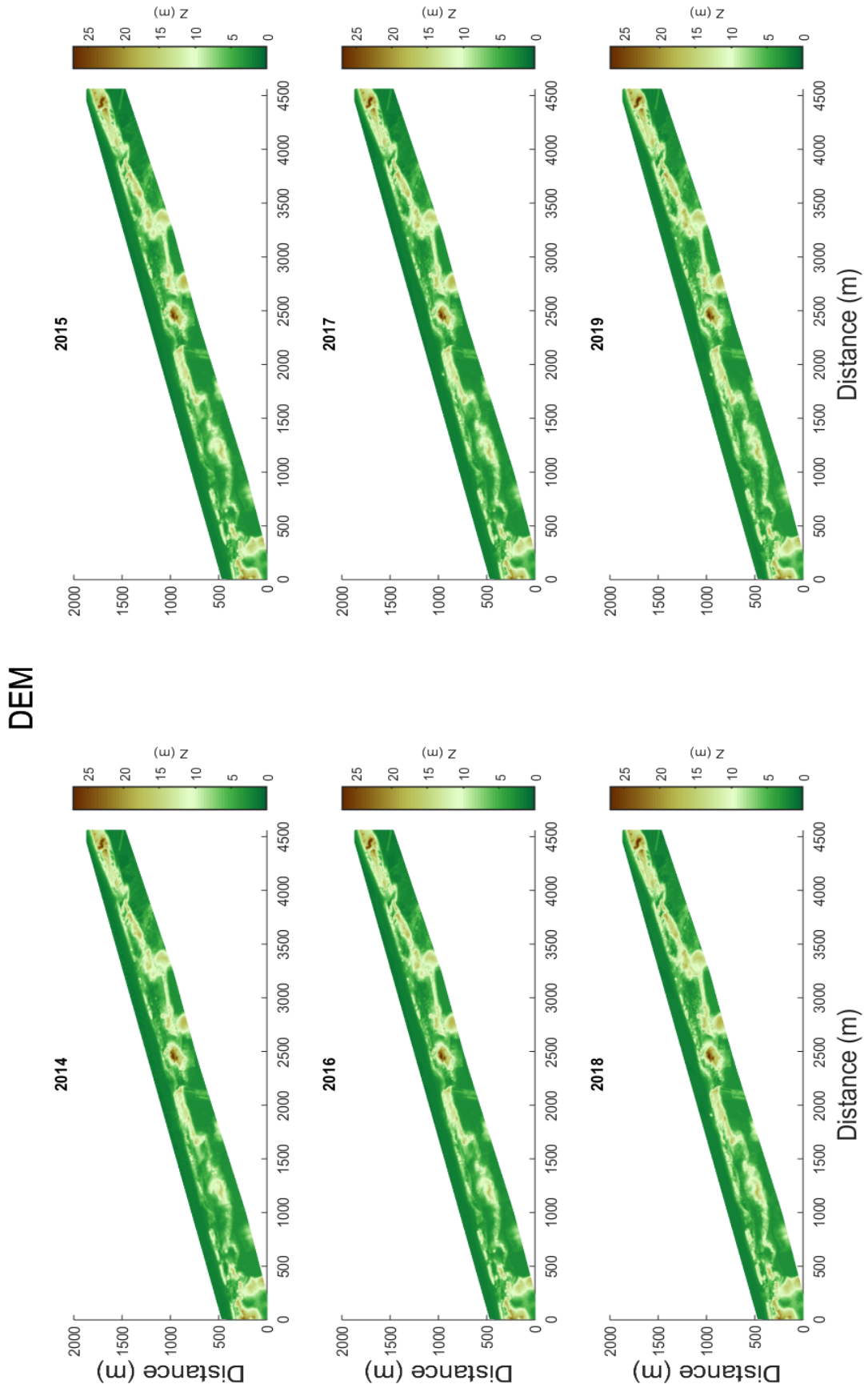

## Appendix 4

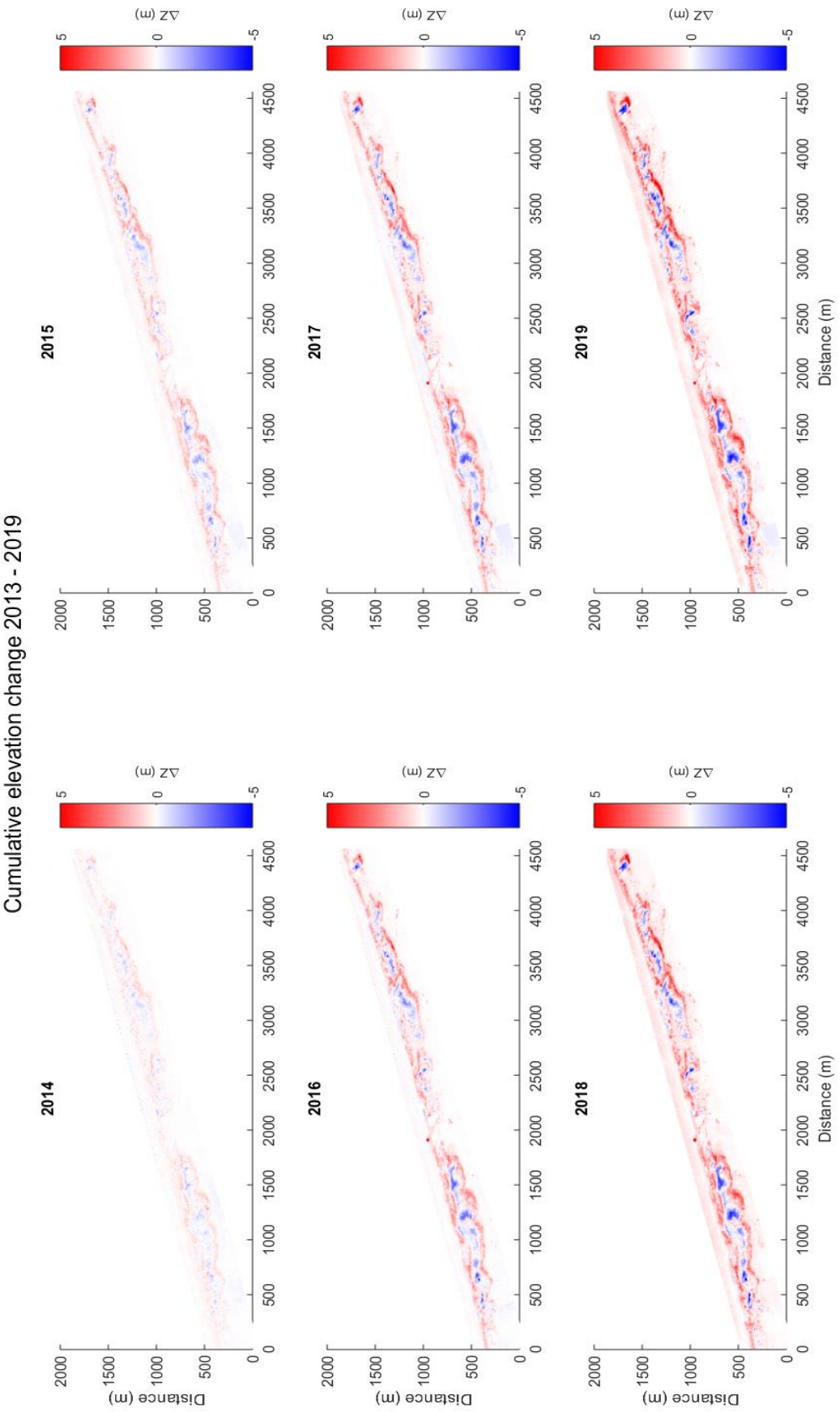
Cumulative elevation change 2013 - 2019
2014
2015
2016
2017
2018
2019
Distance (m)
ΔZ (m)